Deltares

Evaluation linear isotach model; laboratory study and literature review

Contribution to Regio Deal Bodemdaling Groene Hart, project 42

Evaluation linear isotach model; laboratory study and literature review
Contribution to Regio Deal Bodemdaling Groene Hart, project 42

Evaluation linear isotach model; laboratory study and literature review
Contribution to Regio Deal Bodemdaling Groene Hart, project 42

Client	Provincie Zuid-Holland
Contact	Rob Ligtenberg
Reference	-
Keywords	Land subsidence, one-dimensional compression, isotach models

Document control	
Version	1.0
Date	26-06-202426-06-2024
Project nr.	11206019-010
Document ID	11206019-010-BGS-0005
Pages	79
Classification	
Status	Final

Author(s)

Summary

This report reports on a sub-study that was carried out in project 42 of the *Regio Deal Bodemdaling Groene Hart* programme (RDBGH). Project 42 focuses on improving the model tools for subsidence calculations. This sub-study involved laboratory testing and literature study to evaluate the suitability of the linear isotach model for land subsidence applications.

Understanding and predicting land subsidence requires the availability of constitutive models that account for the visco-plastic behaviour of soils. The engineering practice typically uses isotach models to predict subsoil compression due to construction induced loads. In recent years, isotach models have also been incorporated in various land subsidence modelling tools that are used in The Netherlands. Despite the successful application for engineering purposes, the applicability of isotach models in the broader land subsidence applications currently is less well established. In contrast to the typical engineering applications, in land subsidence applications load increments are virtually absent or small and initial strain rates play an important role. To test the validity of the isotach model for small load increments, a literature study and laboratory tests have been conducted.

The assessment of strain rates in the overconsolidated region relies strongly on the position of the isotachs. The present implementation of the isotach model used in Dutch engineering practice, here referred to as the reference implementation, is based on the following assumptions:

1. The isotachs are linear in the log(σ'_v) – natural strain field.
2. The isotachs have an equidistant spacing. This means that in time creep slows down, but never stops.
3. The isotachs are independent of the loading path.

These assumptions were tested in laboratory tests conducted on high plasticity clay samples obtained from the RDBGH land subsidence monitoring site at Bleskensgraaf. A series of two incremental loading (IL) tests and 12 constant rate of strain(CRS) tests were performed. These experimental results are complemented by a literature study on the latest developments in isotach modelling. The outcome of both the laboratory testing and literature study is compared to the reference isotach implementation, yielding the following results for the three underlying assumptions:

1: The isotachs are linear in the log(σ'_v) – natural strain field.
Literature shows that isotachs get distorted upon unloading due to swelling of the soil and therefore isotachs are nonlinear for unloading – reloading conditions. This is confirmed by the results of the IL tests, which show that the strain rates found in the overconsolidated range could not be predicted using the reference implementation. The mismatch between the predicted and measured strain rates increases with increasing OCR, in which the predicted strain rate underestimates the measurements. The difference in measured and calculated strain rate reaches multiple orders in magnitude in the range of OCR = 2 to 4.5. For normally consolidated conditions, OCR = 1, the predicted and measured strain rate matches reasonably well.

The tests further illustrated the sensitivity to different strain measures. The limited sample thickness results in a stiffening effect when presenting the data in terms of linear strain (also: engineering strain) or void ratio. This results in a bending of the DLDS at large strain. The use of natural strain eliminates the end-layer effect and, therefore, is the superior or preferred strain measure for the reference implementation.

The test results were analysed in the log(σ'_v) – natural strain field, but also in the log(σ'_v) – linear strain field and log(σ'_v) – void ratio field. The last two were added to be able to make a comparison to literature data.
The CRS tests, which do not include disturbance by unloading, constrain the position of the different isotachs rather well. For the applied range of strain rates, the isotachs run parallel to each other and changing the displacement rate shifts the stress – strain curve from one isotach to the other, as expected. The positions of individual isotachs were found differ among different samples that are but a small distance apart (order of dm's). This demonstrates the role of heterogeneity, and hampers comprehensive testing of the assumption(s).

2: The isotachs have an equidistant spacing.
To test the assumption of equidistant isotach spacing, CRS tests were used with displacement rates ranging from10.8 mm/h – 0.00108 mm/h which corresponds to strain rates ranging from 1×10^{-4} 1/s to 1×10^{-8} 1/s. This represents the range in strain rate that is achievable under laboratory circumstances. Under field conditions strain rates typical for land subsidence are orders in magnitude lower, 10^{-11} 1/s or less. Consequently, the results obtained in laboratory testing for relatively high strain rates need to be translated to much lower strain rates under field conditions.

The literature indicates that for many clays the isotach spacing reduces for decreasing strain rate and finally reaches an end of creep isotach. This behaviour could not be reproduced from the CRS measurement data. For high strain rates, 10^{-4} 1/s – 10^{-5} 1/s a reduction in isotach spacing was observed. However, this observation might be a spurious finding, caused by excess pore water pressure developing at the higher strain rates. For low strain rates, 10^{-6} 1/s – 10^{-8}1/s, no clear change in isotach distance was observed.

3: The isotachs are independent from the loading path.
The literature study indicates that the validity of the assumptions of linear and stress path independent isotachs is compromised by unloading. Due to unloading and corresponding elastic strain, the soil structure changes, which distorts the isotachs. This explains the findings of the IL tests described above.

For systematic loading applied in the CRS tests, the isotachs are found to be unique and independent from loading history.

The distortion of the isotachs, and the non-equidistant spacing of the isotachs are two elements that are not included in the reference isotach implementation. Both elements have important consequences for the use of the reference implementation for land subsidence applications. Land subsidence applications primarily concern prediction of subsidence, be it for undisturbed conditions or effects of small load changes. The results show that the theoretical framework of the isotach model does not presently yield reliable predictions, limiting the applicability of the model in such applications. The potential to improve the applicability through model adjustments may be explored – numerical solutions for non-equidistant isotachs are available for instance. However, increased reliability of prediction mostly requires empirical data on creep behavior from dedicated field monitoring and testing. Important steps in this direction have been made in RDBGH projects 10 "
Uitbreiding monitoring proefvakken" and 44 "Bodemdaling in kaart en kijken in de bodem; meten, monitoring en ontrafelen van bodemdalingsprocessen".

Contents

1 Introduction

1.1 Background

The work presented in this report was conducted in the framework of the research programme ‘Regio Deal Bodemdaling Groene Hart’ (RDBHG) project 42: Prognosis of land subsidence and a new subsurface (lithological) model for ‘het Groene Hart’. ‘Het Groene Hart’ (English: The Green Heart) is the relatively thinly populated area in the west of The Netherlands between the cities of Rotterdam, The Hague, Amsterdam, and Utrecht. The area is dominated by peat meadows – hence ‘Green Heart’, includes reclaimed lakes, and is underlain by Holocene soft soils (clay/peat). The area suffers from land subsidence associated with land drainage and construction loads.

The Regio Deal programme aims to develop innovative approaches to deal with the subsidence. Project 42 is concerned with the modelling tools for land subsidence calculations. These tools include software/codes that are being used to produce land subsidence prognosis maps for extensive areas (national, provincial, Groene Hart) for policy makers. But also, software for more specific, local applications such as subsidence/settlement estimates for urban activities (new residential areas, renovations, interferences that modify groundwater levels). Project 42 aims to enhance insight in the adequacy and limitations of the tools, and to seek ways to improve them.

1.2 This study

Compression, also referred to as compaction, of soft soils plays an important part in the land subsidence modelling tools. Presently, an isotach model that is typically used in the Dutch engineering practice (D-Settlement; Deltares, 2021), is implemented in the land subsidence tools (e.g., Atlantis; Bootsma et al., 2020, SUB-CR; Kooi et al., 2018).

The isotach framework covers the prediction of creep strain in the soil compression. The isotach framework relates strain to strain-rate and load or effective stress (increments). The prediction methods based on the isotach framework are well established for construction purposes, for example embankments for roads or railways or water retaining embankments. Typically, these purposes include large load increments, which cause the stress conditions to exceed the yield stress. For these conditions, the stress history and initial stress conditions are of minor relevance, allowing fairly accurate prediction of settlement. By contrast, in the context of land subsidence the load increments are typically small (for example due to a lowered groundwater table or re-elevation of pavements and roads) or absent.

Under these circumstances creep strain also contributes to land subsidence and therefore requires quantification. For small or negligible load increments, in which the stress conditions remain below the yield stress, subsidence modelling is challenging as the initial stress conditions and corresponding stress history have a strong impact on the prediction. This report explores the applicability of the isotach framework to prediction of the compression due to small load increments. This exploration includes both laboratory testing and literature review.

1.3 Structure of the report

The report is organized as follows. Chapter 2 starts with a description of the isotach model as implemented in the engineering and land subsidence tools referred to in paragraph 1.2. This is referred to as the reference implementation.

Chapter 3 elaborates the problem and lists the presumptions of the reference implementation that determine its applicability for small load increments. Chapter 4 presents the laboratory experiments that have been conducted to test the presumptions. The tests were done on clay samples from one of the newly installed land subsidence monitoring sites of the RDBGH (project 44). Chapter 5 presents information and insights from the (international) literature on the isotach framework and isotach modelling. Chapters 6 and 7 close with a general discussion and conclusions, respectively.

2 Reference implementation

2.1 Model description

The implementation of the isotach model which is used as a reference in this study is the same as used in the software D-Settlement (Deltares 2021). This implementation is based on the work by Den Haan (Den Haan, 1992, 1994, 1999; Den Haan & Edil, 1994; Den Haan & Selmeijer, 2000) and summarised by Visschedijk, 2010. Parts of the following text are taken from Zwanenburg (2021).

Buisman (1940) introduces a simple relation to evaluate compression of a soil mass:

$$z = \alpha_p + \alpha_s \log(\tau) \tag{2.1}$$

In which z represents compression, α_p represents the direct compression, α_s the coefficient for secular or visco-plastic compression and τ the loading duration. This expression contains two parts. The direct compression, which is stress dependent, given by α_p and the secular or visco-plastic compression given by $\alpha_s \log(\tau)$.

When assuming α_s to be stress independent and replacing compression, z, by strain, ε, the visco-plastic component can be described by:

$$\varepsilon_s = C_\alpha \log\left(\frac{\tau}{\tau_0}\right) \tag{2.2}$$

In which τ_0 represents a reference time, typically, τ_0 = 1 day, C_α the visco-plastic coefficient and ε_s the visco-plastic strain. In the following, the term creep will also be used for visco-plastic strain, ε_s and C_α will be referred to as the creep parameter.

The creep strain rate, $d\varepsilon_s / d\tau$ follows from Equation (2.3):

$$\frac{d\varepsilon_s}{d\tau} = \frac{d}{d\tau}\left(C_\alpha \log\left(\frac{\tau}{\tau_0}\right)\right) = \frac{C_\alpha}{\ln(10)}\frac{\tau_0}{\tau} = \frac{C_\alpha}{2.3\,\tau} \tag{2.3}$$

According to Equation (2.3) the creep strain rate depends on C_α and creep duration τ, resulting in a creep strain rate that decreases with time. If C_α is independent from stress and strain, the amount of creep strain that develops over a time period is independent of stress conditions.

This was acknowledged by Bjerrum (1967), resulting in Figure 2.1. This Figure shows a compression curve during sedimentation in which a soil layer develops, indicated by ‘instant compression during sedimentation’. The Figure uses void ratio, e, as a measure for compaction. At some point the sedimentation process stops, and vertical pressure remains constant. However, settlement and corresponding void ratio reduction, continues due to creep, in Figure 2.1 referred to as delayed compression. When time progresses, the creep strain rate slows down; the creep strain in Figure 2.1 which develops between 3 years and 30 years is the same as between 30 years and 300 years, however the time required to reach this amount of strain is 10-times longer. The same holds for the strain developed between 300 years and 3000 years, etc.

The lines representing age, 3 years, 30 years etc. are running parallel to the instant compression line.

This indicates that irrespective of the stress level to which the stress is raised during instantaneous compression, after a 3-year period of creep, the combination of strain and $\log(\sigma'_v)$ is such that it falls on the 3-year line. The same holds for the 30, 300- and 3000-year line. The age lines, therefore, also connect points in the stress-strain diagram that have accumulated the same amount of creep strain, relative to the instant compression line; below referred to as compression lines.

The creep strain rate follows from the time derivative of the creep strain, ε_s. Equation (2.3) shows that the lines representing age, a constant value for τ, are also lines of constant strain rate. This explains their name; isotach is Greek for constant velocity.

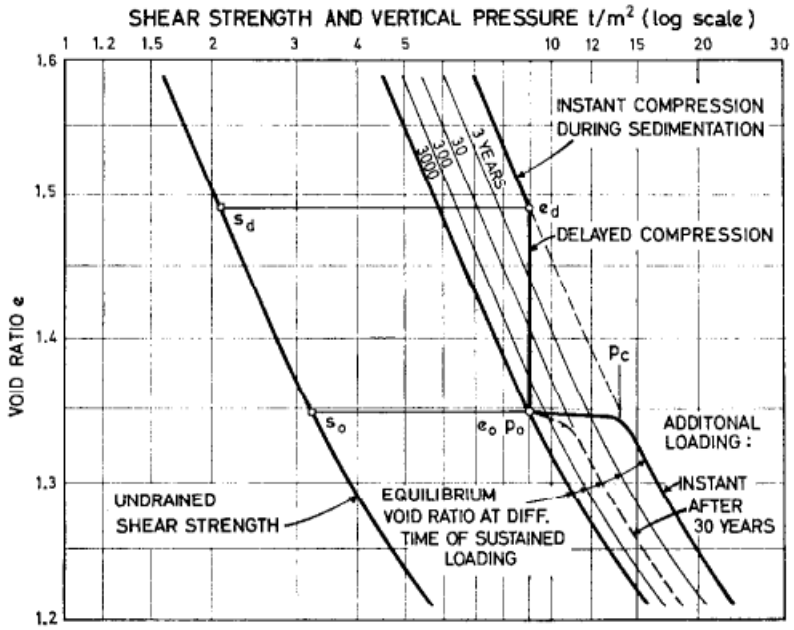

Figure 2.1, the isotach concept from Bjerrum (1967).

Intrinsic time, τ

Figure 2.2 sketches the isotachs in more detail. In analysing laboratory testing data expressing time in days is more practical than years and consequently Figure 2.2 sketches the 1-, 10-, 100- and 1000-day compression line. Not only time causes the stress-strain state to move from one isotach to the other, thereby changing the creep strain rate. Also, loading and unloading steps cause shifts to different isotachs and corresponding acceleration or a slowdown of the creep strain rate. This is shown by Figure 2.2. A soil being loaded to point *a* in Figure 2.2 and then allowed to creep for 100 days reaches point *b* and has a corresponding creep strain rate. If, after the 100-day creep period, the soil is loaded to point *c*, which is on the 10-day compression line, the creep strain rate increases and is equivalent to a strain rate that would be found for the 10-day compression line. Alternatively, if, when reaching point *b*, the soil is unloaded to point *d,* the creep strain rate drops and will be equivalent to the strain rate that would be found after a 1000-day creep period.

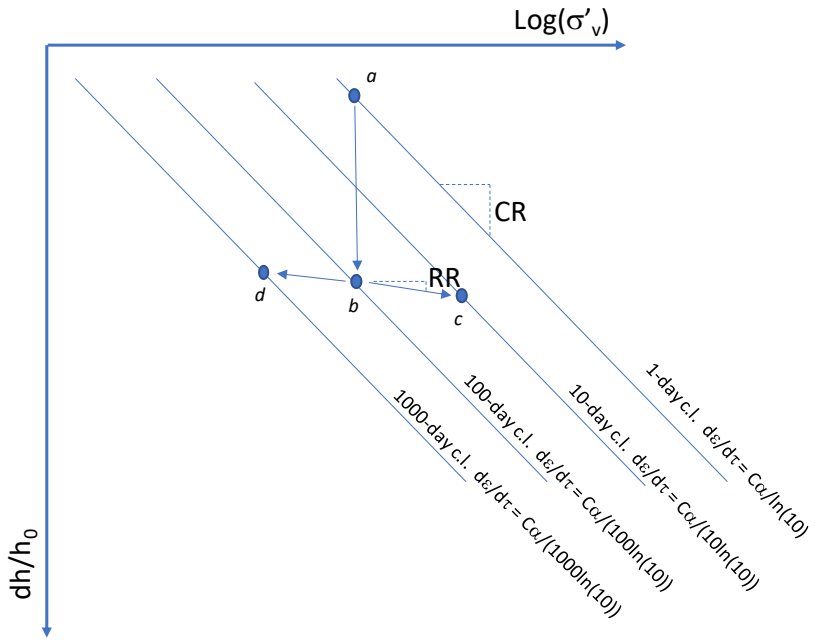

Figure 2.2 Influence loading and unloading on creep strain rate and intrinsic time. CR = compression ratio representing the slope of the isotachs in log σ'_v – dh/h_0 space; RR = recompression ratio representing the slope of the recompression line in log σ'_v – dh/h_0 space.

In construction or laboratory testing, the time *t* is set to zero when a load increment is applied or at the first load increment when multiple increments are applied. Under those conditions, two timescales have to be considered. The first timescale represents the time scale according to which creep develops. The second timescale represents the construction or laboratory testing time, *t*, with *t* = 0 the start of the loading. To account for the first timescale, the concept of intrinsic time, τ, is introduced (den Haan & Edil, 1994). The intrinsic time τ of a soil refers to the isotach which represents the stress – strain – strain rate conditions of the soil. The intrinsic time τ for point *a* in Figure 2.2 is 1 day, for point *b* 100 days etc.

For the first step in an oedometer test τ is typically large. After all, when retrieving the soil sample from the field, the sample was (strongly) unloaded. The small first loading step typically keeps the stress – strain conditions well below the 1-day compression line, and consequently τ>>*t*. Only when large loading steps are applied, which clearly bring the soil conditions beyond the 1-day compression line, the difference between the test time *t* and the intrinsic time, τ becomes negligible.
In elaborating laboratory test data, the time - settlement curve is typically presented as a function of the test time, *t* and the intrinsic time τ is not determined. The creep strain development, as given by Equation (2.3) follows the intrinsic time, τ. Using *t* instead of τ results in a shift in the time – settlement curve. The time shift, t_r is given by:

$$t_r = t - \tau \tag{2.4}$$

In which:

- *t* = loading time, typically set to zero when loading starts, or a load increment has been applied.
- τ = intrinsic time; the time scale according to which the soil is creeping.
- t_r = time shift.

Due to the use of the log-axis when plotting the time-settlement curve, the linear relation between creep strain, ε_s, and the logarithm of the intrinsic time, log (τ), becomes a non-linear relation between creep strain, ε_s, and the logarithm of the loading time, log(*t*).

As shown by Figure 2.3, the time shift t_r has a strong influence for small values for t and a small influence for large values for t. Consequently, the creep index C_α can be determined sufficiently accurately from the ε - log(t) curve when either t_r is small or the loading period is sufficiently long. It should be noted that besides the time shift t_r, consolidation also accounts for initial non-linearity in the ε - log(t) curve.

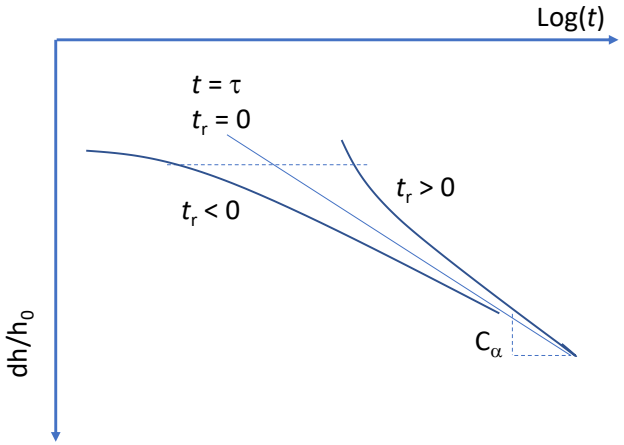

Figure 2.3 Influence of time shift, t_r on the time – development of soils.

The influence of loading and unloading on the intrinsic time

Figure 2.2 shows that loading and unloading causes changes in the intrinsic time. Loading results in a creep rate increase, which according to Equation (2.3), corresponds to a reduction of intrinsic time, τ. While unloading results in a creep rate decrease and according to Equation (2.3) to an increase of τ. A mathematical expression linking a load increment to the change in intrinsic time follows from Figure 2.4.

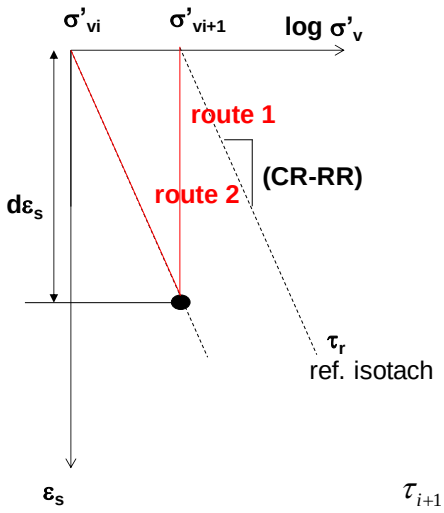

$$\text{route 1: } d\varepsilon_s = C_\alpha \log\left(\frac{\tau_{i+1}}{\tau_i}\right)$$

$$\text{route 2: } d\varepsilon_s = (CR-RR)\log\left(\frac{\sigma'_{v,i+1}}{\sigma'_{v,i}}\right)$$

$$d\varepsilon_{s,1} = d\varepsilon_{s,2}, \quad C_\alpha \log\left(\frac{\tau_{i+1}}{\tau_i}\right) = (CR-RR)\log\left(\frac{\sigma'_{v,i+1}}{\sigma'_{v,i}}\right),$$

$$\log\left(\frac{\tau_{i+1}}{\tau_i}\right)^{C_\alpha} = \log\left(\frac{\sigma'_{v,i+1}}{\sigma'_{v,i}}\right)^{(CR-RR)},$$

$$\tau_{i+1} = \tau_i \left(\frac{\sigma'_{v,i+1}}{\sigma'_{v,1}}\right)^{\frac{CR-RR}{C_\alpha}} \tag{2.5}$$

Figure 2.4 Relation between load increment and intrinsic time increment. The vertical axis represents creep strain only. That is, the stress-dependent, reversible, or direct strain due to the load increment is removed relative to Figure 2.2. This results in the reduced slope CR-RR of the isotachs, compared to CR in Figure 2.2.

The isotach model in predicting settlement:
The concept of intrinsic time allows for an efficient settlement prediction especially when settlement due to a succession of loading, unloading and re-loading steps are applied, (Visschedijk, 2010). The scheme is elaborated in 5 steps, as shown by Figure 2.5.

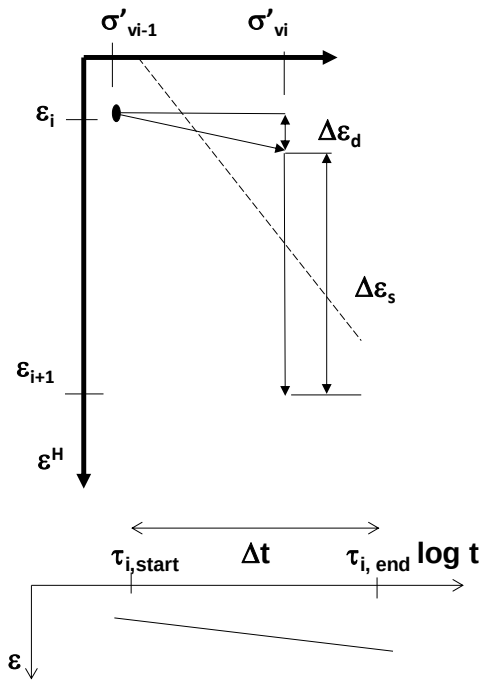

1. Direct strain:

$$\varepsilon_d = RR \log\left(\frac{\sigma_i}{\sigma_{i-1}}\right)$$

2. Intrinsic time, τ, directly after loading

$$\tau_i = \tau_{i-1}\left(\frac{\sigma'_{i-1}}{\sigma'_i}\right)^{\frac{CR-RR}{C_\alpha}}$$

3. Intrinsic time, τ, at the step

$$\tau_{i,end} = \tau_i + \Delta t$$

4. Creep strain

$$\varepsilon_s = C_\alpha \log\left(\frac{\tau_{i,end}}{\tau_{i,start}}\right)$$

5. Total strain and settlement

$$\varepsilon = \varepsilon_d + \varepsilon_s, \quad \Delta h = \varepsilon h_0$$

Figure 2.5 Calculation procedure.

The first step determines the direct strain using the recompression index, *RR* and the total load step. The second step uses the intrinsic time principle to derive the intrinsic time, τ directly after the load application. The third step determines the intrinsic time, $\tau_{i,end}$, at the end of the step. Step 4 applies Equation (2.3) to derive the creep strain that develops during the step. Finally, step 5 calculates the total strain, ε, by summing the direct strain, ε_d, and creep strain, ε_s, and calculates the settlement.

The yield stress, also: pre-consolidation stress, is not mentioned directly in Figure 2.5. However, the yield stress, or Over Consolidation Ratio, OCR, which is the ratio of yield stress and in situ vertical effective stress is required to estimate the initial intrinsic time. Therefore, the position of the reference isotach is relative to the initial state. Figure 2.5 is well suited for a step wise procedure, in which the final conditions in terms of effective stress and intrinsic time form the initial conditions of the next step.

When applying the scheme in Figure 2.5, the initial conditions, σ'_{vi-1} and τ_{i-1}, at the first loading step, $i = 1$, need to be known. The initial vertical effective stress, σ'_{vi-1} follows from the weight of the individual soil layers and pressure heads. The initial intrinsic time τ_{i-1} can be found by using Equation (2.5). With the yield stress being the yield point on the reference isotach, which corresponds to $\tau = \tau_0 = 1$ day and the initial vertical effective stress given by σ'_v, follows:

$$\tau = \tau_0\left(\frac{\sigma'_{vy}}{\sigma'_v}\right)^{\frac{CR-RR}{C_\alpha}} = \tau_0 OCR^{\frac{CR-RR}{C_\alpha}} \qquad (2.6)$$

In which:

RR	= Re-compression index.
CR	= Compression index.
C_α	= Creep parameter.
τ_0	= Intrinsic time reference isotach; τ_0 = 1 day.
σ'_{vy}	= Yield stress related to reference isotach.
OCR	= Over consolidation ratio.

The creep strain rate is related to intrinsic time and OCR as follows:

$$\dot{\varepsilon}_s = \frac{C_\alpha}{\ln 10\tau} = \frac{C_\alpha}{\ln 10\tau_0 OCR^{\frac{CR-RR}{C_\alpha}}} \tag{2.7}$$

2.2 Linear and natural strain

2.2.1 Strain definitions

Soil layers in situ and soil specimen in laboratory tests will have a finite thickness. Even after large deformation, their thickness will not reduce to zero, irrespective of the load level. Consequently, the log(σ'_v) - ε curve will not be linear at large strain, and compression ratios, based on linear strain, will not be constant. To deal with the non-linearity at large strain, a different strain measure is introduced.

The conventional engineering strain, also referred to as linear or Cauchy strain, ε^C relates deformation to the initial dimensions:

$$\varepsilon^C = \frac{\Delta h}{h_0} \tag{2.8}$$

In which:

ε^C = Cauchy strain or engineering strain.
Δh = change in layer thickness or specimen height in laboratory testing.
h_0 = original layer thickness or specimen height in laboratory testing.

The natural strain or Henky strain, ε^H relates the increment in layer thickness or specimen height in laboratory testing, dh, to the actual height, h. Since the actual height is constantly changing ε^H contains the summation of infinitesimal increments, dh, related to their actual sample height, h:

$$\varepsilon^H = \int_{h=h_0}^{h=h_0-\Delta h} \frac{dh}{h} = -\ln\left(\frac{h_0-\Delta h}{h_0}\right) = -\ln\left(1-\varepsilon^C\right) \tag{2.9}$$

In which:

ε^H	= Natural strain.
ε^C	= Linear strain.
dh	= Infinitesimal incremental change in height, *h.*
h	= Sample or layer thickness.
h_0	= Initial sample or layer thickness.
Δh	= Total change in sample or layer thickness.

Figure 2.6 illustrates the differences between the two strain measures. For linear strain a constant increase in strain with increasing reduction in layer thickness is found.

For ε^C = 0, the layer thickness is compressed to 0, which is physically impossible. For natural strain ε^H goes to infinity when the layer thickness reaches 0.

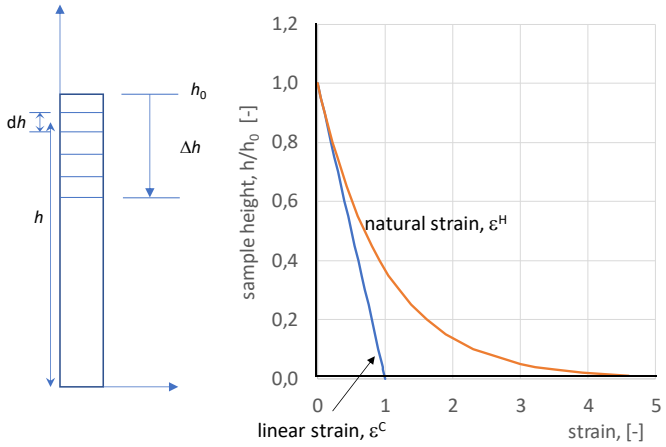

Figure 2.6 Linear and natural strain.

Figure 2.7 shows the results of an incremental loading test, IL, on a peat sample. The results are plotted against linear and natural strain. The difference between the two strain definitions is negligible for a strain level up to ε = 0.2. For a strain level beyond ε^C = 0.5, the curve of the linear strain measure starts to bend as the sample behaviour stiffens due to a final sample thickness. For the loading steps beyond ε^C = 0.5, the compression ratio, CR is no longer constant and reduces for increasing strain. The natural strain develops linearly for increasing log(σ'_v) even at large strain.

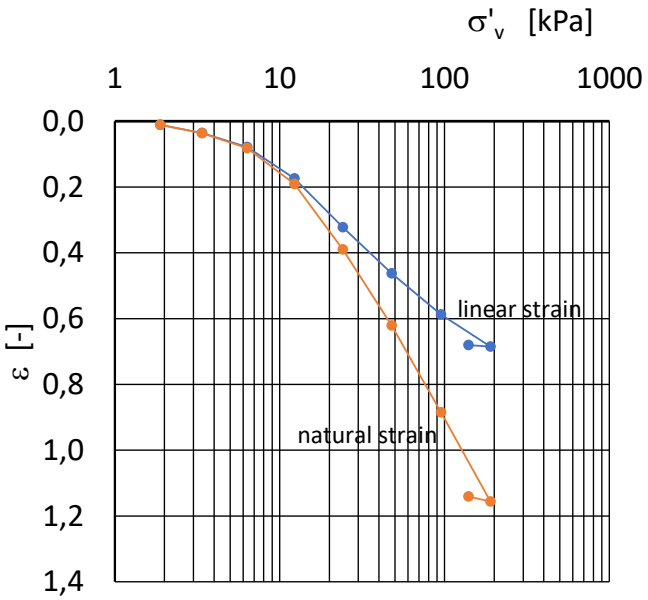

Figure 2.7 Results of an Incremental loading test on peat plotted for linear and natural strain, properties of the tested material, saturated weight, γ_w = 10 kN/m^3, water content, w *= 1124 %, loss on ignition, LOI = 87%.*

2.2.2 1D compression model in natural strain

Figure 2.7 shows that the application of the natural strain definition changes the stress strain curve and consequently, the values for the compression ratios. Equivalent to the model described in Section 2.1 Den Haan (Den Haan, 1992, 1994, 1999) developed a 1D compression model based on natural strain, also referred to as the *abc* model.

The model introduces the parameter *a* for the recompression ratio, *b* for compression ratio, see Figure 2.8 and *c* for the creep parameter. It should be noted that this model uses the natural logarithm, *ln*, for the stress dependency and the stress – strain curves are described in the ln(σ'_v) - ε space. Also, the *abc* model uses the natural logarithm in modelling creep behaviour, yielding the following expression for 1D settlement:

$$\varepsilon^H = a \ln\left(\frac{\sigma'_{vy}}{\sigma'_i}\right) + b \ln\left(\frac{\sigma'_u}{\sigma'_{vy}}\right) + c \ln\left(\frac{\tau}{\tau_0}\right) \qquad (2.10)$$

In which:
ε^H = Henky strain, see Equation (2.9).
a = Recompression index.
b = Compression index.
c = Creep parameter.
τ, τ_0 = Equivalent time, see Equation (2.4) and (2.6), τ_0 = 1 day.

And corresponding creep strain rate becomes:

$$\frac{d\varepsilon_s^H}{d\tau} = c\frac{\tau_0}{\tau}\left(= \frac{c}{\tau}, \text{ for } \tau_0 = 1 \text{ day}\right) \qquad (2.11)$$

Figure 2.8 re-plots the isotach field in the ln(σ'_v) - ε^H space, providing the definitions for *a*, *b*. The creep parameter, *c*, determines the distance between the isotachs.

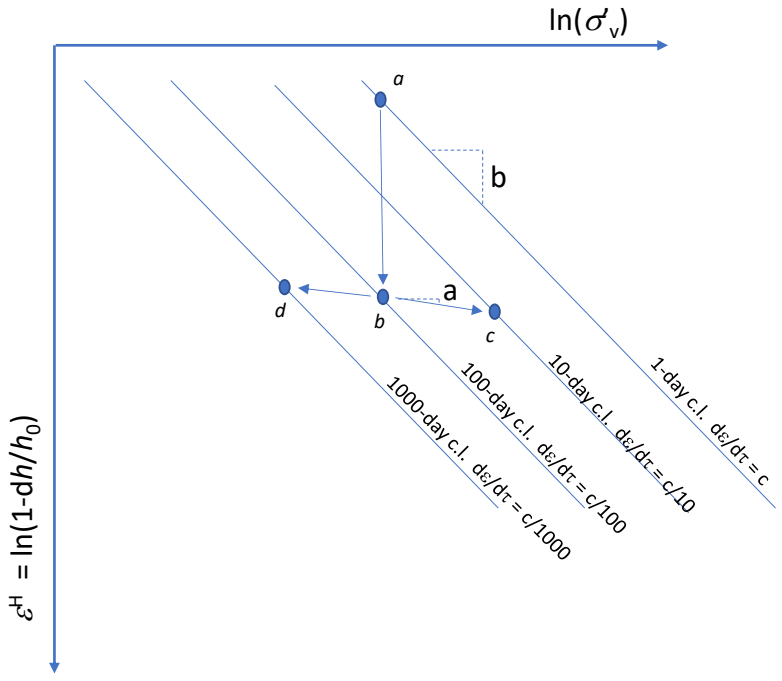

Figure 2.8 Isotach field in the ln(σ'_v) - ε^H space.

Figure 2.9 gives the calculation procedure for settlement in the ln(σ'_v) - ε^H space. This procedure is equivalent to the procedure presented in Figure 2.5 for the log(σ'_v) - ε space.

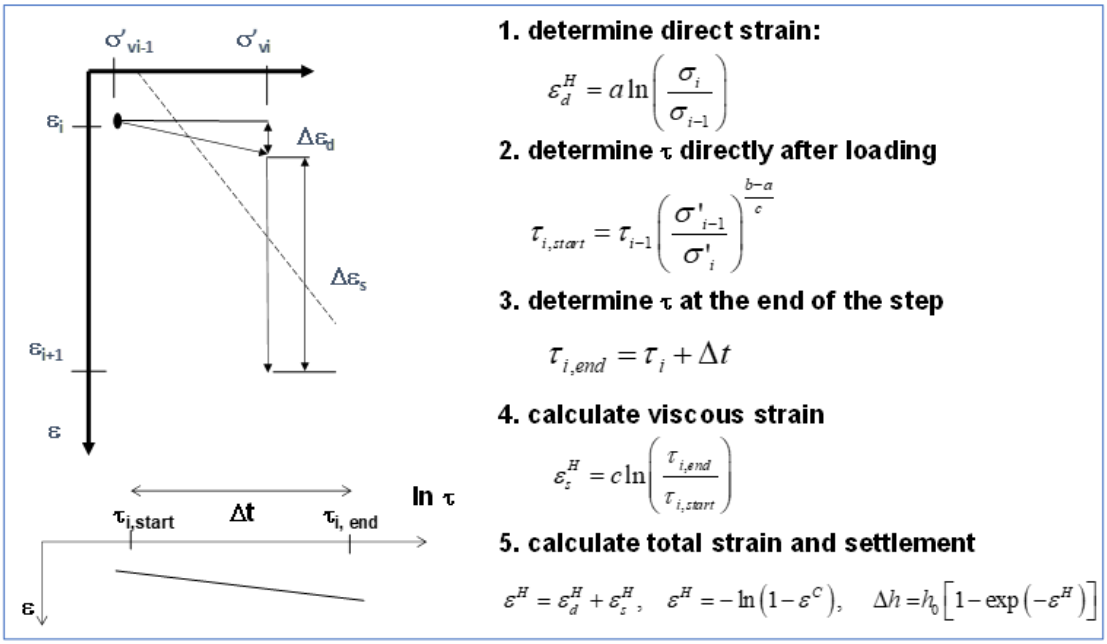

Figure 2.9 Calculation procedure for settlement in the ln(σ'v) - ε^H space.

3 Problem description

While sufficiently accurate settlement predictions can generally be made with the reference implementation of the isotach framework (Chapter 2) for applications involving large load increments, due to heavy constructions, the applicability of the implementation in land subsidence modelling, the drivers of which typically are small load increments, is largely unknown (Section 1.2). Figure 3.1 elucidates the issue using the state diagram for the reference implementation:

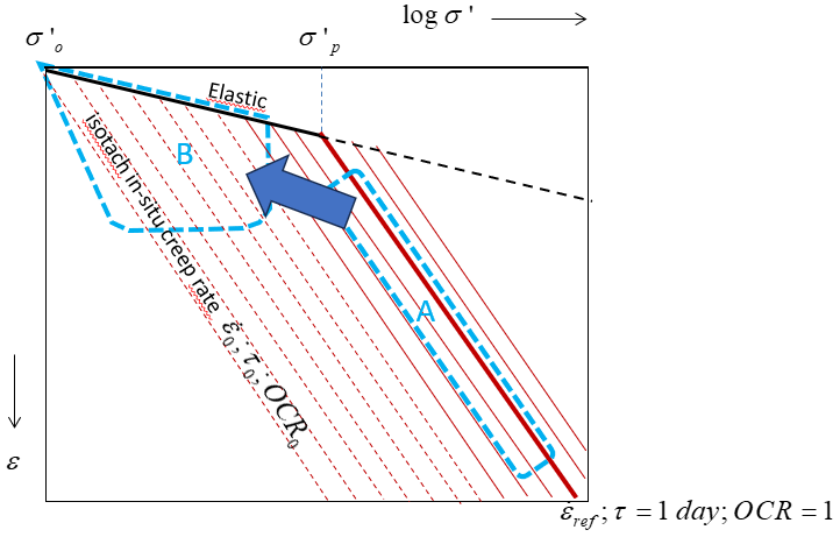

Figure 3.1 Qualitative illustration of the problem. The isotach parameters and creep behaviour of soils are constrained/measured for stress, strain, and creep strain rate conditions in zone A. In land subsidence modelling, the parameters and behaviour are applied for conditions in zone B. The thick red line is the reference isotach.

The isotach parameters and creep behaviour of soils are constrained/measured for stress - strain conditions in zone A, which involve high creep strain rates in the realm of the reference isotach. Zone A also roughly represents early conditions developing in applications involving heavy constructions in which the yield stress or pre-consolidation stress, σ'_p, is exceeded. In land subsidence modelling, the isotach parameters and behaviour are, or need to be, applied for conditions in zone B to quantify very low creep strain rates. Applicability of the reference implementation for this purpose clearly is uncertain as it requires several model characteristics/presumptions to be valid over the entire range of states: from virgin compression, at the reference isotach, to significantly over-consolidated states represented by the in-situ conditions.

These presumptions are:

1. Isotachs are linear in $\log\sigma' - \varepsilon$ space.
2. Isotachs are 'equidistant' in $\log\sigma' - \varepsilon$ space, for log-cycle differences in creep strain rate. In other words, the creep coefficient C_α or c is truly constant, not dependent on stress and strain.
3. The isotachs are fixed in $\log\sigma' - \varepsilon$ space, independent of the path, strain and or stress history.

These presumptions are tested in this report through and laboratory experiments, Chapter 4 and literature study, Chapter 5.

4 Laboratory tests

4.1 Testing plan

4.1.1 Introduction

Two types of tests were conducted to investigate the presumptions listed in Chapter 3:

Incremental loading tests, IL. These tests are designed (1) to derive the isotach parameters, (2) to measure the creep strain rate at the end of load steps for both low (OCR<1) and high stress conditions (OCR=1). The measured creep strain rates subsequently are compared against the creep strain rates predicted by the reference model for the derived isotach parameters. These experiments test, in a straightforward manner, if the reference model applies over a large range of states and, thereby, test the validity of the ensemble presumptions (all three).

Constant Rate of Strain tests, CRS. These tests are designed to constrain the position and the shape of isotachs for different creep strain rates. These tests specifically allow evaluation of the linearity (presumption 1) and equidistant nature (presumption 2) of the isotachs.

For this purpose, clay was sampled at the new RDBDGH land subsidence monitoring site at Bleskensgraaf. The tests were conducted on 'natural' samples to avoid influences of modified structure due to remoulding.

4.1.2 IL tests

Incremental loading tests were done on two samples. The loading schemes of both tests are listed in Table 4-1.

Table 4-1 Loading scheme incremental loading tests.

Step nr	condition	Test 1		Test 2	
		σ_v [kN/m^2]	OCR	σ_v [kN/m^2]	OCR
1	loading	2.5	8.0	1.9	10.5
2	loading	4.5	4.5	4.5	4.4
3	loading	9.3	2.2	9.4	2.1
4	loading	19.2	1.0	19.2	1.0
5	loading	38.9	1.0	39.1	1.0
6	loading	78.8	1.0	79.1	1.0
7	unloading	20.0	3.9	20.0	4.0
8	loading	40.0	2.0	40.0	2.0
9	loading	60.0	1.3	60.0	1.3
10	loading	70.0	1.1	70.0	1.1
11	loading	80.0	1.0	80.0	1.0
12	loading	139.3	1.0	139.3	1.0

All load steps last 24 hours

Estimated natural yield stress, σ'_{vy} = 20 kN/m^2.

4.1.3 CRS tests

13 CRS tests have been conducted. The loading scheme of the tests is given in the tables below. Tests CRS1-2 and CRS2-2 following a conventional loading scheme and serve as a reference. The tests CRS3 – CRS9 contain steps with different displacement rates. Finally, the tests 10 to 12 each include a constant displacement rate.

Table 4-2 Loading scheme tests CRS1-2 and CRS2-2.

Step	σ_{end} [kPa]	Δh/Δt [mm/y]	Remark
1	80	0.07	Loading
2	40	-0.04	Unloading
3	120	0.07	Re-loading
4	[a]	0	Relaxation
5	140	0.07	Re-loading
6	0	-0.07	Unloading

[a] *= the final stress reached at the end of the relaxation phase depends on soil properties; the relaxation phase extends over 15 hours.*

Table 4-3 Loading scheme Test CRS 3.

Phase nr	Displacement rate [mm/h]	Strain rate [1/s]	Period [hours]	Displacement [mm]	Strain [-]
1	10.8	0.0001	0.42	4.50	0.150
2	1.08	0.00001	2.78	3.00	0.100
3	0.108	0.000001	13.89	1.50	0.050
4	0.0108	0.0000001	69.44	0.75	0.025
5	0.00108	0.00000001	694.44	0.75	0.025

Table 4-4 Loading scheme Test CRS 4.

Phase nr	Displacement rate [mm/h]	Strain rate [1/s]	Period [hours]	Displacement [mm]	Strain [-]
1	10.8	0.0001	0.69	7.50	0.250
2	1.08	0.00001	2.78	3.00	0.100
3	0.108	0.000001	13.89	1.50	0.050
4	0.0108	0.0000001	92.58	1.00	0.033
5	0.00108	0.00000001	925.83	1.00	0.033

Table 4-5 Loading scheme Test CRS 5.

Phase nr	Displacement rate [mm/h]	Strain rate [1/s]	Period [hours]	Displacement [mm]	Strain [-]
1	0.108	0.000001	55.56	6.00	0.200
2	0.0108	0.0000001	277.78	3.00	0.100
3	0.00108	0.00000001	1388.89	1.50	0.050

Table 4-6 Loading scheme Test CRS 6.

Phase nr	Displacement rate [mm/h]	Strain rate [1/s]	Period [hours]	Displacement [mm]	Strain [-]
1	10.8	0.0001	0.42	4.50	0.150
2	1.08	0.00001	2.78	3.00	0.100
3	0.108	0.000001	27.78	3.00	0.100

Table 4-7 Loading scheme Test CRS 7 and 7B.*

Phase nr	Displacement rate [mm/h]	Strain rate [1/s]	Period [hours]	Displacement [mm]	Strain [-]
1	1.08	0.00001	5.56	6.00	0.200
2	0.108	0.000001	27.78	3.00	0.100
3	0.0108	0.0000001	138.89	1.50	0.050
4	0.00108	0.00000001	1388.89	1.50	0.050

* *Test 7 is stopped after 508 hours*

Table 4-8 Loading scheme Test CRS 8.

Phase nr	Displacement rate [mm/h]	Strain rate [1/s]	Period [hours]	Displacement [mm]	Strain [-]
1	1.08	0.00001	5.56	6.00	0.200
2	0.108	0.000001	13.89	1.50	0.050
3	0.0108	0.0000001	277.78	3.00	0.100
4	0.00108	0.00000001	2046.78	2.07	0.069
5	0.108	0.000001	41.00	4.30	0.143

Table 4-9 Loading scheme Test CRS 9.

Phase nr	Displacement rate [mm/h]	Strain rate [1/s]	Period [hours]	Displacement [mm]	Strain [-]
1	0.108	0.000001	55.56	6.00	0.200
2	0.0108	0.0000001	416.67	4.50	0.150
3	0.00108	0.00000001	1860.33	1.80	0.060
4	0.108	0.000001	42.00	4.33	0.144

Table 4-10 Loading scheme Tests 10, 10B, 11 and 12.

Test nr	Displacement rate [mm/h]	Strain rate [1/s]	Period [hours]	Displacement [mm]	Strain [-]
10	1.06	0.000010	11.1	11.75	0.39
10B	1.06	0.000010	11.1	11.75	0.39
11	0.106	0.000001	111.1	11.73	0.39
12	0.0108	0.00000010	715.5	7.74	0.26

CRS tests apply a constant displacement rate, and the development of the load or total stress is recorded. In the tests, pore water drains at the top and pore pressure is measured with a pressure transducer at the base of the sample, which is closed to flow. The average pore pressure in the sample is estimated to be $2/\pi \times \sigma_{w,max}$., with $\sigma_{w,max}$ the measured pressure at the base.

The factor $2/\pi$ corresponds to a (quarter wavelength) sine-shaped pressure curve over the height of the sample. This differs slightly from the conventional correction, which assumes a hyperbolic shape, which yields $2/3 \times \sigma_{w,max}$. The required state variable is effective stress rather than total stress[1], which is assessed by taking the difference between the measured load or total stress and the average pore pressure.

The following steps are taken to evaluate the spacing between the isotachs:

- For tests in which the strain rate is varied, tests 3 to 9, the stress – strain curves are fitted for the parts with constant strain rate. The fits are made both for natural and linear strain, to comply to literature data. The fits are made by linear regression and provide information on:
  - Possible changes in slope angle when reducing the strain rate.
  - Horizontal isotach distance $\log(\sigma'_{v,1}/\sigma'_{v,2})$, see Figure 4.1.
  - Vertical isotach distance which can be calculated from on slope angle and horizontal distance, see Figure 4.1.
- The results are compared to literature data, which provides the $(\sigma'_{v,1}/\sigma'_{v,ref})$ versus $d\varepsilon/dt$ relation. In this relation a reference strain rate of $d\varepsilon/dt_{ref} = 1 \times 10^{-7}$ 1/s is selected and $(\sigma'_{v,1}/\sigma'_{v,ref})$ is the corresponding vertical distance to the isotach representing the reference strain rate.
- Combination of the stress strain curves of different tests. To account for differences between samples the combined graphs are analysed in terms of void ratio instead of strain. It should be noted that stress – strain curves by definition start at $\varepsilon = 0$ and small differences due to heterogeneity of the samples will mask the changes in isotach when loaded by different strain rates.

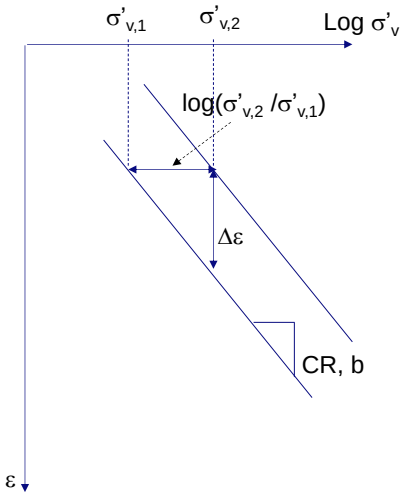

Figure 4.1 definition sketch of horizontal isotach distance $\log(\sigma'_{v,1}/\sigma'_{v,2})$ and vertical istach distance, $\Delta\varepsilon$.

4.2 Characteristics of tested material

The tested clay is sampled at the Bleskensgraaf monitoring site. Sampling was done with the Deltares Large Diameter Sampler, DLDS. The DLDS is a block sampler resulting in sample diameter of 0.4 m and sample height of 0.5 m. Details of the sampler are given by Zwanenburg (2017). Specimens were cut from the samples by hand.

The tested material plots as an extremely plastic clay in the plasticity chard, category ClV according to NEN-EN-ISO 17892:12.

[1] Formally, the strain rate assigned to the isotach need to be corrected for the direct (elastic) strain rate. As the correction is exceedingly small, this is usually not applied.

Specimens have been taken in the range of 2.88 – 3.10 m below ground level. The samples show a variation in organic content, water content and density. This heterogeneity introduces some differences between the tested specimens. The specimen characteristics are given in the tables below.

Table 4-11 Measured characteristics of the tested samples.

Sample ID	Depth [m gl]	water content [%]	density [kN/m^3]	loss on ignition [%]
IL-1	-3.01 to -3.04	62.44	15.20	3.6[a]
IL-2	-3.04 to -3.07	117.72	13.02	6.5[a]
CRS 1_2	-3.01 to -3.04	104.87	13.61	6.5[a]
CRS 2_2	-3.06 to -3.09	82.52	14.09	6.5[a]
CRS 3	-3.05 to -3.08	102.00	13.61	6.8[b]
CRS 4	-3.02 to -3.05	118.16	13.27	9.0[b]
CRS 5	-2.99 to -3.10	59.00	15.37	3.6[b]
CRS 6	-2.99 to -3.10	111.48	13.17	6.5[a]
CRS 7	-2.99 to -3.10	115.61	12.12	13.4[a]
CRS 7b	-2.95 to -2.98	156.92	12.26	13.4[b]
CRS 8	-2.91 to -2.94	151.97	12.23	13.6[b]
CRS 9	-2.95 to -2.98	144.98	12.26	15.0[b]
CRS 10	-2.94 to -2.97	142.54	12.55	14.0[b]
CRS 10b	-2.94 to -2.97	159.37	12.66	15.7[b]
CRS 11	-2.95 to -2.98	138.18	13.09	13.5[b]
CRS 12	-2.92 to – 2.94	160.76	12.53	15.9[b]

[a] *= estimated from nearby samples.*

[b] *= measured after testing.*

The analysis of the data requires the assessment of the void ratio, *e*. The assessment of *e* is done in the following steps:

- The specific density of the solids is measured for each specimen, except for IL-1, IL-2 and CRS 7. For those specimens G_s is estimated from (Den Haan & Kruse 2007):

$$\frac{1}{G_s} = \frac{LoI}{1.4} + \frac{1-LoI}{2.7} \tag{4.1}$$

- The void ratio follows from:

$$e = \frac{G_s w}{S_r} \tag{4.2}$$

In which *w* represents the water content and S_r the degree of saturation. Since S_r is not measured directly, additional information is needed. The unit sample weight follows from:

$$\gamma = S_r n \gamma_w + (1-n)\gamma_s \tag{4.3}$$

In which *n* represents porosity, γ_w the unit weight of water and γ_s the solid weight. Rewriting Equations (4.2) and (4.3), equating for S_r and using $e = n/(1 - n)$ yields:

$$S_r = \frac{G_s w}{e} = \frac{\gamma - (1-n)\gamma_s}{n\gamma_w},$$
$$n = 1 - \left(\frac{\gamma}{\gamma_w G_s w + \gamma_s} \right), \quad (4.4)$$
$$e = \frac{n}{1-n}$$

Table 4-12 provides the results of Equations (4.2) to (4.4) for each of the tested samples.

Table 4-12 Results Equation (4.1) to (4.4).

Sample ID	G_s [-]	S_r [-]	n [-]	e [-]
IL-1	2.57[a]	0.95	0.63	1.68
IL-2	2.50[a]	0.95	0.76	3.10
CRS 1_2	2.49	0.98	0.73	2.66
CRS 2_2	2.53	0.95	0.69	2.20
CRS 3	2.48	0.97	0.72	2.60
CRS 4	2.54	0.97	0.76	3.08
CRS 5	2.58	0.95	0.62	1.61
CRS 6	2.50	0.95	0.74	2.92
CRS 7	2.37[a]	0.88	0.76	3.12
CRS 7b	2.45	0.96	0.80	4.02
CRS 8	2.45	0.95	0.80	3.93
CRS 9	2.47	0.94	0.79	3.82
CRS 10	2.46	0.96	0.78	3.65
CRS 10b	2.45	1.00	0.80	3.90
CRS 11	2.46	1.01	0.77	3.39
CRS 12	2.46	0.99	0.80	3.98

[a] = *G_s is derived from Equation (4.1).*

Test 7 has a low degree of saturation, S_r, which has an impact on the measurement data. Therefore, test 7 is replaced by test 7b. Test 10 includes a high displacement rate and corresponding large pore pressure development. Test 10b is done additionally to measure the pore pressure more accurately.

To test the validity of Equation (4.1) a comparison has been made to the data presented by Den Haan & Kruse (2007), see Figure 4.2. The blue dots, representing the data presented in this report, match well with the literature data.

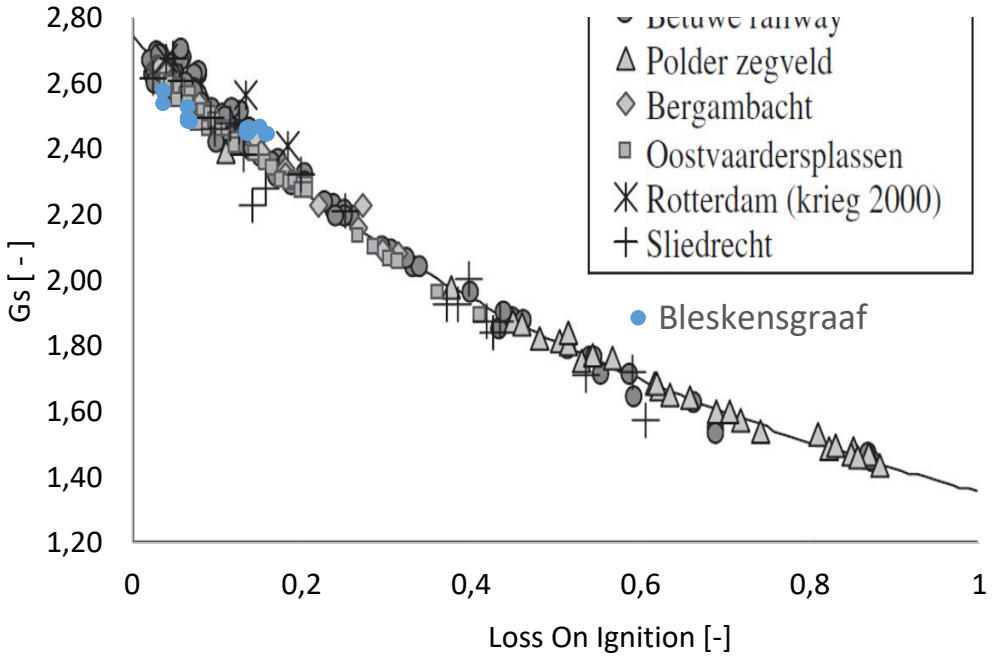

Figure 4.2 Relation between density of the solids, G_s and the loss on ignition, LOI. Comparison of present data, Bleskensgraaf, to Den Haan & Kruse (2007).

4.3 Results IL tests

Figure 4.3 shows the time – strain curves of both IL tests. Figure 4.4 displays the corresponding stress – strain and stress - void ratio curves. The samples used in the tests are quite different (Table 4-11). The lower organic matter content and corresponding larger density of sample 1 are clearly reflected in a stiffer behavior.

Table 4-13, Parameters for IL1 and 2.

Test	RR	CR	C_α	$(CR-RR)/C_\alpha$	σ'_{vy} [kPa]
1	0.011	0.16	0.0059	25.2	20
2	0.025	0.29	0.029	9.3	20

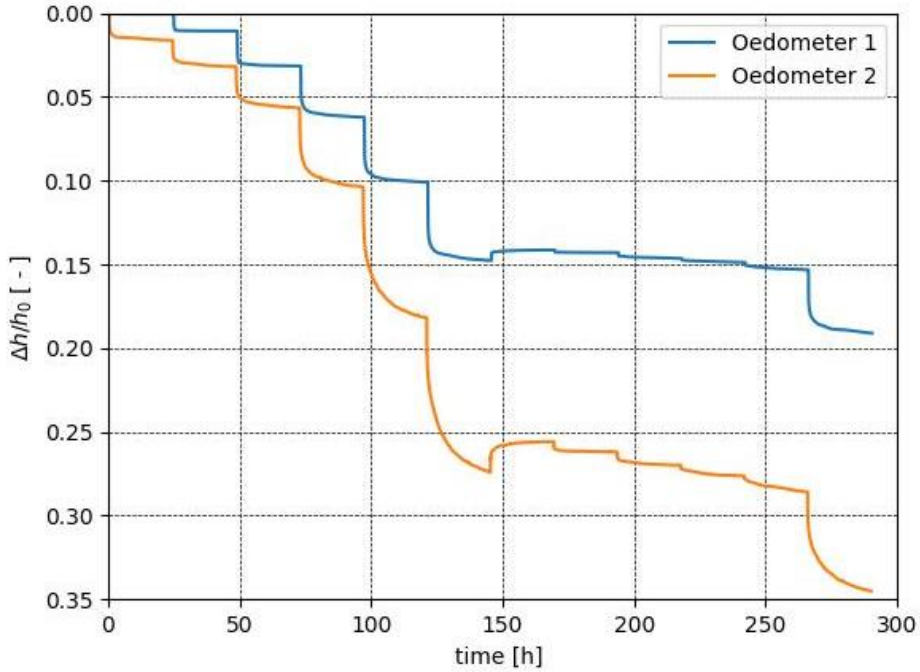

Figure 4.3 Time – strain curves of the two oedometer tests.

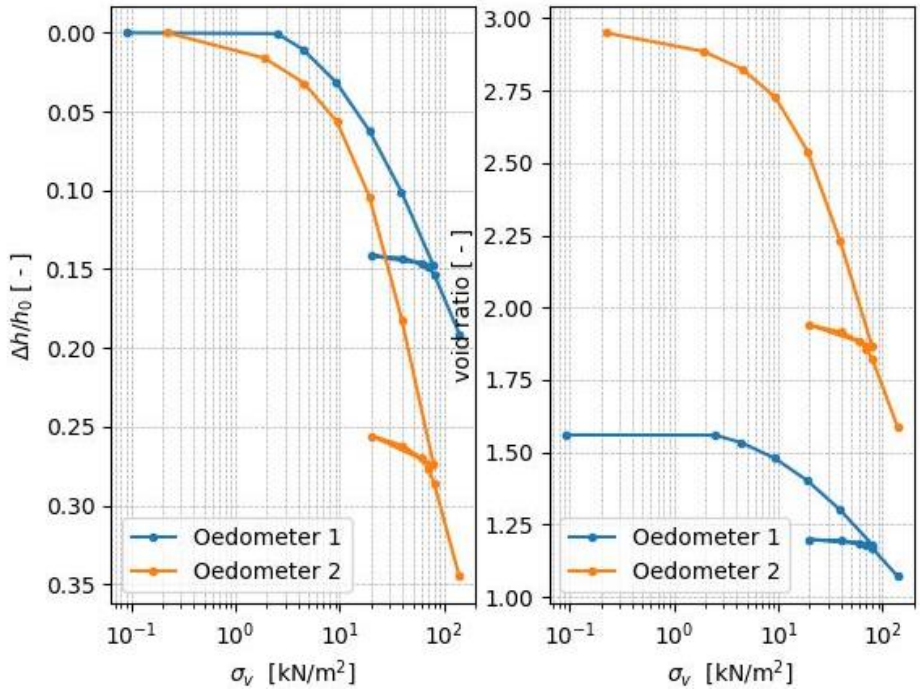

Figure 4.4 Stress – strain and stress – void ratio curves of the two oedometer tests.

Table 4-14 and Table 4-15 list the measured and the model-predicted creep strain rate for each loading step, and their ratio. The measured strain rate was obtained from the slope of the time-strain curve at the end of the load step. The predicted strain rate was calculated with Equation (2.6) and the parameters obtained from the tests (Table 4-13). Strain rates per year are included as the values can be more readily appreciated in terms of land subsidence; 0,001 yr^{-1} for instance corresponds to 1 mm subsidence in a year for a 1 m thick layer.

Table 4-14 IL test 1, measured and predicted strain rates at the end of each loading step.

Step nr	conditions	OCR	dε / dt [1/s]; [1/yr] measurement	dε / dt [1/s]; [1/yr] predicted	$(dε / dt)_m / (dε / dt)_p$
1	Loading	8.0			
2	Loading	4.5	1.50×10^{-9}; 0,047	1.03×10^{-24}; 0,000	1.45×10^{15}
3	Loading	2.2	6.99×10^{-9}; 0,220	1.09×10^{-16}; 0,000	6.40×10^{7}
4	Loading	1.0	2.85×10^{-8}; 0,900	7.56×10^{-9}; 0,238	3.77
5	Loading	1.0	2.69×10^{-8}; 0,848	1.48×10^{-8}; 0,467	1.82
6	Loading	1.0	3.29×10^{-8}; 1,040	1.48×10^{-8}; 0,467	2.23
7	Unloading	3.9			
8	Loading	2.0	6.90×10^{-10}; 0,022	1.07×10^{-15}; 0,000	6.44×10^{5}
9	Loading	1.3	4.79×10^{-9}; 0,151	3.00×10^{-11}; 0,001	160
10	Loading	1.1	8.06×10^{-9}; 0,254	1.40×10^{-9}; 0,044	5.75
11	Loading	1.0	1.01×10^{-8}; 0,319	1.48×10^{-8}; 0,467	0.69
12	Loading	1.0	3.59×10^{-8}; 1,130	1.48×10^{-8}; 0,467	2.43

Table 4-15 IL test 2, measured and predicted strain rates at the end of each loading step.

Step nr	conditions	OCR	dε / dt [1/s]; [1/yr] measurement	dε / dt [1/s]; [1/yr0 predicted	$(dε / dt)_m / (dε / dt)_p$
1	Loading	10.5			
2	Loading	4.4	1.52×10^{-8}; 0,479	1.53×10^{-13}; 0,000	99565.91
3	Loading	2.1	2.45×10^{-8}; 0,773	1.32×10^{-10}; 0,004	186.06
4	Loading	1.0	5.64×10^{-8}; 1,780	5.77×10^{-8}; 1,820	0.98
5	Loading	1.0	1.18×10^{-7}; 3,720	7.16×10^{-8}; 2,260	1.65
6	Loading	1.0	1.93×10^{-7}; 6,090	7.16×10^{-8}; 2,260	2.69
7	Unloading	4.0			
8	Loading	2.0	3.71×10^{-9}; 0,117	2.56×10^{-10}; 0,008	14.45
9	Loading	1.3	3.19×10^{-9}; 0,101	1.03×10^{-8}; 0,325	0.31
10	Loading	1.1	1.86×10^{-8}; 0,587	3.49×10^{-8}; 1,100	0.53
11	Loading	1.0	5.01×10^{-8}; 1,580	7.16×10^{-8}; 2,260	0.70
12	Loading	1.0	1.17×10^{-7}; 3,690	7.15×10^{-8}; 2,260	1.63

4.4 Discussion and conclusions IL tests

The results of both tests show that the reference model performs reasonably well for normally consolidated conditions (OCR=1): predicted and measured strain rates are of the same order of magnitude. However, for overconsolidated conditions (OCR > 1), the reference model systematically underestimates the creep strain rate significantly. The underestimation increases with increasing OCR. For test 1, differences of more than two orders of magnitude are found starting at OCR = 1.3; for test 1 such differences are found starting at OCR = 2.1. The significance of these difference for land subsidence is apparent for instance, for load step 9 in test 1, where the reference model would predict about 1 mm of subsidence for a 1 m thick layer per year, while the measured creep rate corresponds to a subsidence of about 150 mm per year for such a layer.

In steps 3 and 8 of both tests, similar over-consolidated OCR values of about 2 are reached; in step 3 during the first loading sequence, in step 8 upon reloading after the unloading step. In the reference model, the same OCR implies the same strain rate (same isotache). However, in the measurements the strain rate in step 8 is about one order of magnitude lower than the rate in step 3.

The IL tests show that unloading has an impact on the strain rate; the strain rate does decline upon unloading, with larger reduction for larger unloading steps. However, as discussed above, measured strain rates strongly exceed the predicted strain rates. This suggests that the IL data violates presumption 3, as defined in Chapter 3. A detailed explanation for this behaviour is found in the literature study, see Section 5.6. More detailed evaluation is presented in Chapter **Error! Reference source not found.**.

4.5 Results CRS tests

4.5.1 Pore pressures

The excess pore pressure profile which develops in a CRS test reflects the equilibrium between pressure dissipation by drainage and pressure enhancement by loading and compression. Higher strain rates induce larger pore pressures. Moreover, during the tests, permeability reduces due to a reduction in void ratio. This enhances pore pressure over the duration of the tests. Both effects can be recognized in the measurement data. For instance, test 6 uses a 100-fold larger displacement rate than test 9. The larger pore pressures in test 6 can be discerned by comparing the left panels of Figure 4.5 (test 6) and Figure 4.6 (test 9). In both figures, during test phases with constant strain rate, the rate of pore pressure increase tends to increase during the late stage of the test phase. This reflects the influence of permeability reduction during the phases.

Figure 4.7 displays the pore pressure and pore pressure ratio for all the tests. Large pore pressures are typically found in tests or test phases which contain a high displacement rate, 10.8 mm/h and 1.08 mm/h. Also, the acceleration in the last phases, to 0.108 mm/h, in tests 8 and 9 are clearly visible. The pore pressure ratio (right panels) shows a different pattern. At the start of the tests, when the total stress and pore pressure are both still low, the pore pressure ratio is high. However, the ratio drops rapidly for increasing displacements. For tests 8 and 9 the increase in displacement rate in the last phase raises the absolute pore pressure to high levels, pore pressure ratio remains at 0.1 for test 9 and 0.07 for test 8.

Buisman (1940, 1996) shows that the pore pressure field is sine-shaped when the dimensionless time factor T, $T = c_v\, t/h^2 > 0.36$. Following the Terzaghi solution to the consolidation problem (a.o. Verruijt, 2012) this is found when $\sigma_w / \sigma_b < 0.34$. Figure 4.7 shows that tests 6, 7b, 10 and 10b experience larger ratios and the correction might underestimate the average pore pressure in these tests.

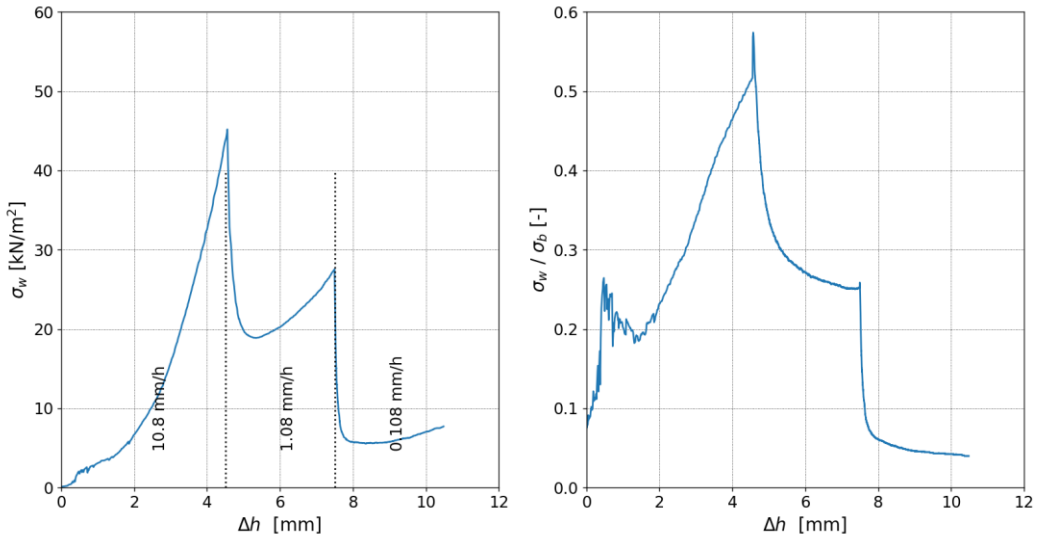

Figure 4.5 Pore pressure development Test 6. Left: absolute pore pressure. Right: ratio of pore pressure and total load. The applied displacement rates are given in the left graph.

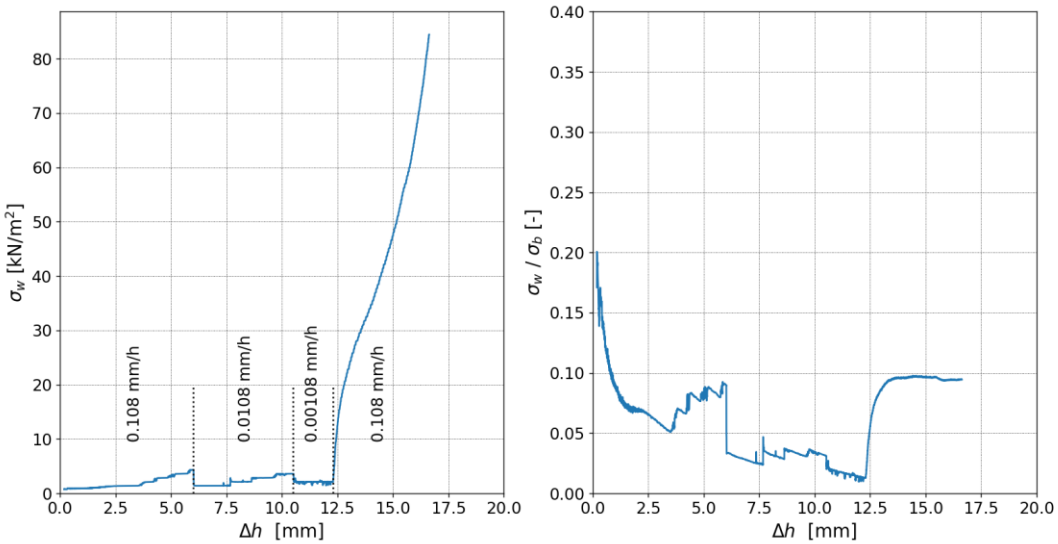

Figure 4.6 Pore pressure development in Test 9. Left: absolute pore pressure. Right: ratio of pore pressure and total load. The applied displacement rates are given in the left graph.

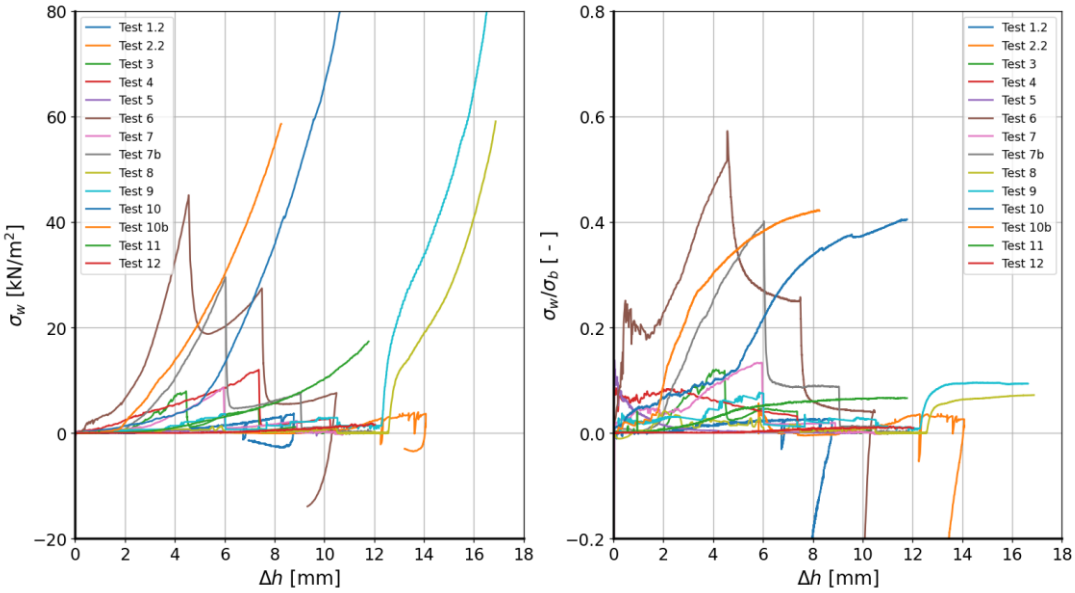

Figure 4.7, Pore pressure and pore pressure ratio in all tests.

4.5.2 Stress – strain representations

The impact of the excess pore pressure development on the stress strain curve is shown in Figure 4.8 for test 6 and in Figure 4.9 for test 9 (left panels). For test 9 the impact is small and virtually negligible, while for test 6 a considerable impact is found. The stress strain curve for the first loading phase rotates when changing from total stress to effective stress.

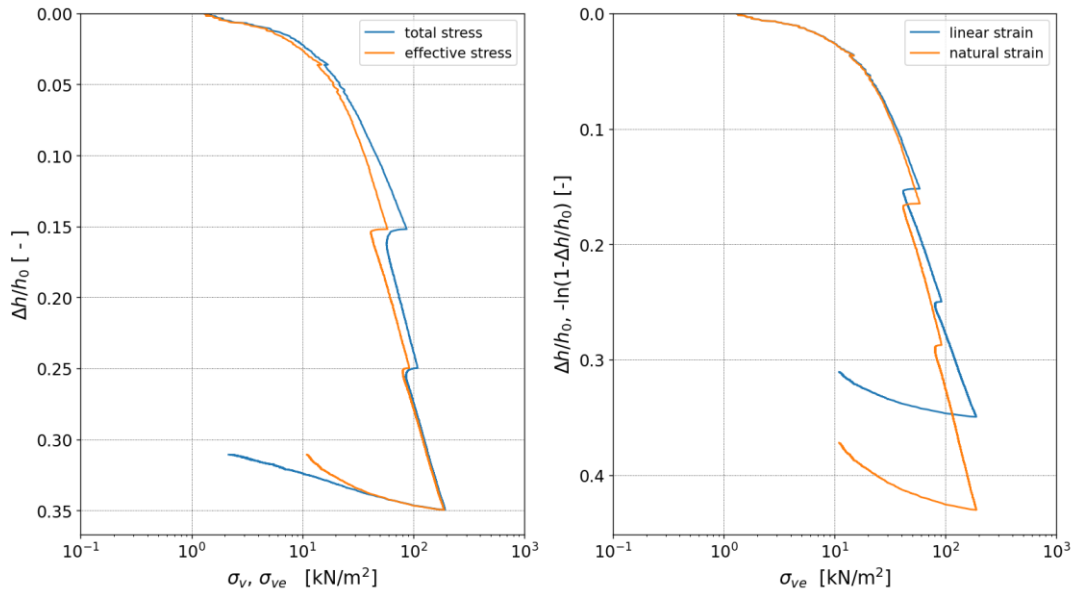

Figure 4.8 Stress – strain curve Test 6, Left: comparison between total stress – strain and effective stress – strain. Right: comparison between effective stress – linear strain and effective stress - natural strain, σ_{ve} = effective stress.

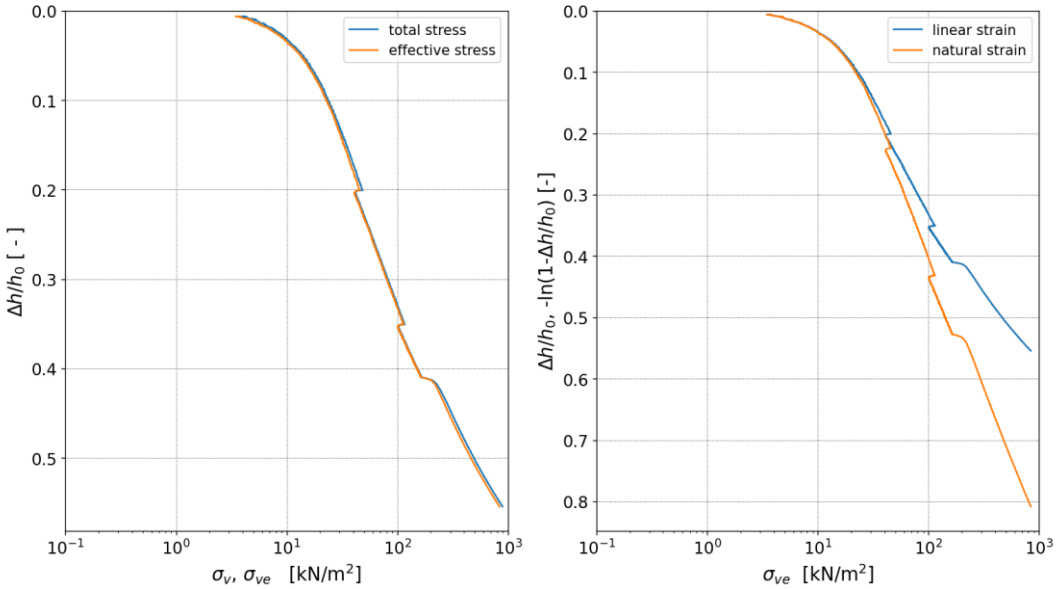

Figure 4.9 Stress – strain curve Test 9, Left: comparison between total stress – strain and effective stress – strain curve. Right: comparison between effective stress – linear strain and natural strain curve, σ_{ve} = effective stress.

The right panels of Figure 4.8 and Figure 4.9 display the results for linear and for natural strain. The effect of stiffening for larger strain – this is more pronounced for test 9 where larger strain is reached - is clearly visible in the bending of the curve for linear strain. As discussed in Section 2.2, the stress – linear strain relationship shows a stiffening effect for larger strain rates, which is absent when using the natural strain. The more linear trend of the curves for natural strain shows that natural strain better fits the reference implementation (presumption 1, Chapter 3). The effective stress – strain curves of all tests are provided in Appendix A both for linear and natural strain.

To provide insight in void ratio development and void ratio differences among samples and tests, Figure 4.10 displays the effective stress – void ratio curves for all tests. The behavior of test 4 and test 5 strongly deviates from observed in the other tests. At the moment of writing there is no clear explanation for this difference. Tests 4 and 5 are omitted from further analysis.

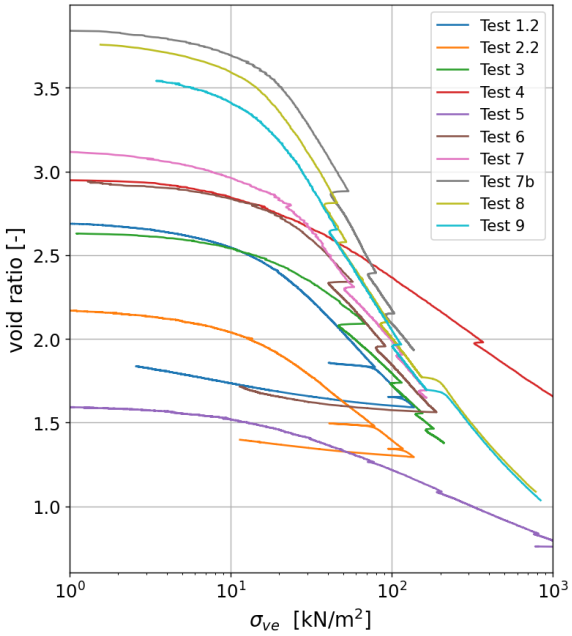

Figure 4.10 Overview of effective stress – void ratio curves.

4.5.3 (Non)linearity of isotachs (presumption 1)

Figure 4.11 and Figure 4.12 show example results of the fitting and parameter estimation for test 9 for linear and natural strain, respectively. The graphical results of all tests are provided in Appendix A. Table 4-16 tabulates the inferred parameter values.

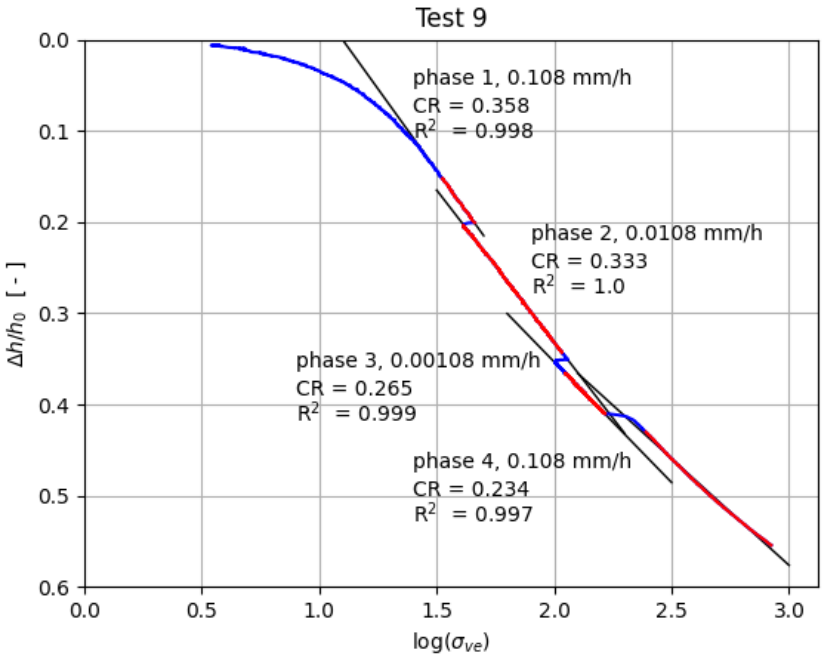

Figure 4.11 Stress – strain curve test 9, based on the logarithm of vertical effective stress, blue represents the measurement data, red the measurement data used for curve fitting, black the best fit for each of the phases. The slope of the lines represents the compression ratio CR, R^2 the weighted least squares sum of the corresponding fit.

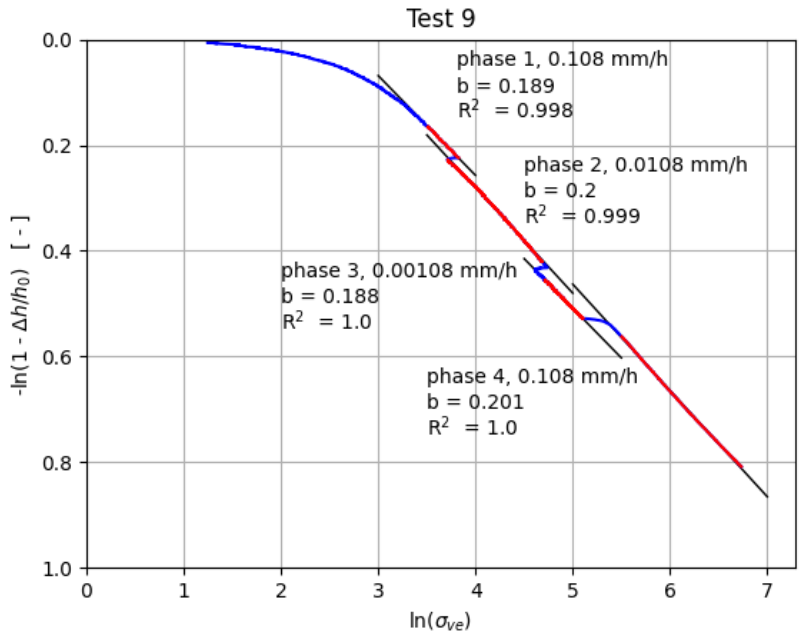

Figure 4.12 Stress – strain curve test 9, based on the natural logarithm of vertical effective stress and natural strain, blue represents the measurement data, red the measurement data used for curve fitting, black the best fit for each of te phases. The slope of the lines represents the compression ratio b, R^2 the weighted least squares sum of the corresponding fit.

Table 4-16 Results of fits of the individual test phases, CR represents the compression ratio for linear strain, b compression ratio for natural strain.

Test nr	Phase	Displacement rate [mm/h]	CR [-]	b [-]
3	1	10.8	0.250	0.127
	2	1.08	0.258	0.146
	3	0.108	0.244	0.148
	4	0.0108	0.219	0.138
	5	0.00108	0.176	0.115
4	1	10.8	0.172	0.092
	2	1.08	0.164	0.101
	3	0.108	0.132	0.088
	4	0.0108	0.102	0.070
5	1	0.108	0.165	0.088
	2	0.0108	0.148	0.089
	3	0.00108	0.141	0.090
6	1	10.8	0.256	0.128
	2	1.08	0.284	0.157
	3	0.108	0.264	0.167
7	1	1.08	0.335	0.174
	2	0.108	0.293	0.177
	3	0.0108	0.270	0.175
	4	0.00108	0.197	0.133

7B	1	1.08	0.328	0.173
	2	0.108	0.374	0.223
	3	0.0108	0.291	0.190
	4	0.00108	0.247	0.175
8	1	1.08	0.353	0.186
	2	0.108	0.336	0.189
	3	0.0108	0.313	0.195
	4	0.00108	0.267	0.192
	5	0.108	0.218	0.196
9	1	0.108	0.358	0.189
	2	0.0108	0.333	0.200
	3	0.00108	0.265	0.188
	4	0.108	0.234	0.201
10	-	1.06	0.288	0.167
10B	-	1.06	0.312	0.187
11	-	0.106	0.307	0.180
12	-	0.0108	0.346	0.185

4.5.4 (Non)constancy of isotach spacing (presumption 2)

From the test data discussed in the sections above, the distances between the isotachs can be derived. Figure 4.13 gives a definition sketch and shows the application to Test 6. The horizontal distance follows from the increment in logarithm of vertical effective stress due to a change in strain rate. The distance between the isotachs in vertical direction is expressed in $\Delta\varepsilon$ and can be derived from the horizontal distance and the isotach slope. In the right graph of Figure 4.13, the measurement data is given by the blue and red line. The red line represents the measurement data that is used for fitting the isotachs. Since the transitions to a new displacement rate introduces some curvature in the measurement data, the horizontal distance between the isotachs is not derived directly from the measurement data. Instead, the fits are used to calculate the horizontal distance between the isotachs. It should be noted that fits are focussed on the end of each phase.

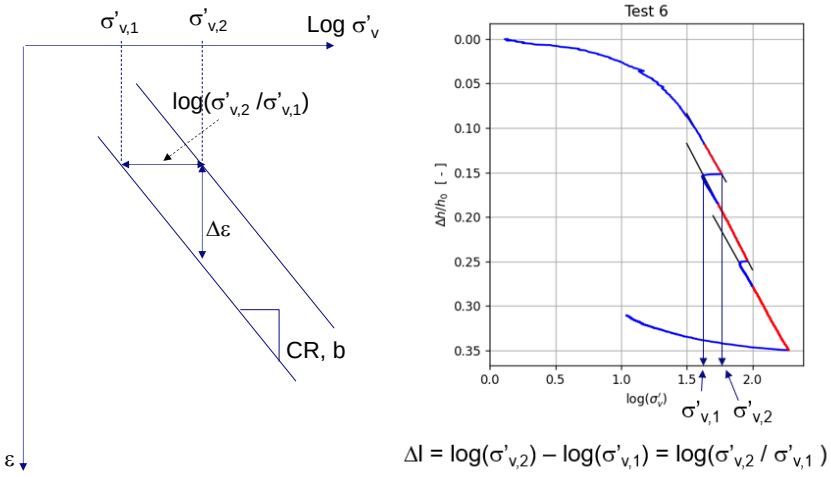

Figure 4.13 Distance between the isotachs, horizontal distance given by log($\sigma'_{v,1}$ / $\sigma'_{v,2}$, vertical distance indicated by $\Delta\varepsilon$, Left; definition sketch, right: results of test 6, blue and red lines measurement data, red lines measurement data used to fit isotachs, black lines represent the best fits.

Table 4-17 and Table 4-18 provide values for the horizontal spacing of isotachs found in the tests based on natural strain and linear strain, respectively. The spacing is listed for a 10-fold change of displacement rate. Table 4-19 includes the additional results of the inferred vertical spacing. The compression ratios and constants are also listed. A discussion of the results is given in Section 4.6.

Table 4-17, Horizontal isotach distance, ln(σ_{v1} / σ_{v2}) between isotachs based on natural strain.

Test nr	10 – 1 [mm/h]	1 – 0.1 [mm/h]	0.1 – 0.01 [mm/h]	0.01 – 0.001 [mm/h]	0.001 – 0.1 [mm/h]
3	0.256	0.138	0.105	0.154	
6	0.316	0.149			
7b		0.226	0.127	0.135	
8		0.206	0.123	0.122	0.170 (0.20)[a]
9			0.108	0.168	0.219

[a] = Values between brackets are visually obtained; other values follow from curve fitting

Table 4-18, Horizontal isotach distance, log(σ_{v1} / σ_{v2}) between isotachs based on linear strain.

Test nr	10 – 1 [mm/h]	1 – 0.1 [mm/h]	0.1 – 0.01 [mm/h]	0.01 – 0.001 [mm/h]	0.001 – 0.1 [mm/h]
3	0.128	0.063	0.046	0.067	
6	0.145	0.073			
7b		0.105	0.057	0.061	
8		0.090	0.058	0.055	0.043 (0.10)[a]
9			0.053	0.067	0.077 (0.10)[a]

[a] = Values between brackets are visually obtained; other values follow from curve fitting

Table 4-19, Horizontal and vertical isotach distance, $\Delta\varepsilon$.

Test nr	phase	*b*	ln($\sigma_{v,2}/\sigma_{v,1}$)	Δε	*CR*	log($\sigma_{v,2}/\sigma_{v,1}$)	Δε
3	1	0.127	0.256	0.032	0.25	0.128	0.032
	2	0.146	0.138	0.020	0.258	0.063	0.016
	3	0.148	0.105	0.016	0.244	0.046	0.011
	4	0.138	0.154	0.021	0.219	0.067	0.015
	5	0.115			0.176		
6	1	0.128	0.316	0.040	0.256	0.145	0.037
	2	0.157	0.149	0.023	0.284	0.073	0.021
	3	0.167			0.264		
7b	1	0.173	0.226	0.039	0.328	0.105	0.035
	2	0.223	0.127	0.028	0.374	0.057	0.021
	3	0.19	0.135	0.026	0.291	0.061	0.018

	4	0.175			0.247		
8	1	0.186	0.206	0.038	0.353	0.090	0.032
	2	0.189	0.123	0.023	0.336	0.058	0.019
	3	0.195	0.122	0.024	0.313	0.055	0.017
	4	0.192	0.170	0.033	0.267	0.043	0.012
	5	0.196			0.218		
9	1	0.189	0.108	0.020	0.358	0.053	0.019
	2	0.2	0.168	0.034	0.333	0.067	0.022
	3	0.188	0.219	0.041	0.265	0.077	0.020
	4	0.201			0.234		

4.6 Discussion and conclusions CRS tests

Practical limitations reduce the range of strain rates that can be applied in the tests. The lower limit of applicable strain rates follows from device specifications and test duration, while for high strain rates, the generation of pore pressure restricts applicable strain rates. These conditions resulted in a range of optional strain rates between 1×10^{-4} 1/s tot 1×10^{-8} 1/s.

Figure 4.10 shows that although the aim of the research is to study the impact of small load increments, the succession of the applied strain rates results in large deformation. Due to large deformation, the slope of the isotach on a linear strain scale is non-constant, as explained in Section 2.2. Using natural strain results in a constant isotach slopes, which facilitates comparison of test results.

Table 4-17 and Table 4-18 show the values for the inter-isotach horizontal distances obtained from the test results. Table 4-19 provides the vertical inter-isotach distances. If the soil behaviour corresponds to the reference implementation, Chapter 2, the isotachs are equi-distanced and the presented values should be the same. Moreover, the $\Delta\varepsilon$ - values presented in Table 4-19 would represent the creep parameter C_α or c.

Since $\Delta\varepsilon$ in Table 4-19 is derived from $\ln(\sigma_1 / \sigma_2)$ and $\log(\sigma_1 / \sigma_2)$ in Table 4-17 and Table 4-18, the tables give practically the same information as Table 4-19. Table 4-17 and Table 4-18 seem to indicate a decline in the isotach distance with decreasing strain rate. The values for $\ln(\sigma_1 / \sigma_2)$ and $\log(\sigma_1 / \sigma_2)$ when moving from 10.8 mm/h (1×10^{-4} 1/s) to 1.08 mm/h (1×10^{-5} 1/s) is approximately double the value for $\ln(\sigma_1 / \sigma_2)$ and $\log(\sigma_1 / \sigma_2)$ when shifting from 1.08 mm/h (1×10^{-5} 1/s) to 0.108 mm/h (1×10^{-6} 1/s). A further reduction in $\ln(\sigma_1 / \sigma_2)$ and $\log(\sigma_1 / \sigma_2)$ is found when shifting from 0.108 mm/h (1×10^{-6} 1/s) to 0.0108 mm/h (1×10^{-7} 1/s). However, a further reduction in applied displacement rate, from 0.0108 mm/h (1×10^{-7} 1/s) to 0.00108 mm/h (1×10^{-8} 1/s) does not further reduce $\ln(\sigma_1 / \sigma_2)$ and $\log(\sigma_1 / \sigma_2)$. Instead, several tests even show an increase.

The 100-fold acceleration at the end of tests 8 and 9, which increases the applied displacement rate from 0.00108 mm/h (1×10^{-8} 1/s) to 0.108 mm/h (1×10^{-6} 1/s) moves the stress strain curve to the right. The corresponding horizontal displacement should be equal to the sum of the horizontal shifts from 0.108 mm/h to 0.0108 mm/h and 0.0108 mm/h to 0.00108 mm/h. As shown by Figure A. 11 and Figure A. 13 the stress – strain curve based on linear strain shows a curvature when reaching large strain. The layer thickness effect explains this effect.

Using the linear fits will result in an underestimation of the horizontal distance between the isotachs. Therefore, Table 4-18 provides an alternative, visually estimated value, in brackets.

The analysis based on natural strain overcomes the disturbance due to layer thickness effect. However, the stress – natural strain curve shows a minor overshoot when adjusting to the new isotach after the acceleration, see Figure A. 12 and Figure A. 14. Again, the use of linear fits underestimate the actual observed shift upon acceleration and visually assessed values for $\ln(\sigma_1 / \sigma_2)$ are given in brackets in Table 4-18.

For both linear strain and natural strain the shift to the right, given in brackets, due to acceleration at the end of the tests 8 and 9 agrees with the summation of the shift in the two previous steps in the test.

For high displacement rates, 10 – 1 mm/h, the values for $\log(\sigma_1 / \sigma_2)$ and $\ln(\sigma_1 / \sigma_2)$ are larger then found for the other increments in displacement rate. This is found for tests 3 and 6 in which the values of $\log(\sigma_1 / \sigma_2)$ and $\ln(\sigma_1 / \sigma_2)$ for the displacement rate reduction 10 – 1 mm/h, are twice or even more the values found at a displacement reduction 1 – 0.1 mm/h. This difference might be explained or partly explained by the correction for the pore pressure reduction for high displacement rates, see Figure 4.5 and Figure 4.7.

Despite the possibility of an incorrect correction for excess pore pressure at high strain rates, the values for $\log(\sigma_1 / \sigma_2)$ and $\ln(\sigma_1 / \sigma_2)$ for a reduction in strain rate from 1 – 0.1 mm/h is consistently larger than the values found for displacement rate reduction 0.1 – 0.01 mm/h.

Regarding the inter-isotach distance, the data don’t show a clear trend. At large displacements rates, 10 – 0.1 mm/h, a reduction in isotach distance with reducing displacement rate is found. However, at low displacement rates, 0.1 – 0.001 mm/h, the isotach distance seems constant.

5 Literature study

5.1 Introduction

This chapter presents the findings from literature study that are deemed relevant for settlement due to small load increments. The presentation addresses the recent developments in the application of the isotach framework for settlement predictions. However, this presentation is not strictly tied to the 3 presumptions introduced in Chapter 3. The evaluation of the presumptions with literature study (Chapter 5) and the conducted laboratory tests (Chapter 4) is included in the integral discussion in Chapter 6.

In literature different approaches are used when relating strain to stress and time. These different approaches are not always clearly indicated in the different papers. However, they are important when comparing either laboratory results, or different constitutive expressions or parameter definitions. Therefore, different approaches are introduced here first.

Typically, constitutive models express the strain of a soil element, induced by external loading by a summation of the elastic, or direct strain, and plastic, or visco-plastic strain, see Equation (5.1):

$$\varepsilon = \varepsilon^d + \varepsilon^p \tag{5.1}$$

In which:

ε, ε^d, ε^p = strain, direct strain and plastic strain respectively

Two different approaches are used in division of total strain in a direct and visco-plastic component and corresponding definition of the compression ratio, *CR*. In approach 1, (e.g. Yuan & Whittle, 2018 or Watabe et al., 2012) the compression ratio, *CR* is directly related to the visco-plastic strain, Equation (5.2).

$$\varepsilon^p = CR \log\left(\frac{\sigma'_{v,u}}{\sigma'_{vy}}\right) + C_\alpha \log\left(\frac{\tau}{\tau_0}\right) \tag{5.2}$$

In which:

CR = Compression ratio for normally consolidated behaviour.

$\sigma'_{v,u}$ = Vertical effective stress after consolidation.

σ'_{vy} = Yield stress.

τ = Intrinsic time.

τ_0 = Reference intrinsic time, typically, τ_0 = 1 day.

Consequently, to derive the value for the compression ratio from laboratory tests, the measured total strain needs to be corrected for the direct strain, according to Equation (5.1), which can only be estimated numerically.

In approach 2, (e.g. Den Haan, 1992, 1999), the compression ratios are related to total strain. Consequently, the expression for the visco-plastic strain component turns into:

$$\varepsilon^p = (CR - RR) \log\left(\frac{\sigma'_{v,u}}{\sigma'_{vy}}\right) + C_\alpha \log\left(\frac{\tau}{\tau_0}\right) \tag{5.3}$$

With:

RR = Re-compression ratio.

When applied correctly, calculated settlement using these equations should provide the same result. However, since the numerical value for *CR* differs, the two approaches should not be mixed. The different approaches have some consequences in the mathematical derivation of the models. Where relevant, these distinctions are indicated in the various sections of this chapter.

Since experimental data only produces total strain the visco-plastic strain can only be derived from experiments when subtracting the direct strain from the measurement data. Also, the direct strain is not measured directly. Instead, it is typically estimated from the recompression ratio, *RR* or recompression index, C_r. Tsutsumi & Tanaka (2011) illustrate the difficulty encountered when using approach 1. For most soils, the unloading – reloading loop results in a hysteresis in the stress strain curve. Consequently, the reloading stiffness is not uniquely defined and typically reloading stiffness for small unloading is higher than found for larger unloading. Tsutsumi & Takani (2011) determine the unloading stiffness C_r at 20% and 80% stress reduction and conclude that in the assessment of visco – plastic strain, the influence of using the different C_r values is small.

Although many scientific papers use approach 1, authors rarely explain how ε^p was derived from total strain, ε. It should be noted that the reference implementation, as explained in the Chapter 2, uses approach 2.

5.2 Spacing isotachs

In modelling soil behaviour, the vertical distance between the isotachs follows from the creep law. A logarithmic time – creep relation gives a constant distance between the isotachs representing a ten-fold reduction in creep strain rate, as shown by Figure 5.2. The use of non-logarithmic creep laws might result in a non-constant spacing of the isotachs.

Leroueil et al. (1985) show experimental data of the position of the isotachs for Batiscan clay. The isotachs follow from Constant Rate of Strain tests conducted at different strain rates ranging from 1.43×10^{-5} 1/s to 1.68×10^{-8} 1/s. The isotachs run mainly parallel to each other except for the lowest strain rate, the dotted line in Figure 5.1. The deviation of this isotach is attributed to thixotropic hardening, but not further explained.

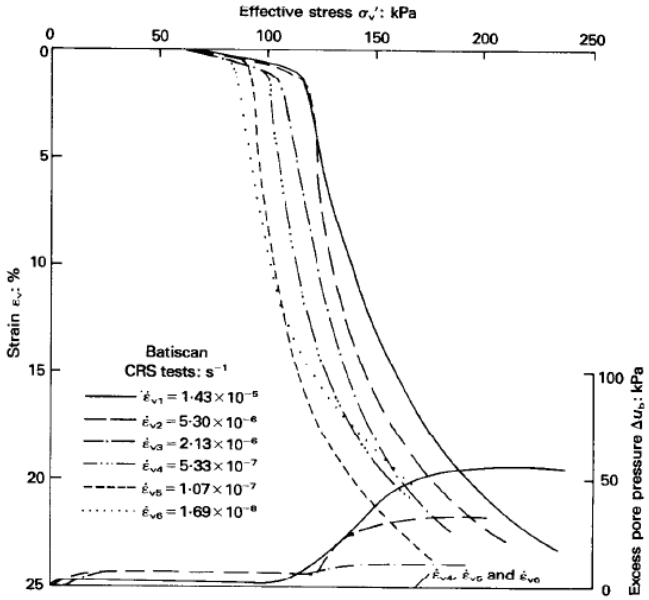

Figure 5.1 Constant Rate of Strain tests on Batiscan clay, total strain on vertical axis, Leroueil et al. (1985).

Typically, in laboratory testing, the yield stress is obtained from the intersection of the re-loading curve and the one – day compression line or the reference isotach. CRS testing uses a constant displacement rate, which might deviate from the strain rate found at the one-day compression line obtained in IL testing. When applying a strain rate below the reference strain rate, a lower yield stress, σ'_{vy} will be found, see Figure 5.2. The ratio of yield stress at lower strain rate and the yield stress at the reference strain rate depends on the isotach spacing.

Leroueil (2006) discusses the rate dependency of the yield stress. When plotting the plastic strain, ε^p - log(σ'_v), the yield stress is found at the intersection of the one-day compression line with the horizontal axis. In constant rate of strain, CRS, testing, different displacement rates can be applied and the stress – strain conditions can follow different isotachs. Each of these isotachs cross the horizontal axis at a different stress level, resulting in different yield stresses for the different isotachs. Figure 5.3 shows the isotach field based on plastic strain. It should be noted that the isotachs in Figure 5.3 have a different slope than the isotachs in Figure 5.2, which are plotted using total strain.

Following Equation (2.3), the one-day creep strain rate follows from $d\varepsilon_s / d\tau = C_\alpha / 2.3$. Several authors apply a reference strain rate at 1.0×10^{-7} 1/s (Watabe et al. 2012, Watabe & Leroueil, 2015). This corresponds to Equation (2.3) when $C_\alpha = 0.02$.

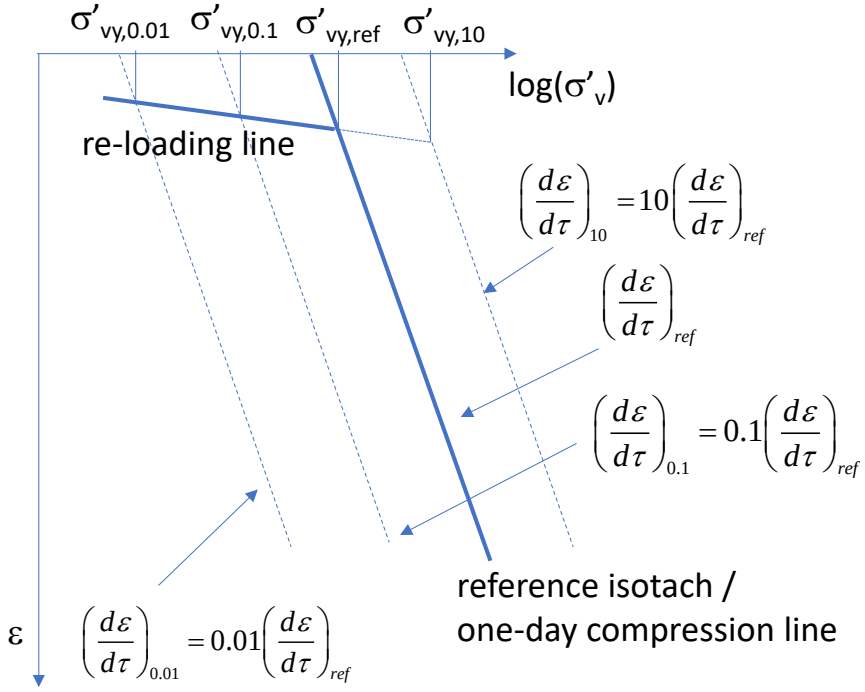

Figure 5.2 Sketch isotachs for different strain rates and corresponding differences in yield stress, using total strain.

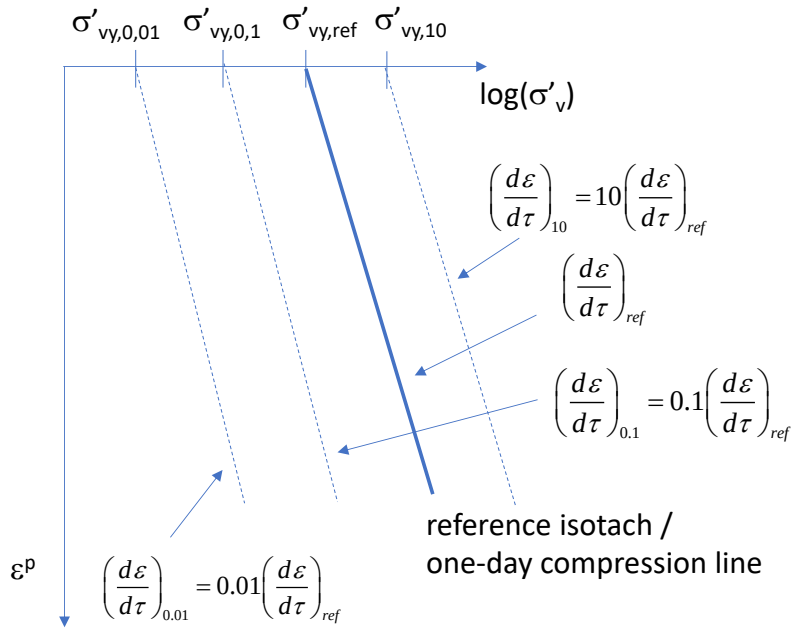

Figure 5.3 Sketch isotachs for different strain rates and corresponding differences in yield stress, based on plastic strain, ε^p

The strain rate dependency of the yield stress follows from numerical formulation of the isotach model, as discussed by a.o. Den Haan (1992, 1999), Visschedijk (2010). The creep strain rate is found by differentiating of the creep law:

$$\varepsilon = C_\alpha \log\left(\frac{\tau}{\tau_0}\right); \quad \frac{d\varepsilon}{d\tau} = \frac{1}{\ln(10)}\frac{C_\alpha}{\tau} \tag{5.4}$$

Consequently, the ratio of different strain rates is the reciprocal of the corresponding intrinsic times:

$$\frac{\left(d\varepsilon/d\tau\right)_1}{\left(d\varepsilon/d\tau\right)_2} = \frac{\tau_2}{\tau_1}$$

Den Haan & Sellmeier (2000), and Visschedijk (2010) discuss the relation between intrinsic time and (yield) stress changes:

$$\tau_2 = \tau_1\left(\frac{\sigma'_{vy,1}}{\sigma'_{vy,2}}\right)^m, m = \frac{CR - RR}{C_\alpha}, \quad \log\left(\frac{\tau_2}{\tau_1}\right) = m\log\left(\frac{\sigma'_{vy,1}}{\sigma'_{vy,2}}\right) \tag{5.5}$$

It should be noted that in the formulation above CR is related to total strain, approach 2 as explained in Section 5.1. When applying approach 1, in which the compression index CR is related to the visco plastic strain, *m* in Equation (5.5) is reduced to *m* = CR/C_α.

When plotting the ratio ($\sigma'_{vy,1}$ / $\sigma'_{vy,1}$) versus dε/d*t* in a double logarithmic graph, a line with slope 1/*m* is to be expected. Figure 5.4 shows Figure 18 from Leroueil (2006). For different laboratory and field data, the relation between yield stress and strain rate is shown. The solid line has a slope α which corresponds to 1/*m*. Despite the scatter, it is concluded in Leroueil (2006) that measurement data deviate from the straight line with slope α or 1/*m*. The consequence of this conclusion is that the measurement data seem to indicate that the isotachs are not equidistant. Instead, the isotachs seem to get closer to each other at low strain rates and have larger distances at higher strain rates.

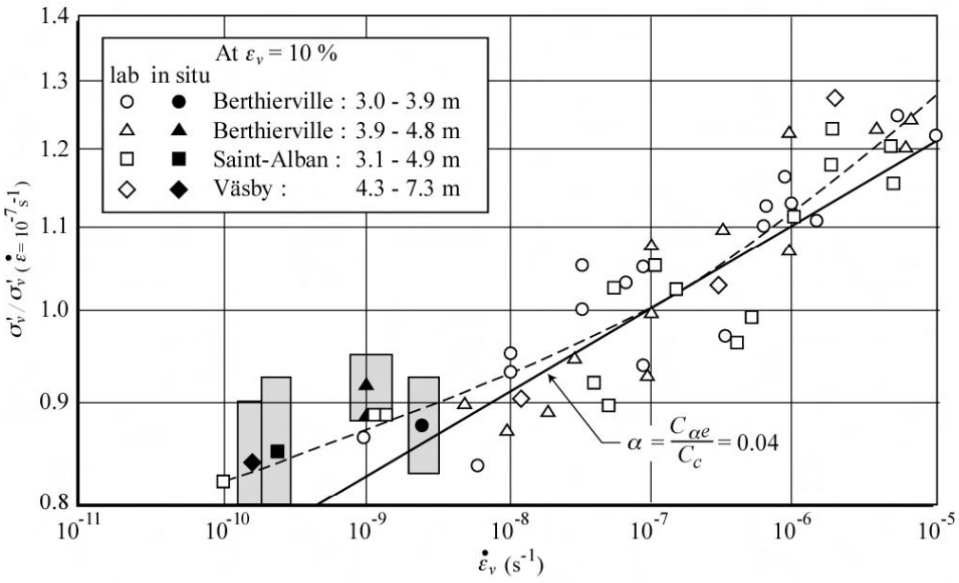

Figure 5.4 Relation between strain rate and yield stress, from: Leroueil, 2006

Leroueil (2006), Watabe et al. (2008), Watabe et al. (2012), Watabe and Leroueil (2015) use the strain rate dependency of yield stress to normalize stress – strain curves for different soil types. Normalizing the reference compression curve by the yield stress related to the reference compression curve, results in a (ε_{vp} – log(σ'_v / σ'_{vy}) curve, see Figure 5.5.

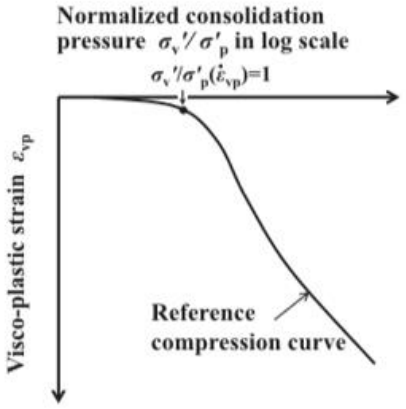

Figure 5.5. Reference compression curve (ε_{vp} – log(σ'_v / σ'_{vy}) curve, after Watabe & Leroueil 2015 σ'_p = yield stress, σ'_{vy}.

The Watabe model (Watabe et al.,2012), uses the relation between the yield stress, σ'_{vy}, and strain rate, given by:

$$\ln \frac{\sigma'_{vy} - \sigma'_{vy,L}}{\sigma'_{vy,L}} = c_1 + c_2 \cdot \ln \dot{\varepsilon}_{vp} \qquad (5.6)$$

Where:

c_1 = $\ln((\sigma'_{vy} - \sigma'_{vy,L})/\sigma'_{vy,})$ at $d\varepsilon_{vp} / dt$ = 1 [1/s].
c_2 = Strain rate dependency.
$\sigma'_{vy,L}$ = Lower limit of $\sigma'_{vy,}$ for $d\varepsilon_{vp} / dt$ = 0.

Watabe et al. (2012) and Watabe & Leroueil (2015) refer to the parameters, c_1, c_2 and $\sigma'_{vy,L}$ as isotach parameters.
It should be noted that by introducing a lower limit for the yield stress, $\sigma'_{vy,L}$, the concept of a zero-strain isotach is accepted. The zero strain isotach is further discussed in Section 5.3.

With σ'_v / σ'_p = f(ε_{vp}) and Equation (5.6), the compressibility of the soil is described by the reference compression curve and the three isotach parameters (c_1, c_2 and $\sigma'_{vy,L}$). For worldwide inorganic clays the authors suggest using a value of $\sigma'_{vy,L}/\sigma'_{vy,0}$ = 0.7, c_1 = 0.935 and c_2 = 0.107. In which, $\sigma'_{vy,0}$ is defined as the σ'_{vy} corresponding to a dε_{vp} / dt value of 1.0×10^{-7} s^{-1}, which is close to the average strain rate obtained in a 24-h incremental loading test. These values have been derived by applying the proposed method on the CRS test results of various clay samples. As can be seen in Figure 5.6 the log(σ'_{vy} / $\sigma'_{vy,o}$) – log(dε_{vp} / dt) relationship for worldwide clays can be adequately described by Equation (5.6) by applying the recommended isotach parameter values for c_1, c_2 and $\sigma'_{vy,L}$. The red line in this figure corresponds to the integrated curve as calculated based on Equation (5.6) for $\sigma'_{vy,L}$ / $\sigma'_{vy,0}$= 0.7, c_1 = 0.935 and c_2 = 0.107.

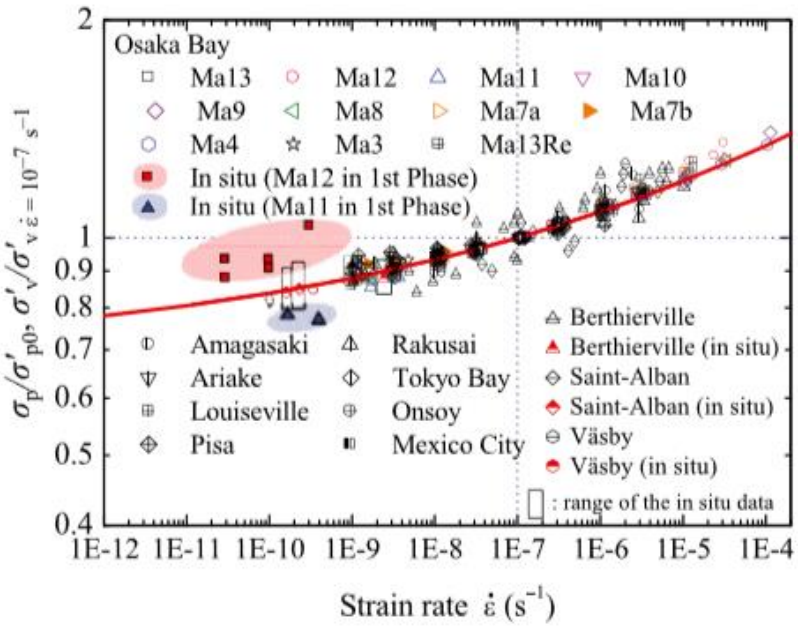

Figure 5.6. The log($\sigma'_{vy}/\sigma'_{vy,0}$) – log(d$\varepsilon_{vp}$ / dt) relationship for worldwide clays compared with the integrated fitting, curve obtained by Eq. (5.6) *with $\sigma'_{vy,L}/\sigma'_{vy,0}$=0.7, c_1=0.935 and c_2=0.107 (from: Watabe and Leroueil 2015).*

Leroueil (2006) explains the practical implications of the yield stress dependency on strain rate. Figure 5.7 shows some typical strain rates observed in laboratory testing and in situ. It is shown that the in-situ strain rates are significantly smaller than applied in laboratory testing. Figure 5.8 shows a comparison between stress – strain curves for laboratory and field conditions.

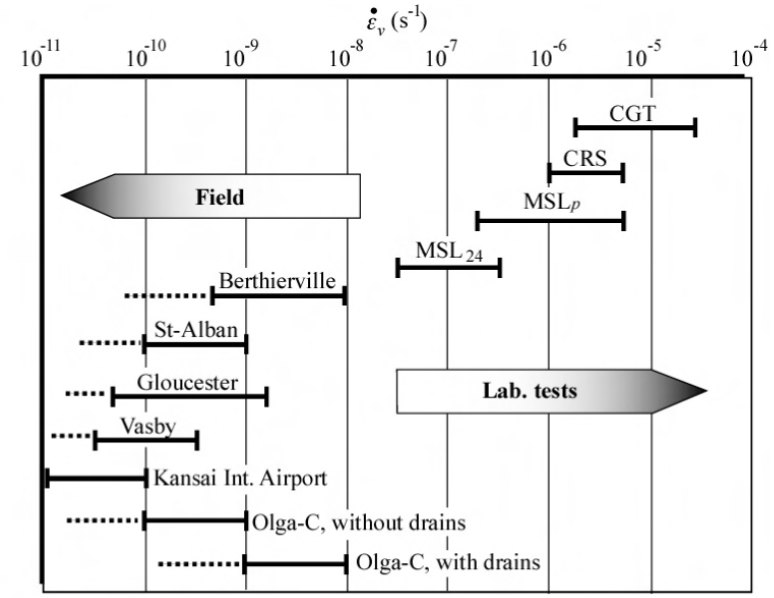

Figure 5.7 Difference in strain rate observed in laboratory testing and in situ, MSL_{24} = conventional 24h incremental loading oedometer test, MSL_p = oedometer test with loading at end of primary, CRS = constant rate of strain tests, CGT = controlled gradient tests, from: Leroueil (2006).

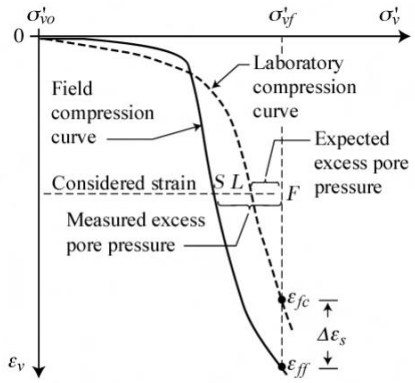

Figure 5.8 Typical compression curve in situ and in laboratory testing, from: Leroueil (2006).

To account for the difference in strain rate under field and laboratory conditions, the authors propose equations to predict settlement due to creep that will occur in the field in addition to the creep settlement obtained from laboratory tests. In engineering practice settlement behaviour is generally estimated based on the $e - \log \sigma'_v$ curve obtained from a 24-h incremental loading oedometer test, which corresponds to a strain rate of about 1.0x10^{-7} s^{-1}, see point D in Figure 5.9. The additional strain, creep strain corresponding to a strain smaller than 1.0x10^{-7} s^{-1}, in the field, represented by point F in Figure 5.9, can be calculated as a function of $C_c/(1+e_0)$ and in situ strain rate as follows:

$$\Delta\varepsilon_{Field} = \Delta\varepsilon_{D\to F} = \frac{C_C}{1+e_0} \cdot \log\left\{\frac{\sigma'_{p0}}{\sigma'_{pL}} \cdot \left[\frac{1}{1+\exp(c_1 + c_2 \ln \dot{\varepsilon}_{Field}}\right]\right\} \quad (5.7)$$

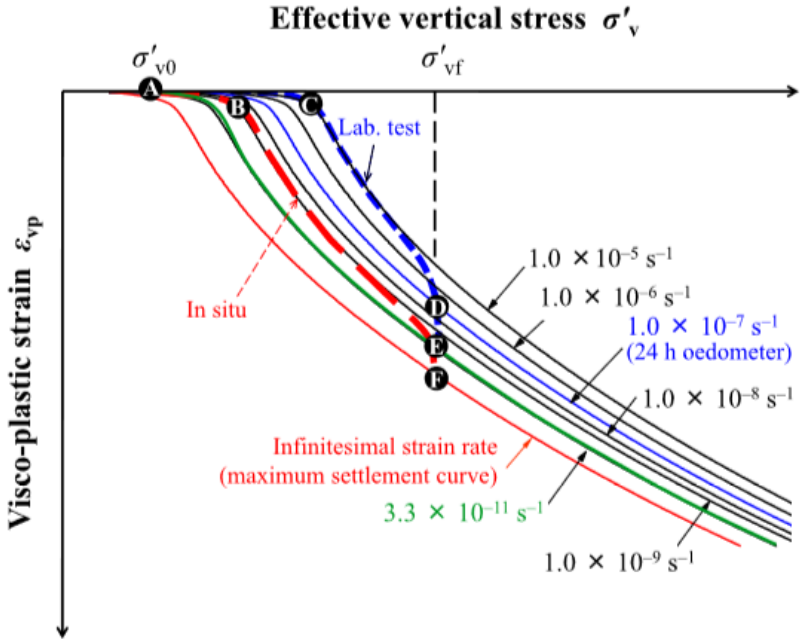

Figure 5.9. Schematic illustration of compression paths for oedometer tests in the laboratory and field behaviour (after: Watabe and Leroueil, 2015).

Equation (5.7) is charted in Figure 5.10.

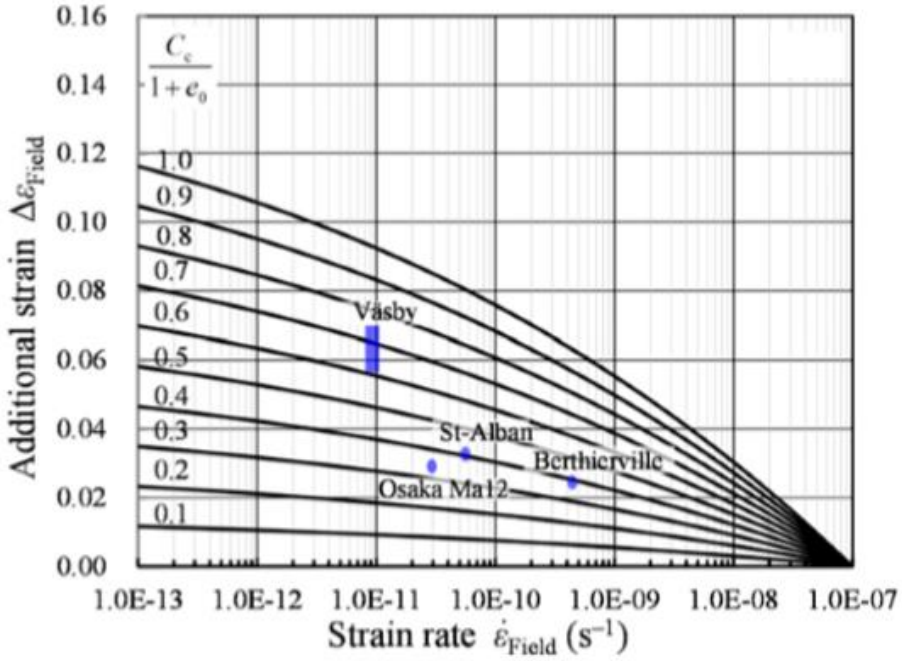

Figure 5.10. Additional strains in the field calculated as a function of Cc/1+e_0 and in situ strain rate (after: Watabe and Leroueil, 2015).

By accepting the presence of a zero strain rate ($\dot{\varepsilon} = 0$) the maximum additional creep strain experienced in the field is given by:

$$\Delta\varepsilon_{ult} = \Delta\varepsilon_{D\to F} = \frac{C_C}{1+e_0} \cdot \log \frac{\sigma'_{p0}}{\sigma'_{pL}} \tag{5.8}$$

This working procedure is summarized by Figure 5.11. A constant rate of strain, CRS, test is used to derive the normalized, reference compression curve. A long-term consolidation test, LT, is used to derive the strain rate development. The authors do not explain how yield stresses are derived. The authors do acknowledge the difficulty in acquiring the soil behaviour at low strain rates. With strain rates in the laboratory typically between 5×10^{-8} and 5×10^{-5} 1/s the ratio of $C\alpha/C_c$, α in Figure 5.4, Figure 5.6, and last graph in Figure 5.11, corresponds well to the values presented by Mesri et al (1995). The deviation of α from a constant $C\alpha/C_c$ manifest itself more clearly at lower strain rates.

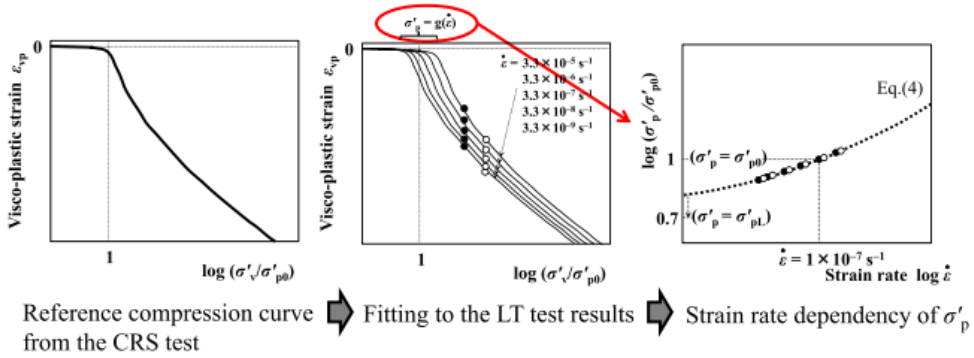

Figure 5.11 Illustration of the method to evaluate the strain rate dependency of yield stress σ'_{vy} from CRS and LT test rests, (from: Watabe & Leroueil, 2015).

5.3 The concept of zero strain rate isotach

The strain rate dependency of the yield stress, as discussed in the previous section results in the model assumption that there is an end to creep, a.o. Leroueil (2006), Watabe & Leroueil (2015). A condition which is represented by the zero strain rate isotach, found for $\sigma'_{vy} = \sigma'_{vy,L}$ in Equation (5.6).

Kawabe & Tatsuoka (2013) and others, provide a further exploration of the zero-strain rate isotach. Figure 5.12 shows the field of isotachs including a zero-strain rate isotach. Starting from the refence isotach, the mutual distance between the isotachs decreases for lower strain rates until the zero-strain rate isotach is reached.

There are basically two ways to reach the zero-strain rate isotach, as shown by Figure 5.12. The first is by development of creep strain, the red, vertical, line in Figure 5.12. The second is by unloading, the blue, horizontal, line in Figure 5.12. It should be noted that reaching the limit isotach in laboratory testing by following the red, vertical, line in Figure 5.12 requires long duration times of the tests and accurate measurements.

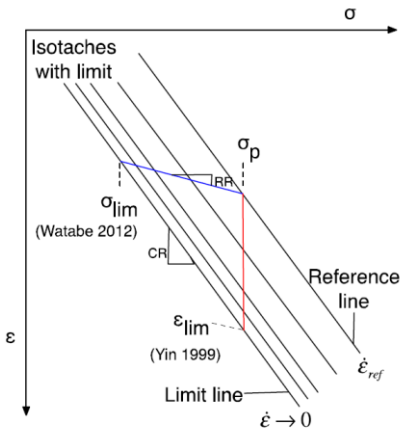

Figure 5.12 Isotachs with creep strain limit, from: Yuan & Whittle (2014).

Kawabe & Tatsuoka (2013) use unloading – reloading loops to establish the isotachs representing low strain rates. The basic rationale behind their way of thinking is represented by Figure 5.13. The strain and corresponding strain rates between the points B and C resemble strain and strain rates between the points B' and C'. Unloading from A to B brings the soil conditions directly at the start of BC, while sustained loading until B' is reached, might require considerable testing time and might not be feasible.

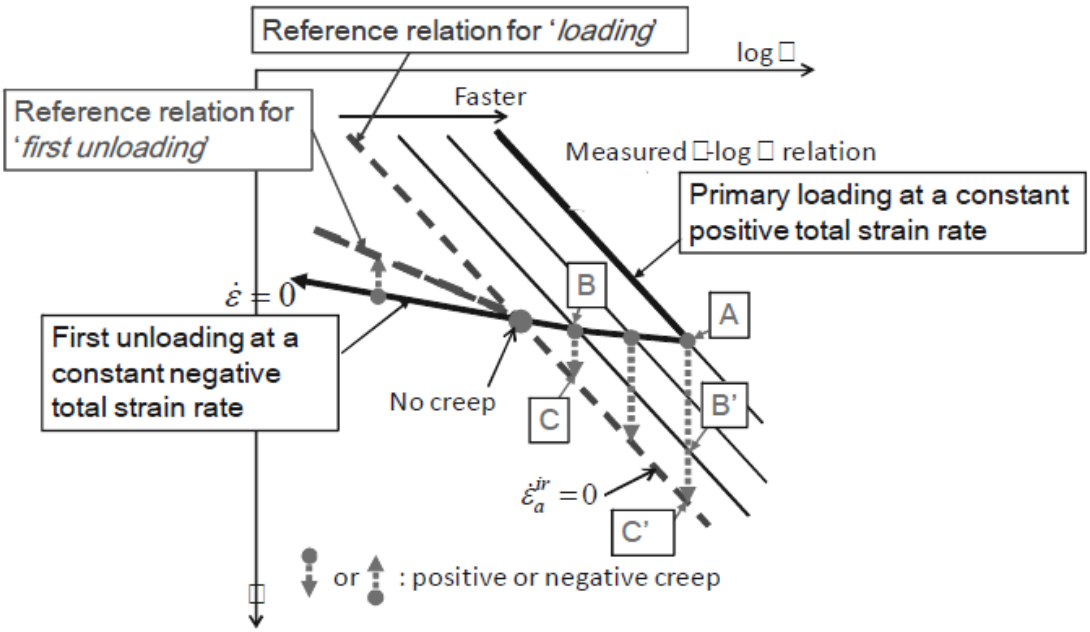

Figure 5.13 Definition of positive and negative creep, from: Kawabe & Tatsuoka, 2013.

In theory, starting from point A in Figure 5.13 unloading could be applied such that soil conditions reach the limit isotach and no creep develops. Kawabe & Tatsuoka (2013) introduce positive and negative creep. When soil is unloaded beyond the limit isotach negative creep develops representing a volume increase or a swelling of the ground level. In contrast, the positive creep represents a volume reduction or settlement of the ground level.

Figure 5.13 defines two limit isotachs referred to as reference relation in Figure 5.13. As long as creep strain rates remain positive the limit isotach is represented by the reference relation for loading.

When exceeding the reference relation for loading, for example due to unloading, negative creep strain and corresponding negative creep strain rates develop until the reference relation for first unloading is reached.

Figure 5.14 shows measurement data of an oedometer test on Fujinomori clay. The test includes loading until an axial stress of 600 kPa followed by sustained loading, SL1, a small unloading followed by sustained loading, SL2, large unloading until an axial strain of 300 kPa followed by sustained loading, SL3, a small reloading in combination to sustained loading, SL4 and finally large reloading. Figure 5.14a shows the stress strain curve. Figure 5.14b zooms in and shows the developed strain rates and corresponding isotachs by the dotted lines. The limit isotach or reference relation for loading is indicated by a continuous line. The graph shows a reduction in strain rate for the lower isotachs and a reduction in mutual distance between the isotachs. It is remarkable that the distance between the isotachs with a strain rate up to 1×10^{-7} 1/s are clearly larger than found for the isotachs with lower strain rates. Kawabe & Tatsuoka (2013) conclude: “The logarithm of creep strain rate decreases rather linearly with creep strain until the creep strain rate becomes a certain low value, followed by a drastic decrease toward zero”.

It should be noted that the strain rates up to 1×10^{-7} 1/s follow from the first sustained loading phase, SL1, while the lower strain rates follow from SL2, SL3 and SL4.

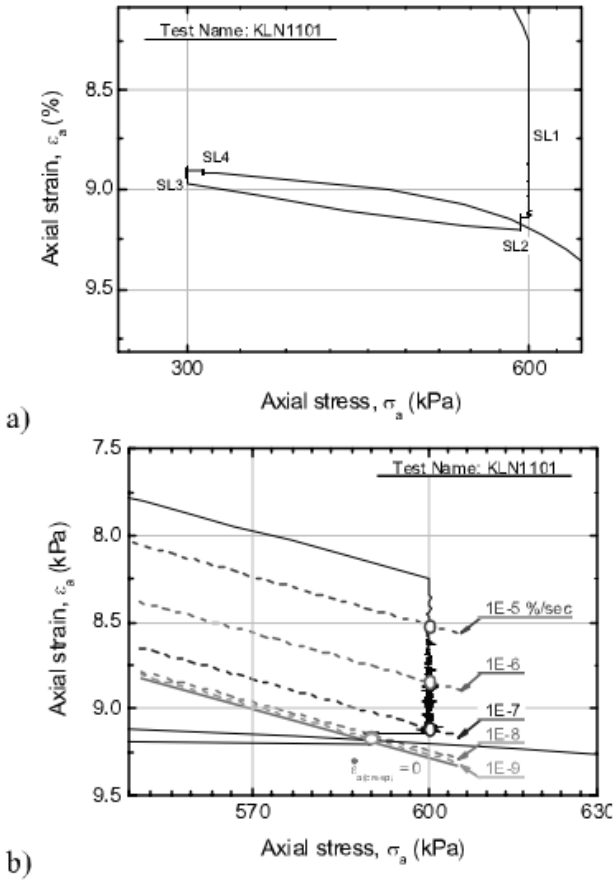

Figure 5.14 Creep rate development during a load cycle including phases of sustained loading, SL after: Kawabe & Tatsuoka, 2013.

Zwanenburg (2017) discusses a series of CRS tests conducted to test the limit isotach concept for peats.

The tests contained unloading followed by relaxation under constant height. The rationale behind application of the relaxation phase in CRS testing follows from swelling that would occur after unloading in conventional oedometer tests. During relaxation, the elastic and visco-plastic deformation is assumed to counterbalance each other and result in a zero-volume change. To avoid the problems in dividing the measured swell in an elastic and visco-plastic part, relaxation was applied rather than unloading. A reduction in vertical stress during relaxation, reflects a tendency for volume reduction and therefore positive creep, while a vertical stress increase reflects a tendency for volume increase and negative creep.

Figure 5.15 shows the results of 5 tests. The level of unloading is reflected in the presented OCR. For increasing OCR the effect of swell becomes more pronounced, however after reaching a peak, the vertical stress declines again indicating a volume reduction and therefore positive creep. In these tests no indication of a limit isotach was found for peats.

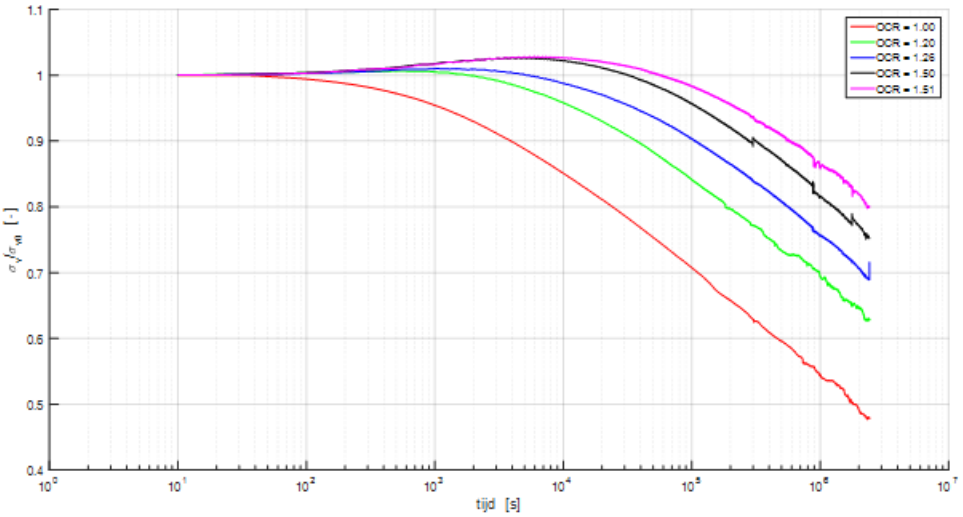

Figure 5.15 Development of vertical stress during a relaxation phase after unloading for different levels of unloading, from: Zwanenburg (2017).

It should be noted that the outcome of Figure 5.15 is consistent with the results presented by Samson (1985). Figure 5.16 shows measurements of the top of an embankment built on a peat foundation, using pre-loading. Removal of the pre-loading induces an immediate rebound followed by swell and finally settlement.

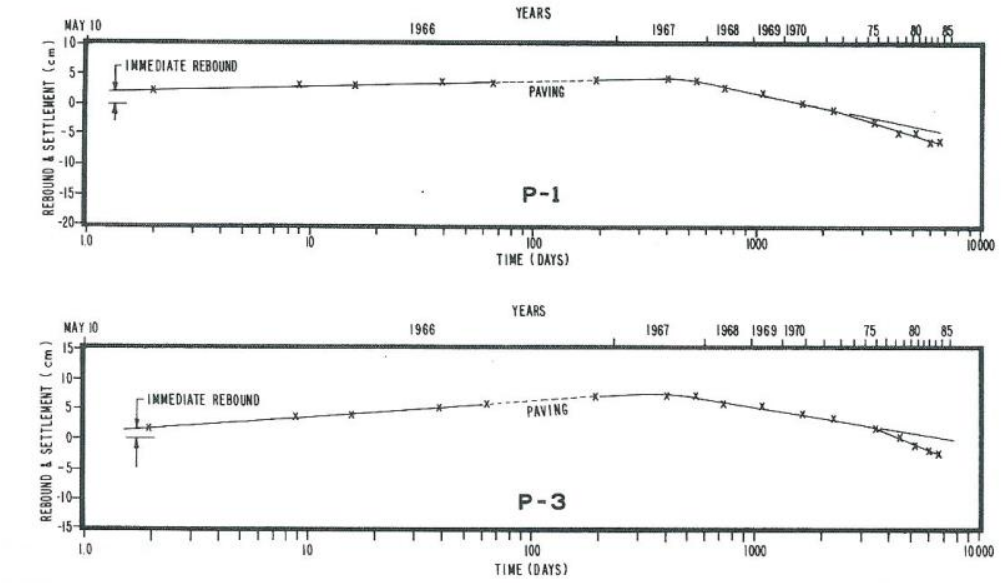

Figure 5.16 Rebound, swell and settlement of road construction using pre-loading, from: Samson (1985).

5.4 The MIT-SR model

Yuan and Whittle (2016) proposed an elasto-viscoplastic formulation for assessing the compression behaviour of clays in which the viscoplastic strain rate is attributed to an internal state variable. This variable represents the perturbation of clay particles due to the prior strain history**.** According to the authors, this formulation overcomes two basic drawbacks of existing isotach models. That is:

(i) Based on the existing isotach model the viscoplastic strain rate is uniquely defined by the state of vertical stress and void ratio. However, in the isotach model the adoption of a reference creep rate as obtained at laboratory scale will likely lead to an overestimation of the creep settlements at the end of primary consolidation. This is because the actual strain rate experienced in the field will be lower than the reference strain rate for the same vertical stress and void ratio applied in the laboratory. The overestimation of settlement due to creep is enhanced as the thickness of the clay layer encountered in the field increases and the time required to reach the end of primary consolidation increases. In the elasto-viscoplastic formulation proposed by Yuan and Whittle (2016) the visco-plastic strain rate is not considered as a function of the vertical stress and void ratio but a function of an internal strain rate, R_a.

(ii) Ladd et al. (1977) frames the hypothesis A and B concepts when it comes to typical observations in settlement behaviour. The isotach model conforms to a Hypothesis B behaviour. Although it is well demonstrated in the literature that the measured time – dependent compressibility of clays agrees very well with creep Hypothesis B behaviour (Degago et al., 2011) there are still laboratory and field data that support both Hypothesis A and B (Mesri, 2009; Choi, 1982). The newly introduced elasto-viscoplastic formulation by Yuan and Whittle (2016) is capable of simulating both hypothesis A and B.

In the proposed formulation, an internal strain rate variable, R_a (≥0), is introduced and the visco-plastic strain rate, $\dot{\varepsilon}_{vp}$, is calculated as follows:

$$\dot{\varepsilon}_{vp} = R_a \cdot \left(\frac{\sigma'_v}{\sigma'_p}\right) \tag{5.9}$$

Where:
σ'_v = The vertical effective stress.
σ'_p = Reference stress state defined in the log(e) – log(σ'_v) space.

The internal strain rate dR_a/dt can be calculated considering a function of the total strain rate, f(dε/dt) and a transient coefficient, m_t:

$$\dot{R}_a = \left[f(\dot{\varepsilon}) - R_a \right] \cdot m_t \tag{5.10}$$

A schematic illustration of Equation (5.10) is given by Figure 5.17 which shows the evolution of R_a during CRS compression and relaxation.

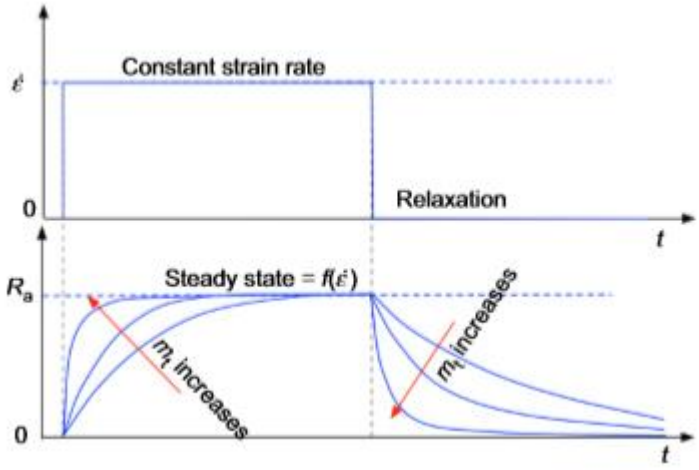

Figure 5.17 Influence of m_t on the evolution of R_a during CRS compression and relaxation (after: Yuan and Whittle, 2018).

The R_a – *value* converges to a steady state condition which is a function of the applied strain rate, f(dε/dt). At the steady state condition dR_a / dt in Equation (5.10) is 0, and f(dε/dt)=R_a. The function f(dε/dt) is defined for matching the normal consolidation characteristics in CRS tests. Consequently:

$$f(\dot{\varepsilon}) = R_a = \left(\frac{\rho_c - \rho_r}{\rho_c}\right) \cdot \dot{\varepsilon} \cdot \left(\frac{\dot{\varepsilon}}{\dot{\varepsilon}_{ref}}\right)^{-\beta} \tag{5.11}$$

And Equation (5.9) becomes:

$$\dot{\varepsilon}_{vp} = \left(\frac{\rho_c - \rho_r}{\rho_c}\right) \cdot \dot{\varepsilon} \cdot \left(\frac{\dot{\varepsilon}}{\dot{\varepsilon}_{ref}}\right)^{-\beta} \cdot \left(\frac{\sigma'_v}{\sigma'_p}\right) \tag{5.12}$$

Where,
ρ_c = Compression ratio.
ρ_r = Recompression ratio.
β = Rate dependent parameter of steady state of R_a.
ρ_a = Creep coefficient.
$\dot{\varepsilon}_{ref}$ = Reference strain rate.

The transient coefficient m_t is assumed to be a function of the visco-plastic strain rate:

$$m_t = \left(\frac{\rho_c}{\rho_a} - 1\right) \cdot \frac{\dot{\varepsilon}_{vp}}{\rho_r \cdot n + \dot{\varepsilon}} \tag{5.13}$$

As can be seen in the equations above, the proposed model has five material constants (ρ_c, ρ_r, ρ_a, β, ε_{ref}) and two internal state variables (σ'_p, R_a). The material constants and the state variable σ'_p can be experimentally determined from CRS and IL oedometer tests. For overconsolidated state [$\sigma'_p/\sigma'_v > 2$], the authors propose an intial $R_{a,0} = 0$ (negligible creep).

For normally consolidated clay the initial creep rate $\varepsilon_{vp,0} \sim R_{a,0}$, see Equation (5.9) for σ'_p/σ'_v =1. The initial creep rate can be calculated by knowing the thickness of the clay layer in the field, the creep coefficient and the soil porosity and by assuming that a degree of consolidation of 99% is achieved.
The parameter β in Equation (5.12) has a constant value irrespective of strain rate. The parameter β value is physically bounded such that $0 \leq \beta \leq \frac{\rho_a}{\rho_c}$. For $\beta = \frac{\rho_a}{\rho_c}$, Equation (5.12) is in agreement with the conventional isotach formulation, which includes parallel compression lines in the void ratio – log σ_v' space with each corresponding to a specific strain rate. For $\beta = 0$, a unique compression curve is obtained independent of the applied strain rates, hypothesis A behaviour. In Figure 5.18, the creep curve as predicted based on the proposed model for different β values is shown for the case of a clay sample in a CRS test.

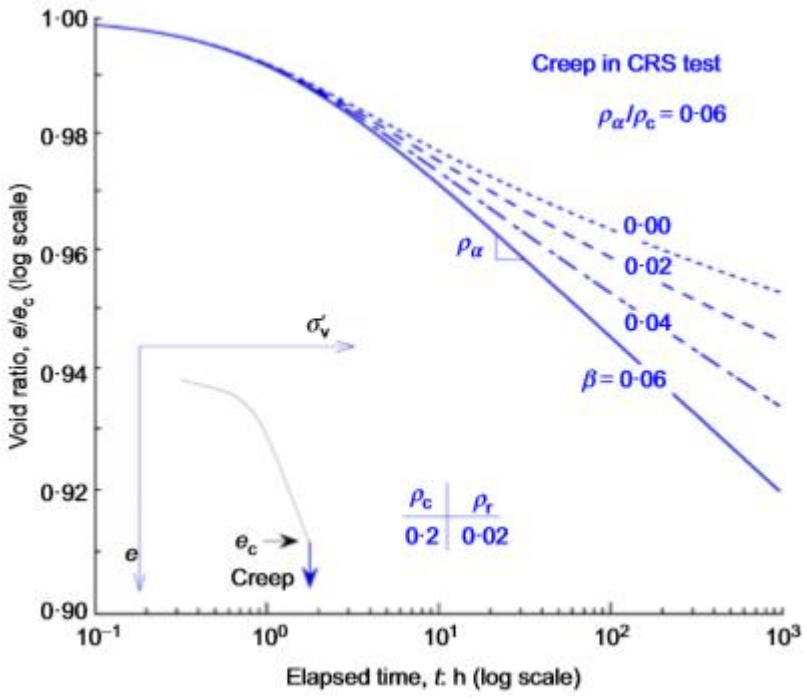

Figure 5.18 Creep for different values of β (after Yuan and Whittle, 2018).

5.5 Modelling non-constant C_α

The MIT-SR model discussed in the previous section can model a non-constant isotach spacing. An alternative approach in modelling a non-constant isotach spacing is found by adopting a non-constant C_α. Yuan et al. (2015) discusses creep behaviour for soils that are unloaded to moderate overconsolidation ratios. The observed creep behaviour can be modelled by a modified isotach formulation in which C_α varies with OCR. In this model, the development of creep strain, ε_s, under constant stress is expressed by a two-parameter model as follows:

$$\varepsilon_s = 0.434 \cdot \hat{C}_{\alpha\varepsilon} \cdot \log\left(\frac{\dot{\varepsilon}_{s,1}}{\dot{\varepsilon}_s}\right) \quad (5.14)$$

The parameters $\hat{C}_{\alpha\varepsilon}$ and $\dot{\varepsilon}_{s,1}$ in the above equation depend on the stress history of the clay (OCR) and are determined experimentally based on a data-fitting approach of oedometer tests on natural clay samples. For an induced OCR of less than 1.5, $\hat{C}_{\alpha\varepsilon}$ and $\dot{\varepsilon}_{s,1}$ are given by:

$$\frac{\hat{C}_{\alpha\varepsilon}}{C_{\alpha\varepsilon}} = \frac{2}{OCR^{\beta}+1} \quad (5.15)$$

$$\frac{\dot{\varepsilon}_{1,s}}{\dot{\varepsilon}_{r,s}} = \left(\frac{1}{OCR}\right)^{m} \quad (5.16)$$

Where:

$C_{\alpha\varepsilon}$ = The secondary compression coefficient of the normally consolidated clay samples.

For OCR = 1, $\hat{C}_{\alpha\varepsilon} = C_{\alpha\varepsilon}$ (conventional isotach model).

β = Parameter that controls the rate of decrease of $\hat{C}_{\alpha\varepsilon}$ / $C_{\alpha\varepsilon}$ with OCR.

$\dot{\varepsilon}_{1,s}$ = The creep rate immediately after unloading.

$\dot{\varepsilon}_{r,s}$ = The strain rate before removal of surcharge.

Based on Equations (5.14), (5.15) and (5.16) it can be concluded that the conventional isotach model ($\hat{C}_{\alpha\varepsilon} = C_{\alpha\varepsilon}$) overestimates the post-unloading creep strains. For instance, for OCR = 1.5 and β = 7.2, as determined for the clay samples in the study of Yuan et al. (2015), Equation (5.15) predicts a $\hat{C}_{\alpha\varepsilon}$ that is approximately 10% of the $C_{\alpha\varepsilon}$ value.

5.6 Modelling of distorted isotachs, C+S model

Den Haan & Edil (1994) noticed that after unloading – reloading of Wisconsin peat, creep strain rate is larger than would be predicted by the reference implementation used in this report described in Chapter 2. The observation is attributed to structural changes due to unloading and reloading. This phenomenon is further explored by Nash (2010) and Nash & Brown (2015). Figure 5.19, taken from Nash & Brown (2015), shows distortion of the isotachs by the dotted lines. The curvature is explained by the destructuration of soil upon reloading. Nash (2010) modified the model by Claesson (2003) to include the curvature of the isotachs around the yield stress as follows:

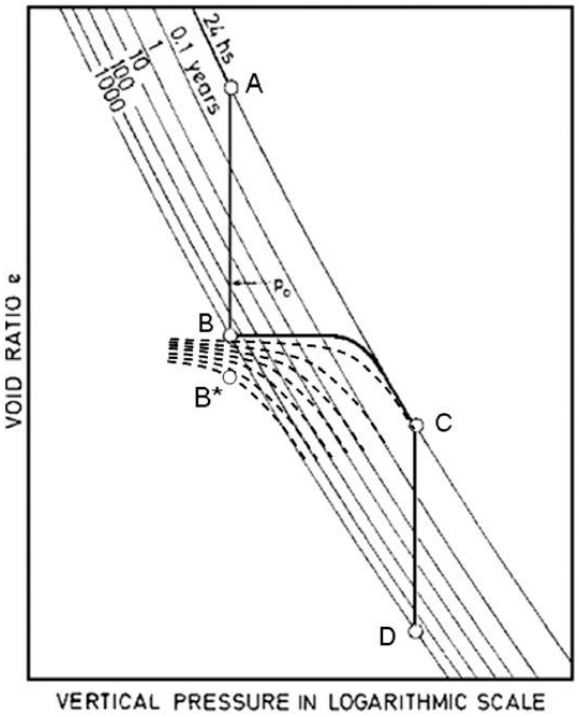

Figure 5.19 Distorted isotachs in overconsolidated region, from: Nash & Brown (2015).

The creep strain and creep strain rate are given by:

$$\Delta\varepsilon^c = \frac{\psi}{v_0}\ln\left(1+\frac{t_e}{t_0}\right); \quad \dot{\varepsilon}^c = \frac{\psi}{v_0\left(t_0+t_e\right)}; \quad \dot{\varepsilon}_0^c = \frac{\psi}{v_0 t_0} \tag{5.17}$$

In which:

ψ = Creep parameter, $\psi = C_\alpha / \ln(10)$.

v_0 = Initial specific volume.

t_0 = Reference time corresponding to the reference isotach, 24 hrs isotach in Figure 5.19, typically t_0 = 1 day.

t_e = Equivalent time, t_e = 0 on the reference isotache.

$\dot{\varepsilon}^c$ = Reference creep strain rate.

Equation (5.17) is used to evaluate creep strain for normally consolidated conditions. The curvature in overconsolidated conditions is found by a reduction in ψ, according to:

$$\psi = \beta\,\psi_{NC} \tag{5.18}$$

In which:

ψ_{NC} = Creep parameter for normally consolidated conditions.

β = Reduction factor.

The reduction factor, β, is expressed as a sine-function. To bound the reduction factor to the overconsolidated region β is linked to the time resistance parameter and time resistance number as used in the Swedish practice and illustrated by Figure 5.20 (Nash & Brown, 2015; Claesson, 2003).

$$\beta = \beta_{\min} + \left(1-\beta_{\min}\right)\sin^a\left(\eta\right), \quad \eta = \frac{\pi}{2}\frac{b-b_0}{b_1-b_0} \tag{5.19}$$

In which:

β_{min} = Minimal value, input parameter.

a = Power.

b = Ratio of actual effective stress over yield stress, $b = \sigma'/\sigma_y$

b_0, b_1 = Stress ratio's see Figure 5.20c.

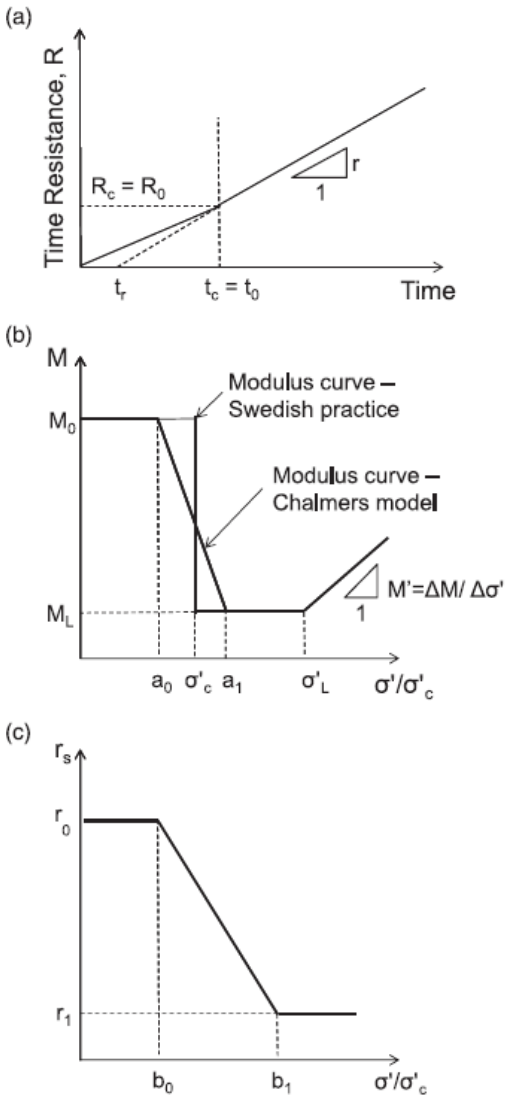

Figure 5.20 Principle sketch of time resistance parameter, R, constrained modulus, M and time resistance factor r as a function of the stress ratio, σ'/σ'_c from: Nash & Brown (2015). R = dt/dε and $\sigma'_c = \sigma_y$

The time resistance parameter, *R* is the inverse of the strain rate *R* = d*t*/dε. The time gradient, *r* of *R* changes in the region of the yield stress, as shown by Figure 5.20c. Equation (5.19) allows β to change from its minimal value to 1 when $b = b_1$. The parameters β_{min} and *a* follow from fitting laboratory test data.

Nash & Brown (2015) explain the curvature of the isotachs by destructuration upon reloading and suggest using the distortion of the isotachs for any reloading condition independent whether the overconsolidation was reached by aging or unloading. This conclusion follows from a qualitative comparison to field experience and a comparison of calculation results found by different models that account and do not account for destructuration.

In contrast, Vergote (Vergote, 2020, Vergote et al., 2020, 2021) explains the distortion of the isotachs by swelling during unloading and proposes a model which includes swelling after unloading. This model is referred to as the Creep and Swell model, C + S model.

The key notion of the C + S model is that swelling is a transient process, which, in contrast to creep, is not modelled by isotach-behaviour.

Figure 5.21 shows how, according to the C + S model, volume change after unloading is followed by an elastic component, a swelling component and creep.

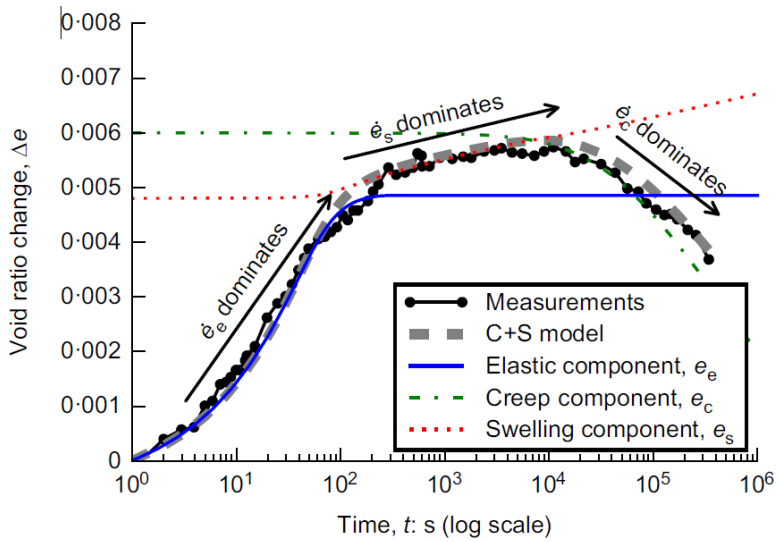

Figure 5.21 Principle of the C+S model: decomposition of strain rates in an elastic, swelling and creep rate component. From: Vergote et al. (2020).

The decoupling of swell and creep in the C+S model results in the use of two definitions for the overconsolidation ratio. Creep rate is related to position of the current stress state in relation to the reference isotach. This position is defined by the yield stress, $\sigma'_{p.ref}$, which is a position on the reference isotach and changes in time due to aging. The swelling rate depends on the level of unloading related to the ratio of the maximum stress before unloading and the actual stress:

$$OCR = \frac{\max(\sigma')}{\sigma'}, OCR_{ref} = \frac{\sigma'_{ref}}{\sigma'} \tag{5.20}$$

The strain rate in the C+S model is a summation of three components, the elastic strain rate, $\dot{e}_e$, the compressive visco-plastic strain rate, $\dot{e}_{vp,c}$ and swelling rate, $\dot{e}_s$:

$$\dot{e} = \dot{e}_e + \dot{e}_{vp,c} - \dot{e}_s \tag{5.21}$$

It should be noted that the swelling strain rate is positive for a volume increase while the elastic and the compressive visco-plastic strain rates are positive for a volume reduction.

The elastic strain rate follows from the loading rate:

$$\dot{e}_e = C_r \frac{\dot{\sigma}'}{\sigma'} \frac{1}{\ln(10)} \tag{5.22}$$

In which:

C_r = Re-loading compression index.

$\dot{\sigma}'$ = Loading rate.

The initial strain rate directly after loading, $\dot{\varepsilon}_{init,c}$ follows from the size of the unloading step, as expressed by OCR and a control parameter β_3:

$$\frac{\dot{\varepsilon}_{init,c}}{\dot{\varepsilon}_{vp,c,ref}} = \left(\frac{1}{OCR_{ref}} \right)^{\beta_3} \tag{5.23}$$

In which:

$\dot{\varepsilon}_{init,c}$ = Creep rate directly after unloading.

$\dot{\varepsilon}_{vp,c,ref}$ = Creep strain rate on the reference isotach.

β_3 = Control parameter creep strain rates.

For $\beta_3 = (C_c - C_r)/C_\alpha$, Equation (5.23) represents the condition of a linear isotach model with equally spaced isotachs. The distortion of the isotachs is found from an update of the creep parameter $\hat{C}_{\alpha,c}$:

$$\frac{\hat{C}_{\alpha,c}}{C_{\alpha,ref}} = \frac{2}{\left(\dot{\varepsilon}_{vp,c} \Big/ \dot{\varepsilon}_{vp,c,ref} \right)^{-\beta_2/\beta_3} + 1} \tag{5.24}$$

In which:

β_2 = Control parameter decay C_α

The C+S models allows for both equidistance isotachs and non-equidistance isotachs. For non-equidistance isotachs the creep parameter C_α declines, see also Section 5.5. In the C+S model the change in C_α follows from:

$$\frac{\hat{C}_{\alpha}}{C_{\alpha,ref}} = \frac{2}{OCR_{ref}^{\beta_2} + 1} \tag{5.25}$$

In which:

$C_{\alpha,ref}$ = Creep parameter C_α at reference isotach.

The swelling rate follows from:

$$\dot{\varepsilon}_{initial,s} = 10^{b_2} \left(OCR_{ref} - 1 \right)^{m_2} \tag{5.26}$$

$$\dot{\varepsilon}_s = -\frac{1}{\hat{C}_{\alpha,s}} \dot{\varepsilon}_s^2 \ln(10) + m_2 \frac{\dot{OCR}}{OCR - 1} \tag{5.27}$$

$$\frac{\hat{C}_{\alpha,s}}{C_{\alpha,ref}} = 10^{b_1} \left(OCR - 1 \right)^{m_1} \tag{5.28}$$

In which:

$e_{initial,s}$ = Initial swelling rate, directly after unloading.

b_2, m_2 = Parameters controlling the change in initial swelling rate

$\hat{C}_{\alpha,ref}$ = Swelling parameter

b_1, m_1 = Parameters controlling the swelling parameter

Figure 5.22 shows an example of the field of distorted isotachs taken from Vergote et al. (2020).

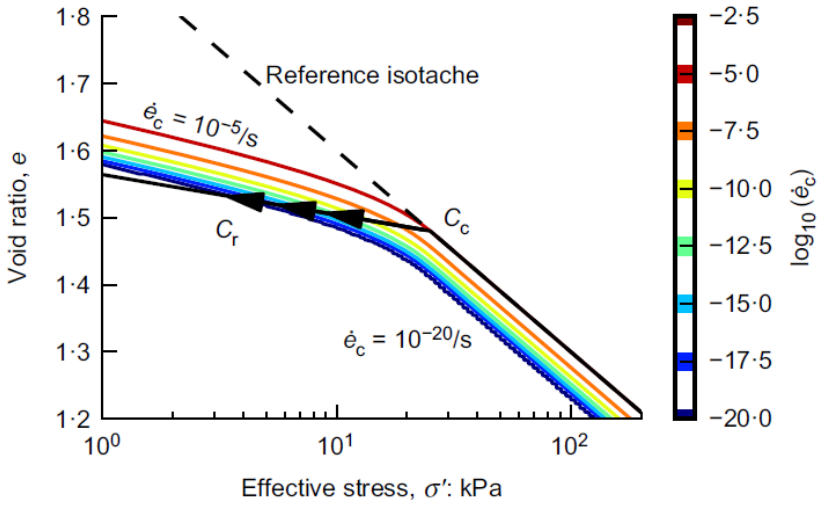

Figure 5.22 Example of distorted creep isotachs based on β_2 = 4 and β_3 = 19, from: Vergote et al. 2020.

The C+S model uses 10 parameters of which four are typically derived from conventional incremental loading or constant rate of strain tests, The remaining parameters can be evaluated from curve fitting and parameter optimization, as shown by Vergote et al (2020) and (2021).

6 Integrative discussion

This chapter compares the laboratory test results, Chapter 4, to the literature findings, Chapter 5.

This integration of results is related to the three presumptions, introduced in Chapter 3:

1. Isotachs are linear in $\log\sigma' - \varepsilon$ space.
2. Isotachs are 'equidistant' in $\log\sigma' - \varepsilon$ space, for log-cycle differences in creep strain rate. In other words, the creep coefficient C_α or c is truly constant, not dependent on stress and strain.
3. The isotachs are fixed in $\log\sigma' - \varepsilon$ space, independent of the path, strain and or stress history.

The laboratory test results and the literature study provide the following insights on these presumptions.

Presumption 1; Isotachs are linear in $\log\sigma' - \varepsilon$ space.

Although the focus of this study is on small load increments, the succession of the different test phases resulted in large displacement and corresponding large strain effects. This is generally accepted, but not often applied when analysing laboratory test data. Often, in literature, the principles introduced by a paper, are explained by isotachs that are linear in the in $\log\sigma' - \varepsilon$ space, while published experimental data typically show bended isotachs at large strain. Also, the experimental results in this study clearly show the impact of large deformations on the stress – strain curve and the benefits of using a large strain definition when analysing the data.

Besides large displacements, unloading also has an impact the linearity of the isotachs. Among others, Vergote (2020) shows that unloading results in distorted isotachs. This distortion is caused by rearrangement of the soil matrix due to swelling. Compared to non-distorted isotachs, distorted isotachs result in larger strain rates after unloading.

Consequently, an isotach model based on non-distorted isotachs cannot be used to predict the strain rates after unloading. This is validated in this study by the IL tests. In these tests soil parameters derived from each test are used to calculate the strain rates at the end of each loading step. For loading steps in normally consolidated conditions a reasonable agreement is found between the measured and calculated strain rates. For re-loading steps, a clear mismatch is found between the measured and calculated strain rates. The mismatch increases with increasing OCR and reaches multiple orders of magnitude.

This behaviour has negative consequences for the prediction of initial conditions under field conditions when some form of unloading has been applied. A typical example are the pre-consolidation techniques that include late-stage unloading used in construction to reduce creep settlement. Moreover, this behaviour has an impact on laboratory testing. Retrieving samples, for instance, typically involves a reduction in effective stress and corresponding swelling. The initial loading stages in testing are then affected by the distorted isotachs and inferred behaviour differs from intrinsic soil behaviour. Moreover, in tests that include unloading to low stress levels and associated high OCR, the measured strain rate does not represent soil behaviour at the same OCR developed by aging in the field.

Presumption 2; Isotachs are equidistant.
Figure 5.4 in Chapter 5 shows experimental data relating yield stress to strain rate. Leroueil (2006) concludes from this graph that isotachs are not equidistant and consequently C_α reduces in time during aging. For equidistant isotachs the relation between yield stress and strain rate would be linear on the log-log scale, and, Leroueil (2006) presents the line for $C_{\alpha e}/C_c = 0.04$ as an example. The data presented by Leroueil are scattered around this line and have the tendency to be above the line $C_{\alpha e}/C_c = 0.04$ for high and low strain rates. Therefore, Leroueil (2006) concludes that a non-constant $C_{\alpha e}/C_c$ ratio represented by the curved, dashed line fits the data better.

To see how the results of the tests performed in the current study compare with the findings of Leroueil (2206), Figure 6.1 plots the data of tests 3, 7b, 8 and 9 in Figure 5.4. The figure uses 1×10^{-7} 1/s for reference strain rate. This strain rate was not reached in test 6 and therefore the results from test 6 were not included. The data for strain rates larger than the reference strain rate, 1×10^{-7} 1/s plot above the line $C_{\alpha e}/C_c = 0.04$. However, for low strain rates, 1×10^{-8} 1/s, the data falls below the line $C_{\alpha e}/C_c = 0.04$, and the dashed line proposed by Leroueil (2006), does not seem to match the experimental data obtained in this study. A line with $C_\alpha/CR = 0.055$ provides a good fit for the strain rates 1×10^{-8} 1/s to 1×10^{-6} 1/s. For higher strain rates the data points are still above the line. It should be noted that the data from the IL tests, Table 4-13 yields RR/CR = 0.069 for test 1 and 0.086 for test 2.

For large strain rates, 1×10^{-4} 1/s, concerns were raised about the pore pressure correction, as discussed at the start of Section 4.5. The consequence of a possible incorrect pore pressure correction is an overestimation of $\sigma_{v,2}/\sigma_{v,1}$ and the data point in Figure 6.1 would move down.

For the strain rates in the range of 1×10^{-5} 1/s to 1×10^{-8} 1/s, the experimental data in Figure 6.1 seems to show a linear spacing of the isotachs. At larger strain rates the data seems to indicate otherwise. The deviation at higher strain rates can be attributed to an incorrect correction for pore pressure development. The found linear spacing contradicts literature findings, in which a gradual spacing reduction is applied. Due to the scatter in the original and new data and the questions on the pore pressure correction, it is hard to decide if the data in Figure 6.1 are best fitted by a constant or a non-constant $C_{\alpha e}/C_c$ ratio.

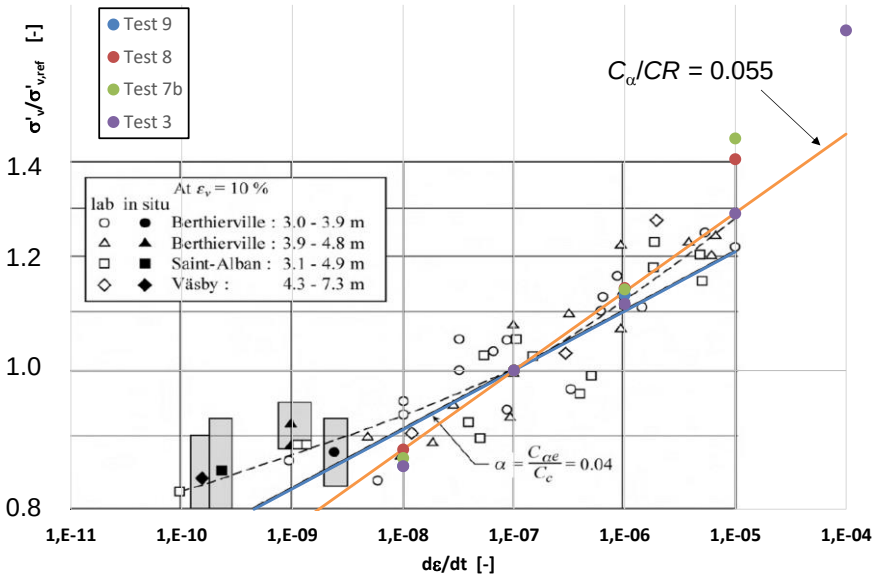

Figure 6.1 Comparison measurement data to Leroeuil (2006).

Applying a spacing reduction and end-of-creep isotach has strong consequences for the prediction of the strain rate development and corresponding OCR development. The reference implementation does not include these effects and predicts a continuous, linear decline in creep strain rate and corresponding increase in OCR. In practical field applications the OCR is assessed more often than strain rates. Typically, field data yield a lower OCR than predicted from the reference implementation, a.o. van Duinen & Stoutjesdijk (2023). This results in the contradicting observations that field data indicates non-equidistanct isotachs, while the laboratory data in Figure 6.1 do seem to show equidistant isotachs.

Presumption 3; the isotachs are fixed in $\log\sigma' - \varepsilon$ *space, independent of the path, strain and or stress history.*

The literature review discusses the different models that are based on the isotach concept. Each of the models assume that the isotachs are fixed in the $\log\sigma' - \varepsilon$ space, for normally consolidated conditions. Upon unloading, the isotachs get distorted and a new field of bended isotachs develop. Despite the general acceptance of the uniqueness of the isotachs, for normally consolidated conditions, there is little experimental evidence published on this. Leroueil et al (1985) show isotachs derived from CRS testing on Batiscan clay for strain rates ranging from 1.43×10^{-5} to 1.68×10^{-8} 1/s. De tests show that the isotachs run parallel to each other with exception of the lowest tested strain rate 1.68×10^{-8} 1/s. For this strain rate an isotach was found that crossed the isotachs representing higher strain rates. Leroueil et al. explain this by thixotropic hardening which was not further elaborated.

To compare the literature finding to the experimental research, the stress strain curves of the individual tests are plotted together in Figure 6.2 to Figure 6.5. To account for variability of the tested samples, the curves are plotted in terms of void ratio. Tests 3 and 6 also show stiffer behaviour as reflected by the values for compression ratio, *CR* given in Table 4-16. Therefore, the tests 3 and 6 are omitted in the comparison in the Figure 6.2 to Figure 6.5.

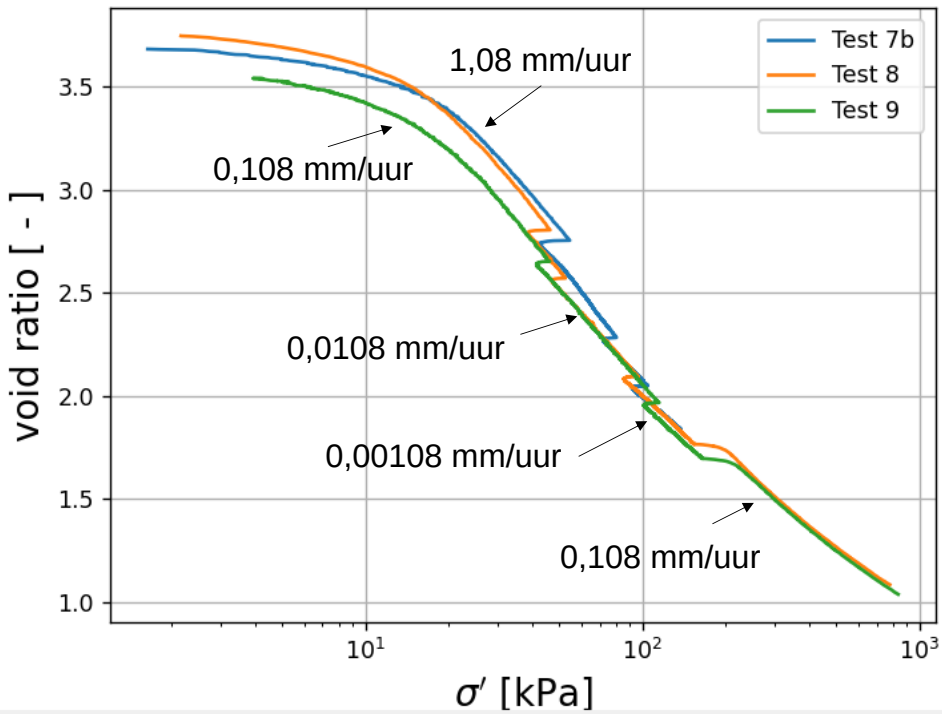

Figure 6.2 Comparison of the test results for Tests 7b, 8 and 9. Initial void ratio for test 7b is adjusted form e_0 *= 3.85 to 3.7.*

Figure 6.2 shows a comparison between the tests 7b, 8 and 9. The results of the different test compare well. Parts of the stress – strain curve with the same displacement rate fall on top of each other. The acceleration at the end of the test, from a displacement rate of 0.00108 mm/h to 0.108 mm/h, brings the stress – strain curve back to the same isotach as was found at earlier stages of the tests at the same displacement rate.

In contrast to Figure 5.1 all isotachs, in the graphs below, run parallel, even for the lowest displacement rate, 0.00108 mm/u which correspond to 1×10^{-8} 1/s. The thixotropic behaviour observed in the test results Batiscan clay, is not found in the test results presented below.

Tests 10, 10b, 11 and 12 use a constant displacement rate, 1.08 mm/h for tests 10 and 10b, 0.108 mm/h for test 11 and 0.0108 mm/h for test 12. A comparison between the results of these tests further improves the establishment of the position of the isotachs, see Figure 6.3, Figure 6.4 and Figure 6.5. In these graphs, the initial void ratio for test 10 is changed from 3.45 to 3.7, for test 11 from 3.21 to 3.45 and for test 12 from 3.72 to 3.6. Despite the required changes in void ratio, there is a good agreement between the tests with a constant strain rate and variable strain rate. Test 11 seems to show a bit stiffer behaviour. This can be explained by natural variability between the samples.

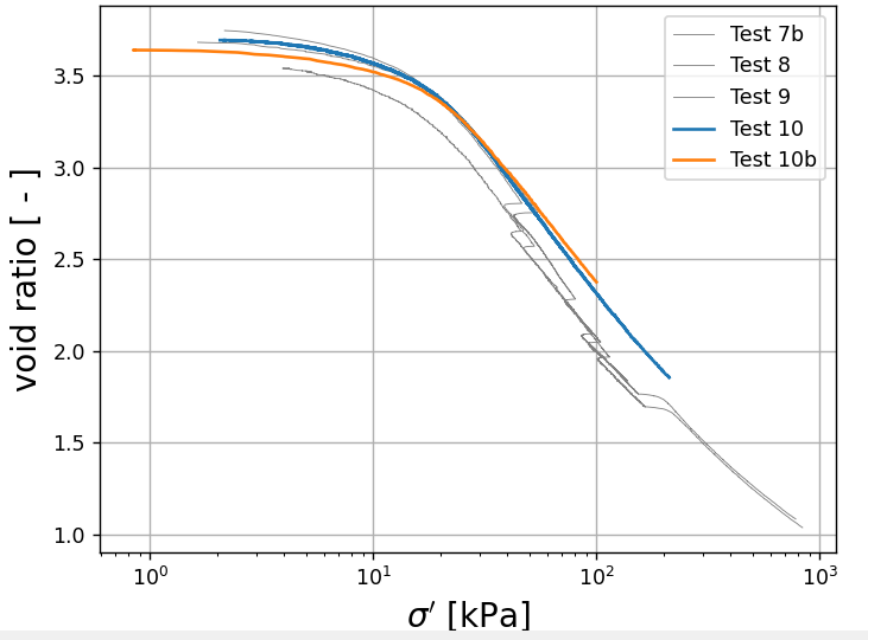

Figure 6.3 Comparison of tests 10 and 10b with displacement rate 1.08mm/h, to tests 7b, 8 and 9.

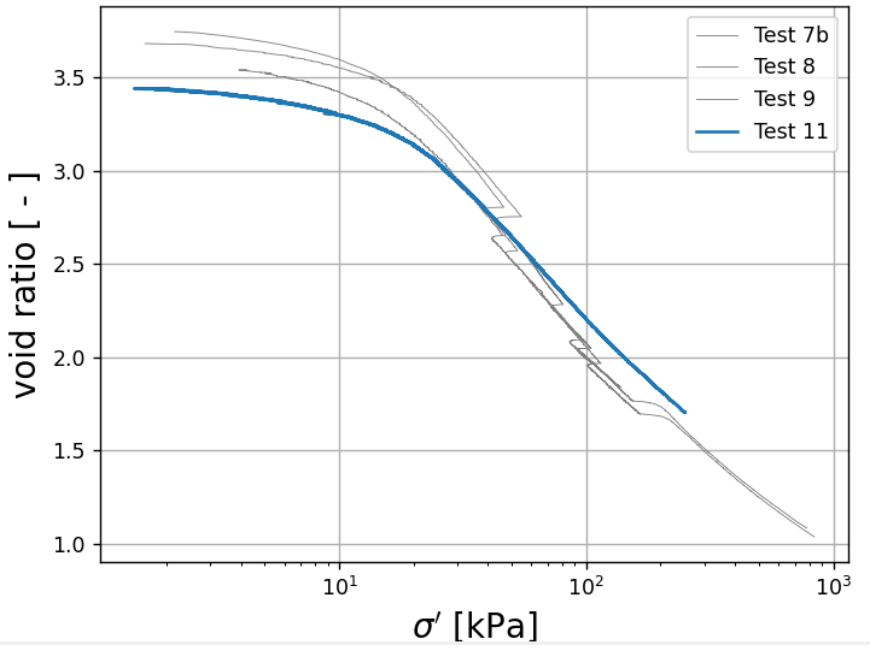

Figure 6.4 Comparison of test 11 with displacement rate 0.108 mm/h, to tests 7b, 8 and 9.

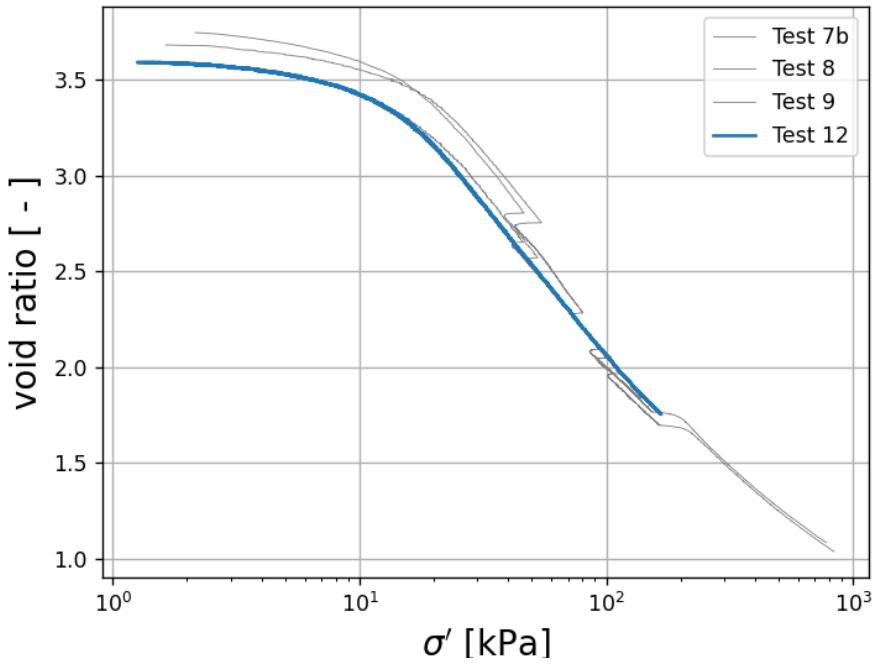

Figure 6.5 Comparison of test 12 with displacement rate 0.0108 mm/h to tests 7b, 8 and 9.

7 Summary and Conclusions

7.1 Summary

This study explored the applicability of the reference isotach implementation for settlement prediction due to small load increments that are common in land subsidence applications. The study is restricted to clay behaviour. Applicability fundamentally depends on three characteristics of the reference implementation being valid over the entire range of states: from virgin compression, at the reference isotach, to significantly overconsolidated states represented by the in-situ conditions:

1. Isotachs are linear in log σ' - ε space.
2. Isotachs are 'equidistant' in log σ' - ε space, for log-cycle differences in creep strain rate. In other words, the creep coefficient C_α or c is truly constant, not dependent on stress and strain.
3. The isotachs are fixed in log σ' - ε space, independent of the path, strain and or stress history.

Validity of these assumptions was investigated through laboratory testing and literature study.

Isotachs are linear in log σ' - ε *space.*
The laboratory tests show that the isotachs are not linear in log σ' - ε space. There are two conditions to which the non-linearity of the isotachs applies. The first condition is related to large strain behaviour. The tests showed that the isotachs start to bend when reaching strain levels of approximately 50%. This is simply explained by the end of layer effect; a soil layer, or a sample in laboratory testing cannot be compressed to a zero-thickness and consequently stiffness increases when reaching large strain levels. The study on land subsidence focusses on small load increments and consequently, small strain and small strain rate. Therefore, the above effect of non-linearity might not be relevant for most land subsidence applications. This differs from laboratory tests in which different loading phases, or for CRS testing, different displacement rates are applied. In analysing the later phases and comparing the results to previous phases, large strain behaviour should be accounted for. The use of the natural strain definition is a valuable tool in analysing large strain behaviour. The laboratory tests show that when using the natural strain definition, the isotachs remain linear even at large strain.

The second condition for which non-linearity is encountered is related to unloading. The literature explains that the isotachs get distorted upon unloading due to structural re-arrangement of the soil skeleton caused by swelling. The IL tests, discussed in Section 4, illustrate this effect. The tests show that after unloading the observed displacement rate is much larger than predicted by the reference isotach model. For increasing OCR an increasing difference is found between the observed and predicted displacement rate. Even for small unloading steps the difference might reach several orders in magnitude. This has two consequences for the application of the reference isotach model for land subsidence applications. The first consequence is a restriction to parameter assessment by laboratory testing. In IL testing, unloading steps cannot be used to quantify low strain rate behaviour which is reached after a long creep period. The second consequence is a restriction to field applications, in which land subsidence is influenced by several loading and unloading effects that might include swelling. The impact of rate effects is unknown at the moment. For example, ground water fluctuations result in loading and unloading conditions and might reduce the applicability of the reference isotach implementation. However, small gradual changes might have a limited impact.

Isotachs are 'equidistant' in log σ' - ε space.
The laboratory tests do not show that the isotachs are not equidistant. It is important to stress that this finding applies to the range of the strain rates that could be applied. The lowest possible strain rate that could be applied by the equipment is still orders in magnitude larger than observed in the field. At large strain rates, induced pore pressure results in some uncertainty on the effective stress level present in the soil sample. However, it is concluded that within the range of strain rates, from 10^{-6} tot 10^{-8} 1/s, the isotachs derived from the laboratory testing are equidistant. This contradicts with the literature findings. Most of the recent publications on isotach modelling include a non-equidistant isotach framework including an end-of-creep isotach. The test results for larger strain rates might indicate a non-equidistant spacing.

For modelling land subsidence, the assumption on equidistant or non-equidistant spaced isotachs has a large impact. The distances between the isotachs control the rate at which the strain accelerates upon loading or slows down during a period of constant load. For equidistant isotachs, the refence implementation provides a good tool to predict strain rates at small load increments. For non-equidistant isotachs the reference isotach implementation results in an overprediction of the undisturbed in-situ strain rate. Upon re-loading non-equidistant isotachs will result in a different acceleration of the in-situ strain rate compared to the reference implementation. These effects have a large contribution to uncertainty in subsidence predictions.

Since the laboratory testing conditions differ from field conditions, in terms of applied strain rates, the validation of the isotach model should be extended to include field data at relevant strain rates.

Isotachs are fixed in log σ' - ε space.
Literature shows that the isotachs get distorted upon unloading. The IL tests conducted in this study illustrate the consequences; the strain rate after unloading could not be predicted correctly with the reference isotach model. The consequence of distorted isotachs is the stress path dependency in assessment of strain rate and corresponding settlement.

When no unloading is applied, literature agrees that the isotachs are fixed in log σ' - ε-space and independent from the followed loading path or stress history. The experimental work in this study supports this as indicated by the following three observations. The first observation is that combining CRS tests, in which different or changing strain rates are applied, results in a unique set of isotachs. The second observation is that acceleration at the end of the test brings the stress – strain curve back to an isotach which was already found earlier in the test at same strain rate. The third observation is that the stress – strain curve from CRS tests with a constant strain rate agree well to the stress strain curves found at the same strain rate in tests in which multiple strain rates are applied.

7.2 Conclusions

The study reveals several shortcomings of the reference isotach model that limit its applicability in land subsidence applications. The laboratory testing and literature study show:

- The isotachs might be non-equidistant in normally consolidated conditions, with smaller spacing for lower strain rates. Application of the reference isotach model would result in an overprediction of in-situ strain rates and contributes to the uncertainty in subsidence prediction.
- Distortion of the isotachs upon unloading followed by swelling. This results in non-unique isotach field for unloading – reloading conditions and strain and strain rates for unloading – reloading conditions become dependent on the loading path.

This is not included in the reference model and consequently the reference model will underpredict strain rates and corresponding settlement after unloading. The underprediction will be stronger for larger unloading steps, e.q. renovation of roads that includes removal of the old construction. The conducted constant rate of strain tests do not provide indications that isotachs are not parallel. Although, literature includes one study that indicates non-parallel isotachs can occur. If the latter is relevant for real soil behaviour, then this would further restrict the applicability of the reference isotach implementation.

These shortcomings have consequences for settlement prediction due to small load increments, as predictions become dependent on the exact loading conditions and stress history. Therefore, using the reference isotach implementation for small load increments will not result in accurate settlement prediction.

The distortion of the isotachs, and the non-equidistant spacing of the isotachs are two elements that are not included in the reference isotach implementation. Both elements have a important consequences for the use of the reference implementation for land subsidence applications. Land subsidence applications primarily concern prediction of subsidence, be it for undisturbed conditions or effects of small load changes. The results show that the theoretical framework of the isotach model does not presently yield reliable predictions, limiting the applicability of the model in such applications. The potential to improve the applicability through model adjustments may be explored – numerical solutions for non-equidistant isotachs are available for instance. However, increased reliability of prediction mostly requires empirical data on creep behavior from dedicated field monitoring and testing. Important steps in this direction have been made in RDBGH projects 10 “Uitbreiding monitoring proefvakken” and 44 “Bodemdaling in kaart en kijken in de bodem; meten, monitoring en ontrafelen van bodemdalingsprocessen”.

References

Bjerrum L. (1967) Engineering geology of Norwegian normally-consolidated marine clays as related to settlement of buildings *Geotechnique* **17**(2) 81-118.

Buisman A.S.K. (1940) Grondmechanica, reprent Balkema Rotterdam (reprint 1996) (in: Dutch).

Bootsma, H., H. Kooi, G. Erkens (2020) Atlantis, a tool for producing national predictive land subsidence maps of the Netherlands. Proc. IAHS, 382, 415–420, https://doi.org/10.5194/piahs-382-415-2020.

Choi, Y. K. (1982). Consolidation behavior of natural clays. PhD thesis, University of Illinois at Urbana-Champaign, UrbanaIllinois.

Degago, S. A., Grimstad, G., Jostad, H.P., Nordal, S. & Olsson, M. (2011). Use and misuse of the isotach concept with respect to creep hypotheses A and B.

Deltares (2021) D-Settlement Embankment design and soil settlement prediction, User Manual, version 21.2, D-Settlement - Deltares.

Den Haan E.J. (1992) The formulation of virgin compression of soils *Géotechnique,* vol 42, p 465-483.

Den Haan E.J. (1994) A simple compression model for non-brittle soft clays and peat *PhD thesis TUDelft.*

Den Haan E.J. (1999) Stress independent parameters for primary and secondary compression *in: Proceedings XIIIth International Conference on Soil Mechanics and Foundation Engineering*, New Delhi, Vol I, p 65 – 70.

Den Haan E.J., Edil T.B. (1994) Secondary and tertiary compression of peat *in: Advances in understanding and modelling the mechanical mbehaviour of peat, den Haan, Termaat & Edil (eds), Balkema Rotterdam.*

Den Haan E.J., Sellmeijer H.J.B. (2000) Calculation of Soft Ground with an Isotach Model *in: Soft ground technology Hanson & Termaat (eds), ASCE geotechnical special publication* no 112, June 2000.

Den Haan E.J. Kruse G.A.M. (2007) Characterisation and engineering properties of Dutch peats *in: Characterisation and Engineering Properties of Natural Soils – Tan, Phoon, Hight & Leroueil (eds)*, Tayor&Francis Group, London.

Van Duinen T.A., Stoutjesdijk T. (2023) DIV Toename sterkte in tijd, veld,-laboratoriumonderzoek en eerste analyse, Deltares rapport nr 11209373-002-GEO-v1.1.

Grimstad, G. & Degago, S.A. (2010). A non-associated creep model for structured anisotropic clay (n-SAC). 7th European Conf. NUMGE, Trondheim, Norway, 3-8.

Kawabe S., Tatsuoka F. (2013) Creep characteristics of clay in one-dimensional compression with unloading / reloading cycles *in: proceedings of the 18th International Conference on Soil Mechanics and Geotechnical Engineering*, Paris.

Kooi, H., Bakr, M., de Lange, G., den Haan, E., and Erkens, G. (2018) User guide to SUB-CR; a MODFLOW package for land subsidence and aquifer system compaction that includes creep, Deltares internal report 11202275-008, http://publications.deltares.nl/11202275_008.pdf.

Ladd, C. C., Foott, R., Ishihara, K., Schlosser, F. & Poulos, H. G. (1977). Stress–deformation and strength characteristics. In Proceedings of the 9th international conference on soil mechanics and foundation engineering, pp. 421–494. Tokyo, Japan: Japanese Society of Soil Mechanics and Foundation Engineering.

Leroueil S., Kabbaj M., Tavenas F., Bouchard R (1985) Stress -strain-strain rate relation for the compressibility of sensitive natural clays *Géotechnique* **35** (2) p 159-180.

Leroueil S. (2006) The isotach approach. Where are we 50years after its development by Professor Šuklje? *in: Proceedings of the 13th Danube-European Conference on Geotechnical Engineering*, Prof. Suklje's memorial lecture, Ljubljana 2006 pp 55-88.

Mesri, G. (2009). Discussion of 'Effects of friction and thickness on long-term consolidation behavior of Osaka Bay clays' by Watabe, Udaka, Kobayashi, Tabata & Emura (2008). Soils Found. 49, No. 5, 823–824.

Nash D., Brown M. (2015) Influence of Destructuration of Soft Clay on Time-Dependent Settlements: Comparison of Some Elastic Viscoplastic Models *International Journal of Geomechanics* 15(5), DOI:10.1061/(ASCE)GM.1943-5622.0000281.

Sivasithamparam, N., Karstunnen, M. & Bonnier, P. (2015). Modelling creep behaviour of anisotropic soft soils. Computers and Geotechnics, 69, 46-57.

Šuklje, L. (1957). The analysis of the consolidation process by the Isotachs method. Proc. 4th Int. Conf. Soil Mech. Found. Engng, London, 1: 200-206.

Visschedijk M. (2010) Isotachen berekeningen op een sigarendoosje *Geotechniek* juli 2010

Vergote T.A. (2020) Deformation of soils: time and strain effects after unloading *PhD thesis* National University of Singapore.

Vergote T.A., Leung C.F., Chain S.C. (2020) Modelling creep and swelling after unloading load and relaxation with Bayesian updating *Géotechnique* DOI:10.1680/jgeot.20.P.106.

Vergote T.A., Leung C.F., Chian S.C. (2021) Elastoviscoplastic modelling with distorted isotaches and swelling for constant strain rate and incremental loading *International journal Analytical Methods in Geomechanics* 2021;1-14 DOI:10.1002/nag.3248.

Watabe, Y., Udaka, K., and Morikawa, Y. (2008). Strain rate effect on long-term consolidation of Osaka bay clay. Soils Found., 48(4), 495–509.

Watabe, Y., Udaka, K., Nakatani, Y. and Leroueil, S. (2012). Long-term consolidation behavior interpreted with isotach concept for worldwide clays. *Soils & Found*., 52(3), 449–464.

Watabe Y., Leroueil (2015). Modeling and implementation of the isotach concept for long term consolidation behaviour. *Int. J. Geomech*., 15(5). DOI: 10.1061/(ASCE)GM.1943-5622.0000270.

Yuan Y., Whittle A.J. (2014) Surcharge Loading On Reduction of Secondary Compression, *2014 CREBS workshop Deltares*, Delft, powerpoint presentation.

Yuan, Y.,Whittle, A., and Nash, D. (2015). Model for predicting and controlling creep settlements with surcharge loading. Deformation Characteristics of Geomaterials. 10.3233/978-1-61499-601-9-931, 931-938.

Yuan, Y., & Whittle, A.J. (2018). A novel elasto-viscoplastic formulation for compression behaviour of clays. Geotechnique 68(12), 1044, doi: 10.1680jgeot.16.P276.

Verruijt A. (2012) Soil Mechanics, TUDelft, downloaded from: http://geo.verruijt.net/.

Visschedijk M. (2010) Isotachen berekeningen op een sigarendoosje *Geotechniek* juli 2010 (in: Dutch).

Watabe Y., Udaka K., Nakatani Y., Leroueil S. (2012) Long-term consolidation behavior interpreted with isotach concept for worldwide clays *Soils and Foundations* 52(3):449-464 Doi: 10.1016/j.sandf.2012.05.005.

Zwanenburg C. (2017) Kruip en Zwel, laboratoriumproeven op veen uit de Bloemendaler polder, Deltares report 1220018-005-GEO-v1 (in: Dutch).

Zwanenburg C. (2017[a]) The development of a large diameter sampler *in: proceedings of the 19th international conference on soil mechanics and geotechnical engineering,* Seoul.

Zwanenburg C. (2021) Lecture notes TUD.

Zwanenburg C. (2017). *The Development of a Large Diameter Sampler,* Proceedings of the 19th International Conference on Soil Mechanics and Geotechnical Engineering, Seoul.

A Results CRS testing

Table 4-16 gives a summary of the first of the stress – strain curves for each test phase. This appendix provides more information on the obtained fits. The following graphs provide the stress – strain and stress – natural strain curves. For each test, the measurement data is presented. The red parts represent the data that is used in the individual fits and blue the remaining data. The fits follow from linear regression on logarithm of strain versus strain relationship. Following Chapter 2 in this report, both linear strain and natural strain are used in which the natural strain is combined to the natural logarithm of the stress. The fits are conducted by the *polyfit* function in the *numpy* package of *python*. For each fit the weighted least squares sum R^2 is given. R^2 = 1 represents a perfect fit.

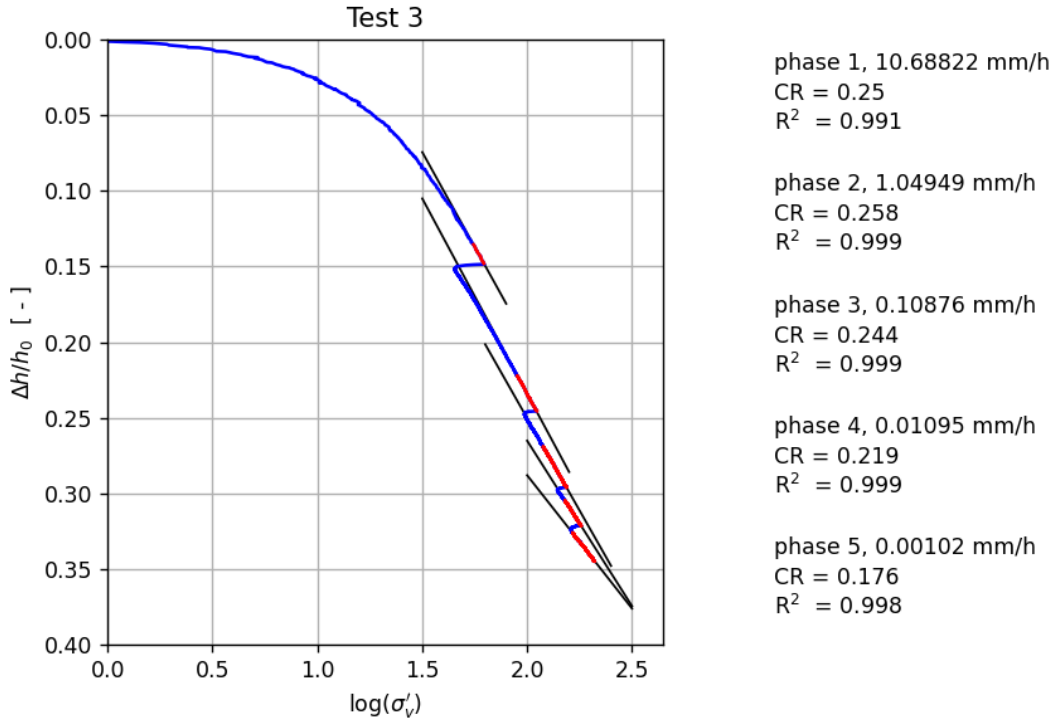

Figure A. 1 Fits stress – strain curve test 3.

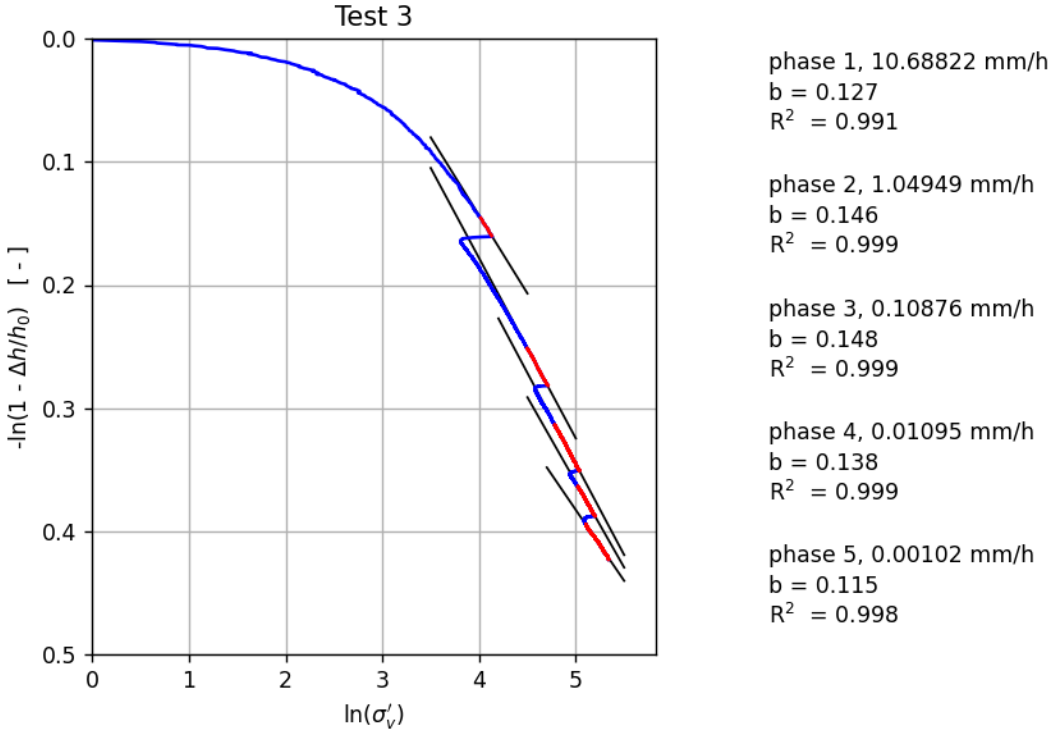

Figure A. 2 Fits stress – natural strain curve, Test 3.

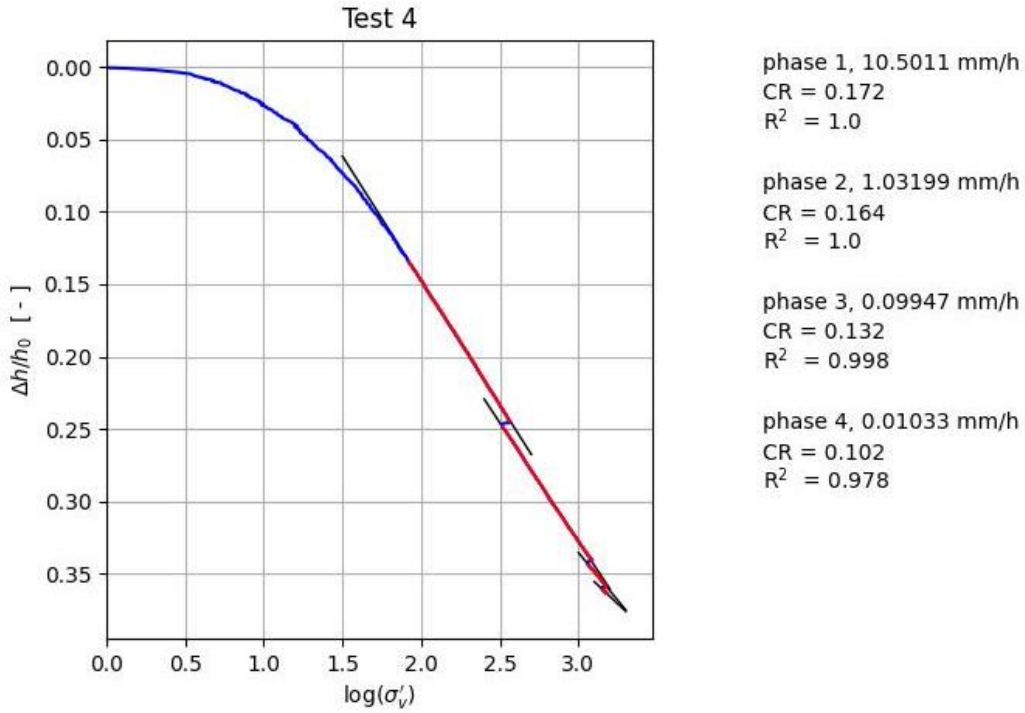

Figure A. 3 Fits stress – strain curve, Test 4.

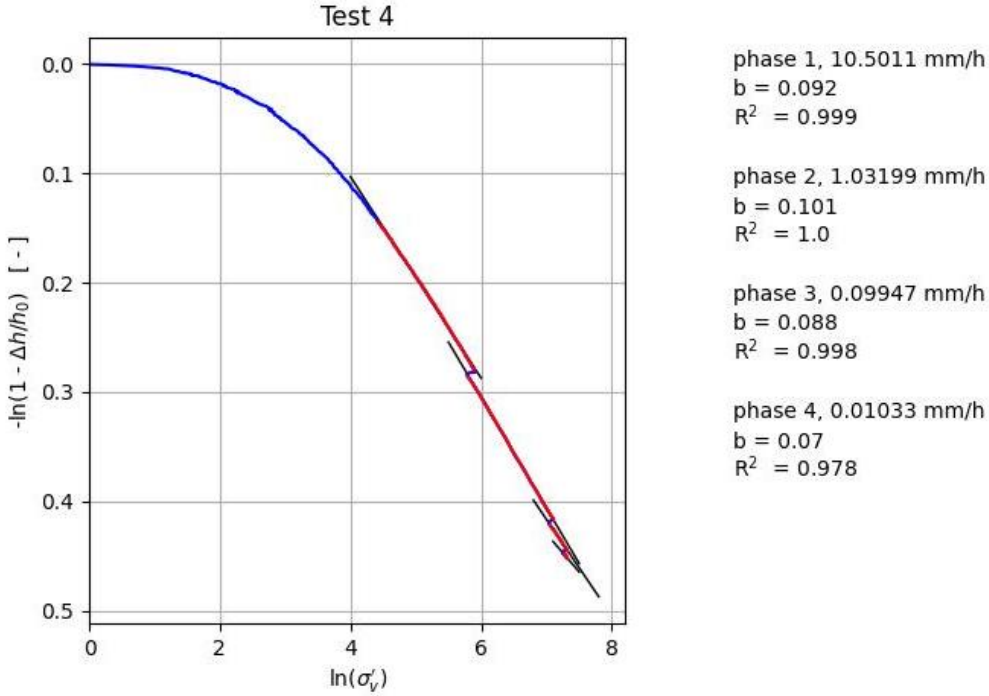

Figure A. 4 Fits stress – natural strain curve Test 4.

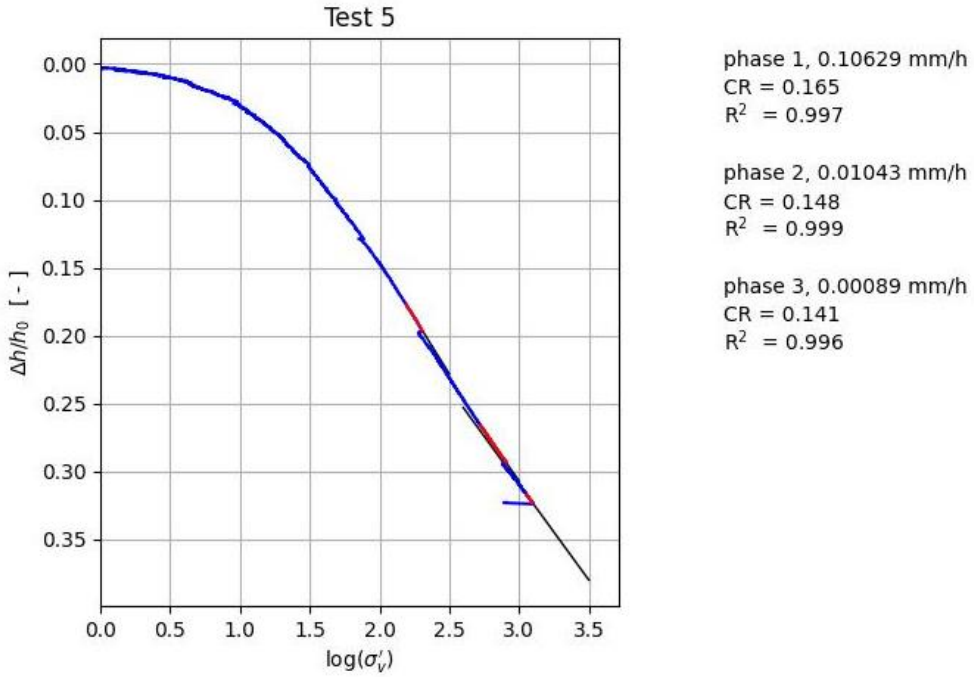

Figure A. 5 Fits stress – strain curve Test 5.

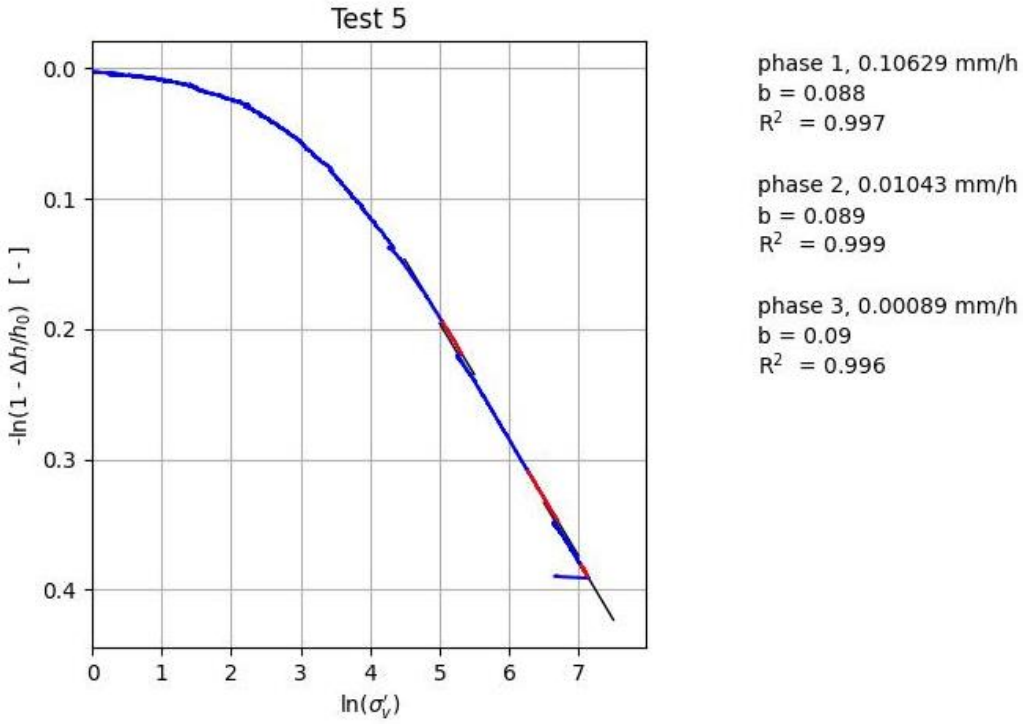

Figure A. 6 Fits stress – natural strain curve Test 5.

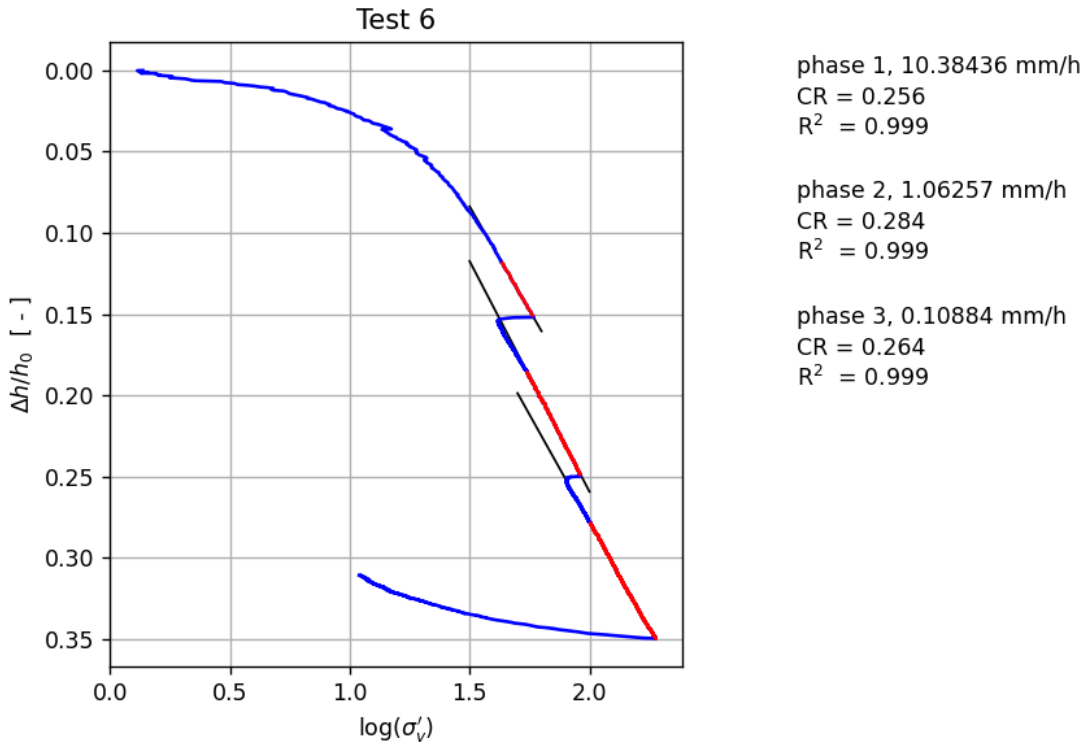

Figure A. 7 Fits stress – strain curve, Test 6.

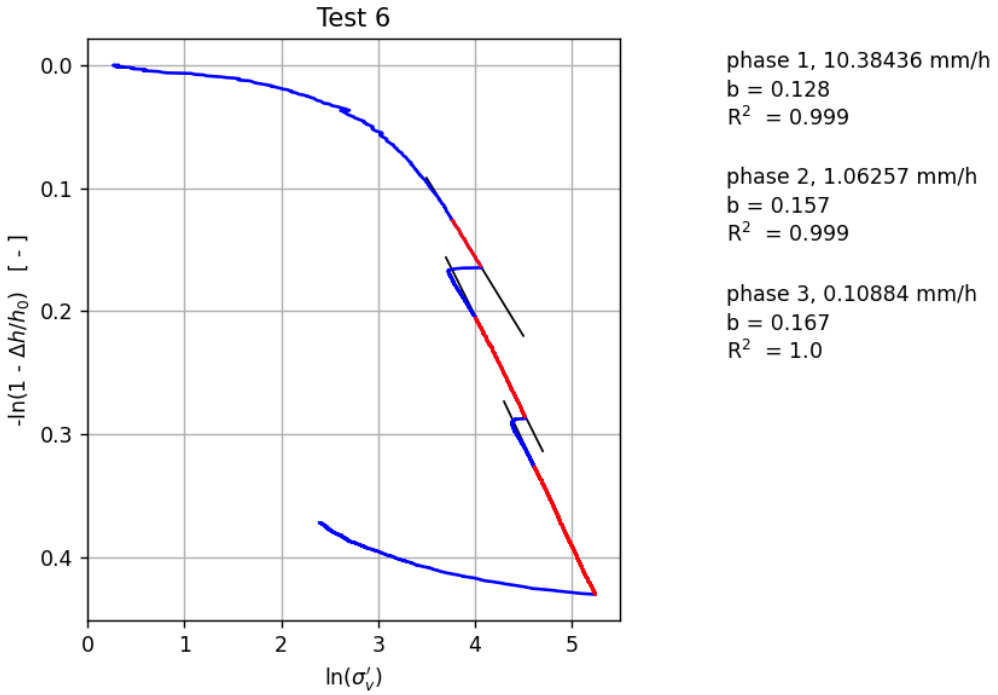

Figure A. 8 Fits stress – natural strain curve Test 6.

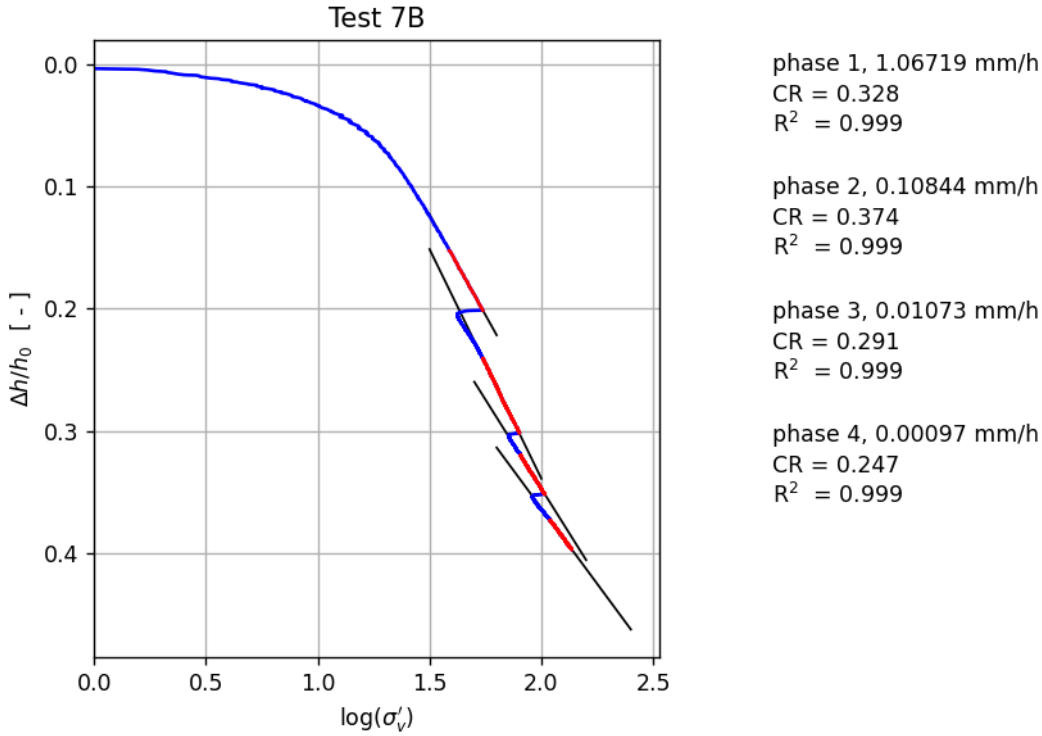

Figure A. 9 Fits stress – strain curve Test 7b.

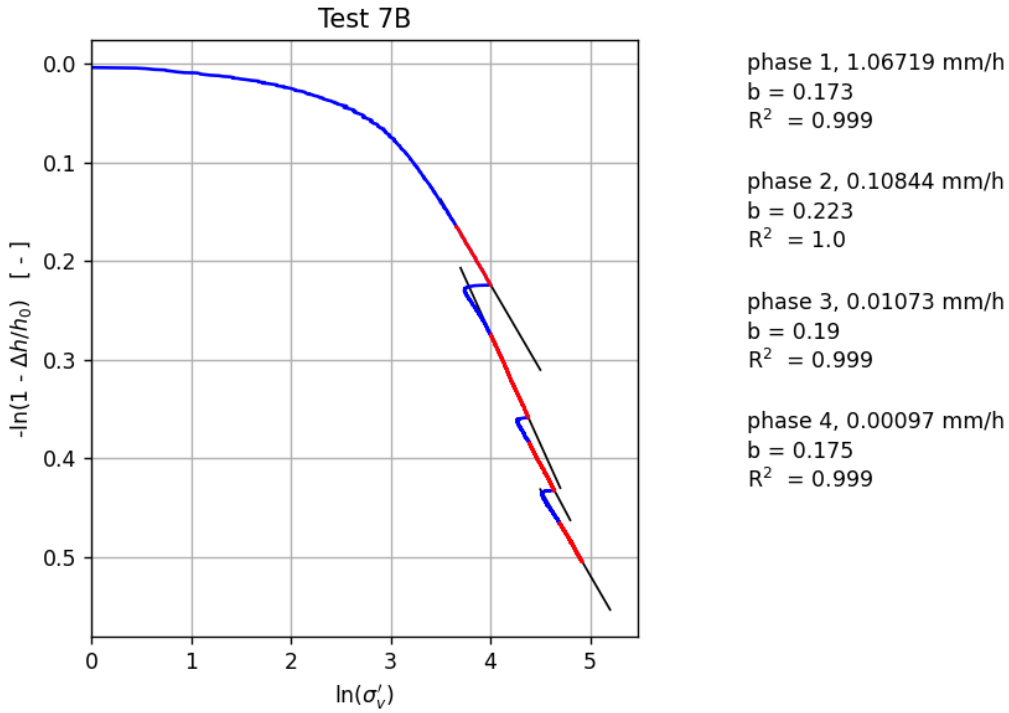

Figure A. 10 Fits stress – natural strain curve Test 7b.

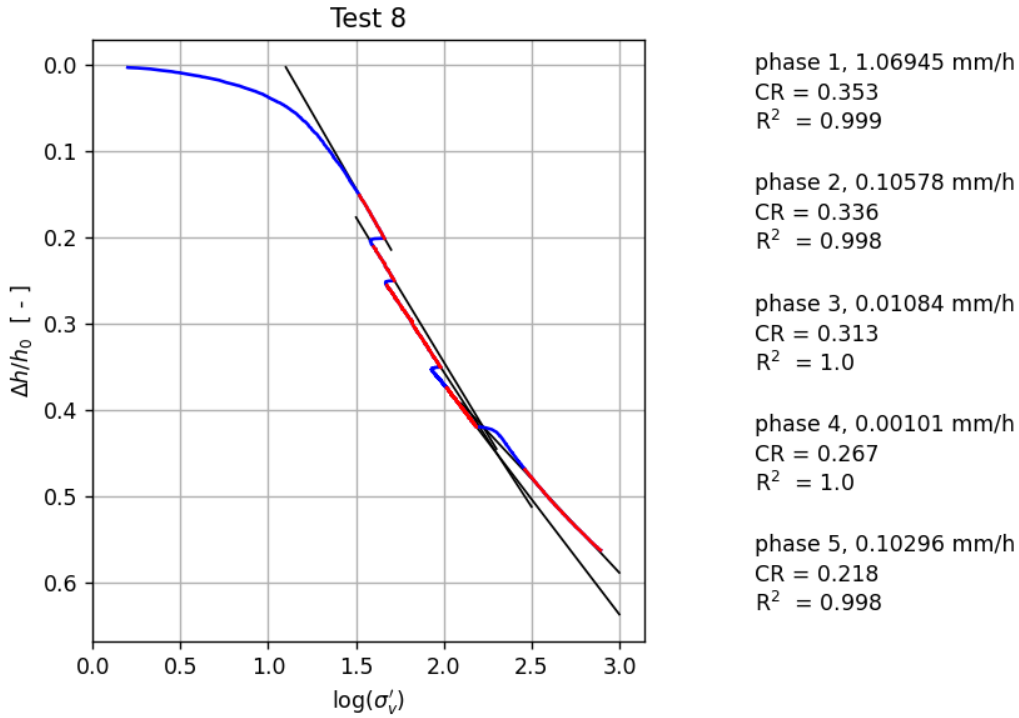

Figure A. 11 Fits stress – strain curve Test 8.

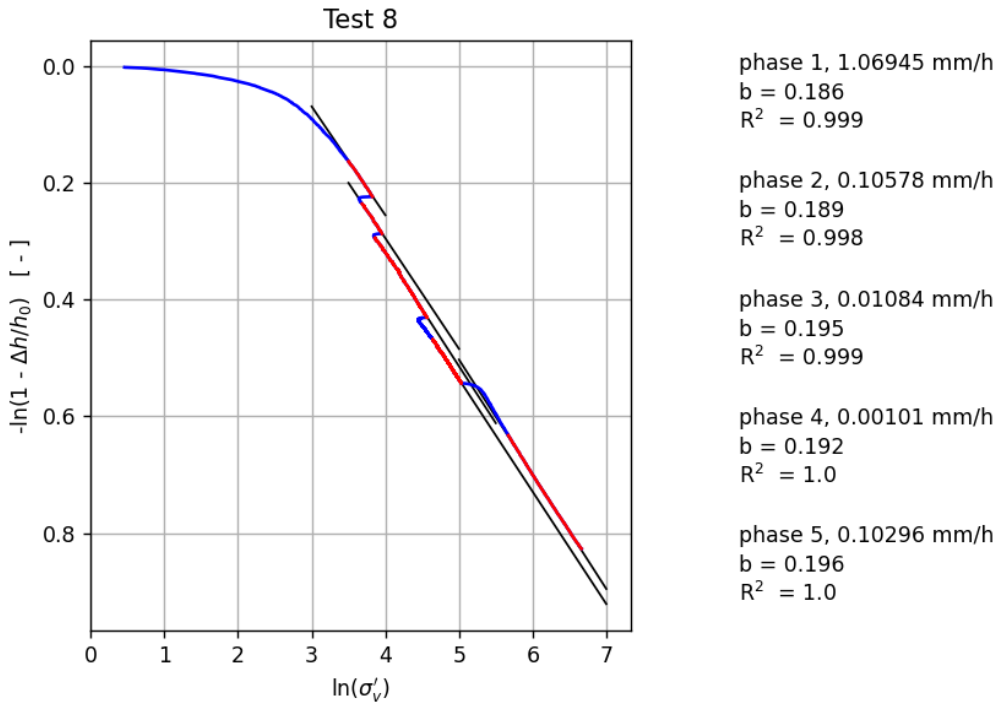

Figure A. 12 Fits stress – natural strain curve Test 8.

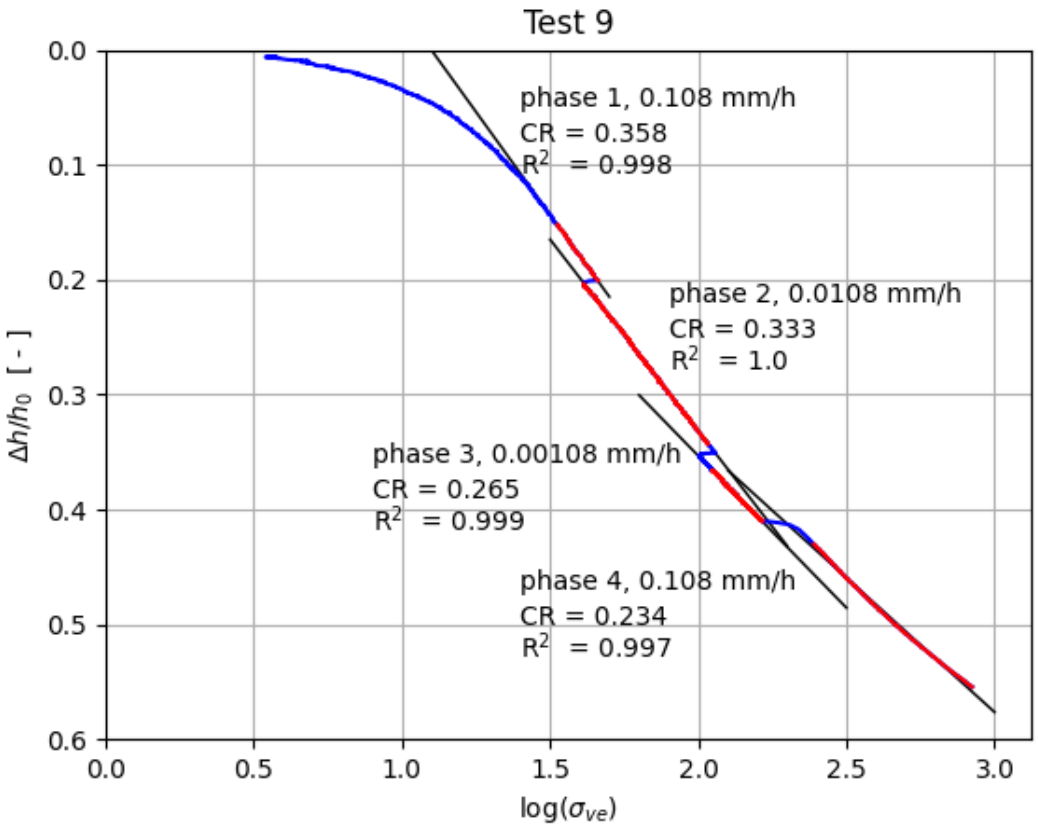

Figure A. 13 Fits stress – strain curve Test 9.

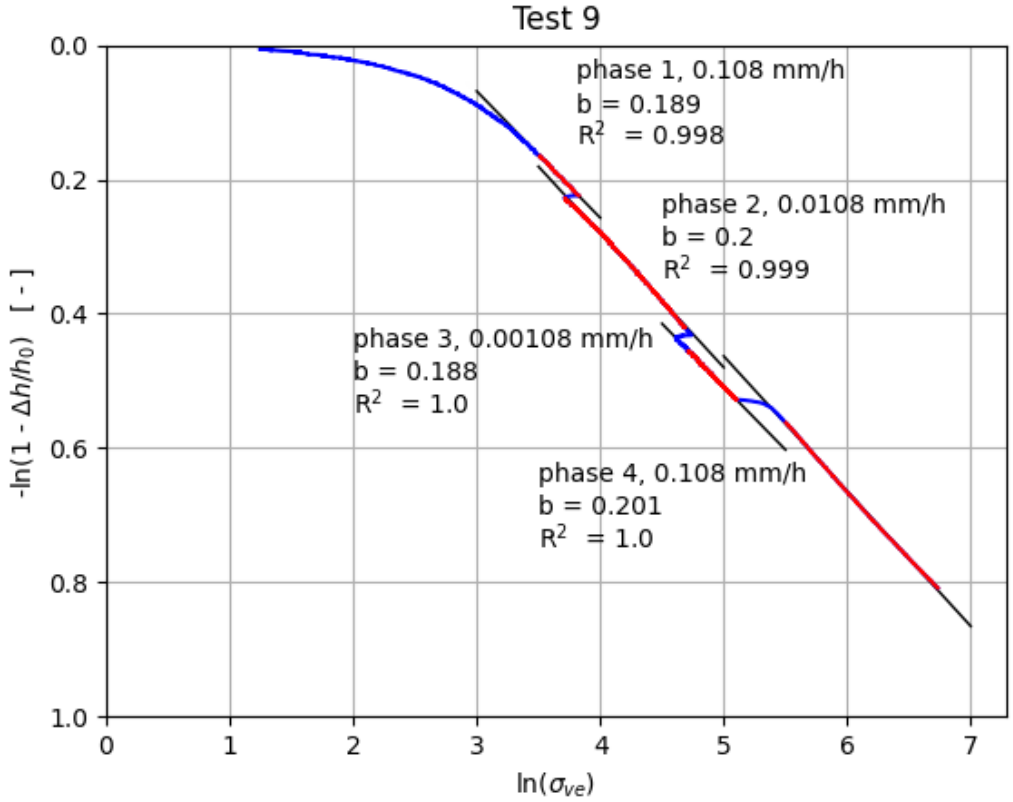

Figure A. 14 Fits stress – natural strain curve Test 9.

Deltares is an independent institute for applied research in the field of water and subsurface. Throughout the world, we work on smart solutions for people, environment and society.

Deltares

www.deltares.nl